ISSN 1949-8470 (online)

World Journal of *Radiology*

World J Radiol 2013 May 28; 5(5): 193-228

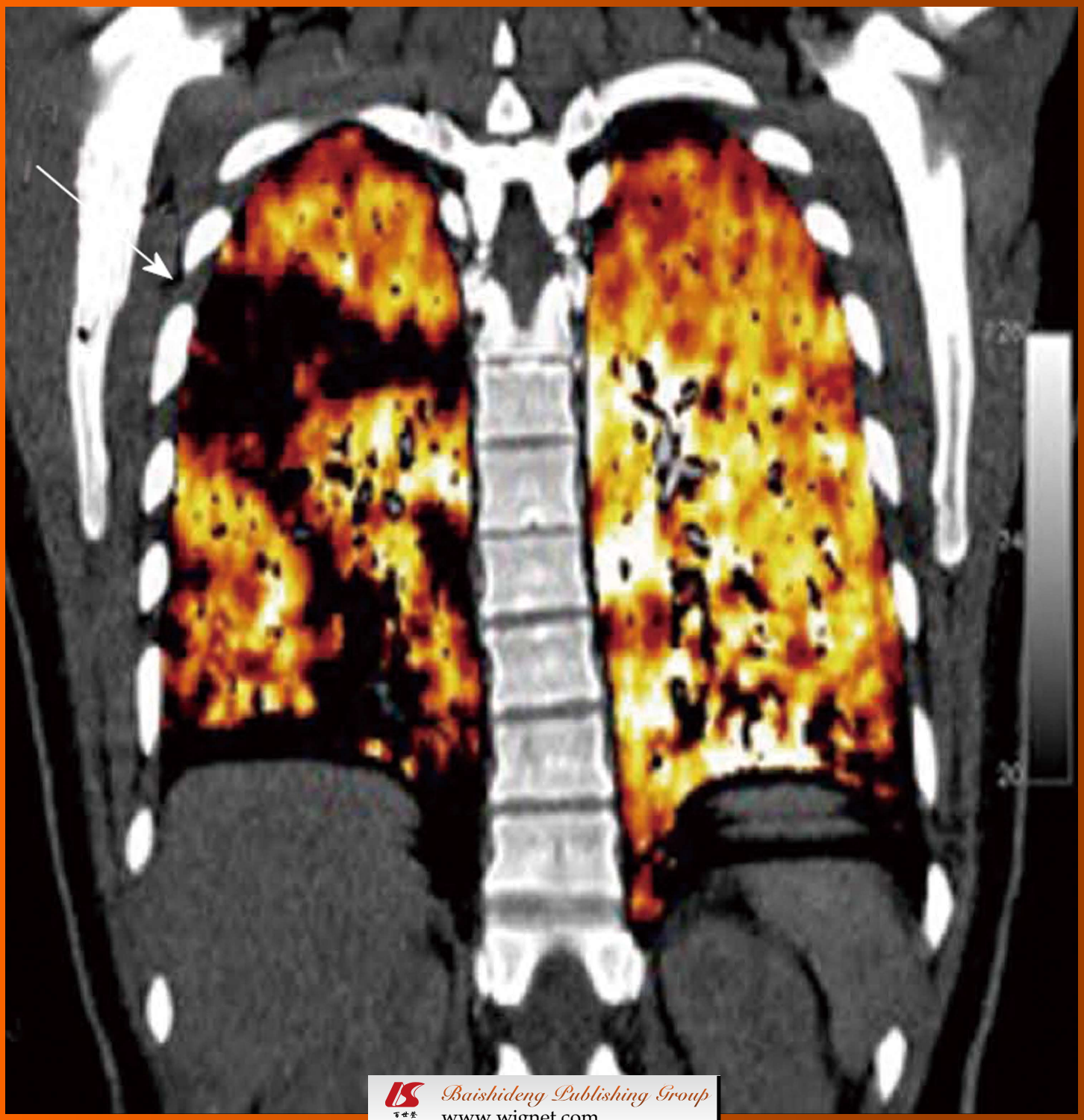

Baishideng Publishing Group
www.wjgnet.com

WJR World Journal of Radiology

A peer-reviewed, online, open-access journal of Radiology

Editorial Board

2009-2013

The *World Journal of Radiology* Editorial Board consists of 319 members, representing a team of worldwide experts in radiology. They are from 40 countries, including Australia (3), Austria (4), Belgium (5), Brazil (3), Canada (9), Chile (1), China (25), Czech (1), Denmark (1), Egypt (4), Estonia (1), Finland (1), France (6), Germany (17), Greece (8), Hungary (1), India (9), Iran (5), Ireland (1), Israel (4), Italy (28), Japan (14), Lebanon (1), Libya (1), Malaysia (2), Mexico (1), Netherlands (4), New Zealand (1), Norway (1), Saudi Arabia (3), Serbia (1), Singapore (2), Slovakia (1), South Korea (16), Spain (8), Switzerland (5), Thailand (1), Turkey (20), United Kingdom (16), and United States (82).

France

Alain Chapel, *Fontenay-Aux-Roses*
Nathalie Lassau, *Villejuif*
Youlia M Kirova, *Paris*
Géraldine Le Duc, *Grenoble Cedex*
Laurent Pierot, *Reims*
Frank Pilleul, *Lyon*
Pascal Pommier, *Lyon*

Germany

Ambros J Beer, *München*
Thomas Deserno, *Aachen*
Frederik L Giesel, *Heidelberg*
Ulf Jensen, *Kiel*
Markus Sebastian Juchems, *Ulm*
Kai U Juergens, *Bremen*
Melanie Kettering, *Jena*
Jennifer Linn, *Munich*
Christian Lohrmann, *Freiburg*
David Maintz, *Münster*
Henrik J Michaely, *Mannheim*
Oliver Micke, *Bielefeld*
Thoralf Niendorf, *Berlin-Buch*
Silvia Obenauer, *Duesseldorf*
Steffen Rickes, *Halberstadt*
Lars V Baron von Engelhardt, *Bochum*
Goetz H Welsch, *Erlangen*

Greece

Panagiotis Antoniou, *Alexandroupolis*
George C Kagadis, *Rion*
Dimitris Karacostas, *Thessaloniki*
George Panayiotakis, *Patras*
Alexander D Rapidis, *Athens*
C Triantopoulou, *Athens*
Ioannis Tsalafoutas, *Athens*
Virginia Tsapaki, *Anixi*
Ioannis Valais, *Athens*

Hungary

Peter Laszlo Lakatos, *Budapest*

India

Anil Kumar Anand, *New Delhi*
Surendra Babu, *Tamilnadu*
Sandip Basu, *Bombay*
Kundan Singh Chufal, *New Delhi*
Shivanand Gamanagatti, *New Delhi*
Vimoj J Nair, *Haryana*
R Prabhakar, *New Delhi*
Sanjeeb Kumar Sahoo, *Orissa*

Iran

Vahid Reza Dabbagh Kakhki, *Mashhad*
Mehran Karimi, *Shiraz*
Farideh Nejat, *Tehran*
Alireza Shirazi, *Tehran*
Hadi Rokni Yazdi, *Tehran*

Ireland

Joseph Simon Butler, *Dublin*

Israel

Amit Gefen, *Tel Aviv*
Eyal Sheiner, *Be'er-Sheva*
Jacob Sosna, *Jerusalem*
Simcha Yagel, *Jerusalem*

Italy

Mohssen Ansarin, *Milan*
Stefano Arcangeli, *Rome*
Tommaso Bartalena, *Imola*
Sergio Casciaro, *Lecce*
Laura Crocetti, *Pisa*
Alberto Cuocolo, *Napoli*
Mirko D'Onofrio, *Verona*
Massimo Filippi, *Milan*
Claudio Fiorino, *Milano*
Alessandro Franchello, *Turin*
Roberto Grassi, *Naples*
Stefano Guerriero, *Cagliari*
Francesco Lassandro, *Napoli*
Nicola Limbucci, *L'Aquila*
Raffaele Lodi, *Bologna*
Francesca Maccioni, *Rome*
Laura Martincich, *Candiolo*
Mario Mascalchi, *Florence*
Roberto Miraglia, *Palermo*
Eugenio Picano, *Pisa*
Antonio Pinto, *Naples*
Stefania Romano, *Naples*
Luca Saba, *Cagliari*
Sergio Sartori, *Ferrara*
Mariano Scaglione, *Castel Volturno*
Lidia Strigari, *Rome*
Vincenzo Valentini, *Rome*

Japan

Shigeru Ehara, *Morioka*
Nobuyuki Hamada, *Chiba*
Takao Hiraki, *Okayama*
Akio Hiwatashi, *Fukuoka*
Masahiro Jinzaki, *Tokyo*
Hiroshi Matsuda, *Saitama*
Yasunori Minami, *Osaka*
Jun-Ichi Nishizawa, *Tokyo*
Tetsu Niwa, *Yokohama*
Kazushi Numata, *Kanagawa*
Kazuhiko Ogawa, *Okinawa*
Hitoshi Shibuya, *Tokyo*
Akira Uchino, *Saitama*
Haiquan Yang, *Kanagawa*

Lebanon

Aghiad Al-Kutoubi, *Beirut*

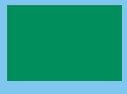

Libya

Anuj Mishra, *Tripoli*

Malaysia

R Logeswaran, *Cyberjaya*
Kwan-Hoong Ng, *Kuala Lumpur*

Mexico

Heriberto Medina-Franco, *Mexico City*

Netherlands

Jurgen J Fütterer, *Nijmegen*
Raffaella Rossin, *Eindhoven*
Paul E Sijens, *Groningen*

New Zealand

W Howell Round, *Hamilton*

Norway

Arne Sigmund Borthne, *Lørenskog*

Saudi Arabia

Mohammed Al-Omran, *Riyadh*
Ragab Hani Donkol, *Abha*
Volker Rudat, *Al Khobar*

Serbia

Djordjije Saranovic, *Belgrade*

Singapore

Uei Pua, *Singapore*
Lim CC Tchoyoson, *Singapore*

Slovakia

František Dubecký, *Bratislava*

South Korea

Bo-Young Choe, *Seoul*
Joon Koo Han, *Seoul*
Seung Jae Huh, *Seoul*
Chan Kyo Kim, *Seoul*
Myeong-Jin Kim, *Seoul*
Seung Hyup Kim, *Seoul*
Kyoung Ho Lee, *Gyeonggi-do*
Won-Jin Moon, *Seoul*
Wazir Muhammad, *Daegu*
Jai Soung Park, *Bucheon*
Noh Hyuck Park, *Kyunggi*
Sang-Hyun Park, *Daejeon*
Joon Beom Seo, *Seoul*
Ji-Hoon Shin, *Seoul*
Jin-Suck Suh, *Seoul*
Hong-Gyun Wu, *Seoul*

Spain

Eduardo J Aguilar, *Valencia*
Miguel Alcaraz, *Murcia*
Juan Luis Alcazar, *Pamplona*
Gorka Bastarrika, *Pamplona*
Rafael Martínez-Monge, *Pamplona*
Alberto Muñoz, *Madrid*
Joan C Vilanova, *Girona*

Switzerland

Nicolau Beckmann, *Basel*
Silke Grabherr, *Lausanne*
Karl-Olof Lövblad, *Geneva*
Tilo Niemann, *Basel*
Martin A Walter, *Basel*

Thailand

Sudsriluk Sampatchalit, *Bangkok*

Turkey

Olus Api, *Istanbul*
Kubilay Aydin, *İstanbul*
Işıl Bilgen, *Izmir*
Zulkif Bozgeyik, *Elazig*
Barbaros E Çil, *Ankara*
Gulgun Engin, *Istanbul*
M Fatih Evcimik, *Malatya*
Ahmet Kaan Gündüz, *Ankara*
Tayfun Hakan, *Istanbul*
Adnan Kabaalioglu, *Antalya*
Fehmi Kaçmaz, *Ankara*
Musturay Karcaaltincaba, *Ankara*
Osman Kizilkilic, *Istanbul*
Zafer Koc, *Adana*
Cem Onal, *Adana*
Yahya Paksoy, *Konya*
Bunyamin Sahin, *Samsun*
Ercument Unlu, *Edirne*
Ahmet Tuncay Turgut, *Ankara*
Ender Uysal, *Istanbul*

United Kingdom

K Faulkner, *Wallsend*
Peter Gaines, *Sheffield*
Balaji Ganeshan, *Brighton*
Nagy Habib, *London*
Alan Jackson, *Manchester*
Pradesh Kumar, *Portsmouth*
Tarik F Massoud, *Cambridge*
Igor Meglinski, *Bedfordshire*
Robert Morgan, *London*
Ian Negus, *Bristol*
Georgios A Plataniotis, *Aberdeen*
N J Raine-Fenning, *Nottingham*
Manuchehr Soleimani, *Bath*
MY Tseng, *Nottingham*
Edwin JR van Beek, *Edinburgh*
Feng Wu, *Oxford*

United States

Athanassios Argiris, *Pittsburgh*
Stephen R Baker, *Newark*
Lia Bartella, *New York*
Charles Bellows, *New Orleans*
Walter L Biffl, *Denver*
Homer S Black, *Houston*
Wessam Bou-Assaly, *Ann Arbor*
Owen Carmichael, *Davis*
Shelton D Caruthers, *St Louis*
Yuhchyau Chen, *Rochester*
Melvin E Clouse, *Boston*
Ezra Eddy Wyssam Cohen, *Chicago*
Aaron Cohen-Gadol, *Indianapolis*
Patrick M Colletti, *Los Angeles*
Kassa Darge, *Philadelphia*
Abhijit P Datir, *Miami*
Delia C DeBuc, *Miami*
Russell L Deter, *Houston*
Adam P Dicker, *Phil*
Khaled M Elsayes, *Ann Arbor*
Steven Feigenberg, *Baltimore*
Christopher G Filippi, *Burlington*
Victor Frenkel, *Bethesda*
Thomas J George Jr, *Gainesville*
Patrick K Ha, *Baltimore*
Robert I Haddad, *Boston*
Walter A Hall, *Syracuse*
Mary S Hammes, *Chicago*
John Hart Jr, *Dallas*
Randall T Higashida, *San Francisco*
Juebin Huang, *Jackson*
Andrei Iagaru, *Stanford*
Craig Johnson, *Milwaukee*
Ella F Jones, *San Francisco*
Csaba Juhasz, *Detroit*
Riyad Karmy-Jones, *Vancouver*
Daniel J Kelley, *Madison*
Amir Khan, *Longview*
Euishin Edmund Kim, *Houston*
Vikas Kundra, *Houston*
Kennith F Layton, *Dallas*
Rui Liao, *Princeton*
CM Charlie Ma, *Philadelphia*
Nina A Mayr, *Columbus*
Thomas J Meade, *Evanston*
Steven R Messé, *Philadelphia*
Nathan Olivier Mewton, *Baltimore*
Feroze B Mohamed, *Philadelphia*
Koenraad J Mortele, *Boston*
Mohan Natarajan, *San Antonio*
John L Nosher, *New Brunswick*
Chong-Xian Pan, *Sacramento*
Dipanjan Pan, *St Louis*
Martin R Prince, *New York*
Reza Rahbar, *Boston*
Carlos S Restrepo, *San Antonio*
Veronica Rooks, *Honolulu*
Maythem Saeed, *San Francisco*
Edgar A Samaniego, *Palo Alto*
Kohkan Shamsi, *Doylestown*
Jason P Sheehan, *Charlottesville*
William P Sheehan, *Willmar*
Charles Jeffrey Smith, *Columbia*
Monvadi B Srichai-Parsia, *New York*
Dan Stoianovici, *Baltimore*
Janio Szklaruk, *Houston*
Dian Wang, *Milwaukee*
Jian Z Wang, *Columbus*
Shougang Wang, *Santa Clara*
Wenbao Wang, *New York*
Aaron H Wolfson, *Miami*
Gayle E Woloschak, *Chicago*
Ying Xiao, *Philadelphia*
Juan Xu, *Pittsburgh*
Benjamin M Yeh, *San Francisco*
Terry T Yoshizumi, *Durham*
Jinxing Yu, *Richmond*
Jianhui Zhong, *Rochester*

WJR World Journal of Radiology

Contents

Monthly Volume 5 Number 5 May 28, 2013

Contents

World Journal of Radiology
Volume 5 Number 5 May 28, 2013

AIM AND SCOPE

World Journal of Radiology (*World J Radiol*, *WJR*, online ISSN 1949-8470, DOI: 10.4329) is a peer-reviewed open access academic journal that aims to guide clinical practice and improve diagnostic and therapeutic skills of clinicians.

WJR covers topics concerning diagnostic radiology, radiation oncology, radiologic physics, neuroradiology, nuclear radiology, pediatric radiology, vascular/interventional radiology, medical imaging achieved by various modalities and related methods analysis. The current columns of *WJR* include editorial, frontier, diagnostic advances, therapeutics advances, field of vision, mini-reviews, review, topic highlight, medical ethics, original articles, case report, clinical case conference (clinicopathological conference), and autobiography.

We encourage authors to submit their manuscripts to *WJR*. We will give priority to manuscripts that are supported by major national and international foundations and those that are of great basic and clinical significance.

INDEXING/ABSTRACTING

World Journal of Radiology is now indexed in PubMed Central, PubMed, Digital Object Identifier, and Directory of Open Access Journals.

NAME OF JOURNAL
World Journal of Radiology

ISSN
ISSN 1949-8470 (online)

LAUNCH DATE
December 31, 2009

FREQUENCY
Monthly

World Journal of Radiology
Room 903, Building D, Ocean International Center,
No. 62 Dongsihuan Zhonglu, Chaoyang District,
Beijing 100025, China
Telephone: +86-10-85381891
Fax: +86-10-85381893
E-mail: wjr@wjgnet.com
http://www.wjgnet.com

PUBLISHER
Baishideng Publishing Group Co., Limited
Flat C, 23/F., Lucky Plaza, 315-321 Lockhart Road,
Wanchai, Hong Kong, China
Fax: +852-31158812
Telephone: +852-58042046
E-mail: bpgoffice@wjgnet.com
http://www.wjgnet.com

PUBLICATION DATE
May 28, 2013

World Journal of Radiology

Online Submissions: http://www.wjgnet.com/esps/
wjr@wjgnet.com
doi:10.4329/wjr.v5.i5.193

World J Radiol 2013 May 28; 5(5): 193-201
ISSN 1949-8470 (online)

REVIEW

Computed tomography of Crohn's disease: The role of three dimensional technique

Siva P Raman, Karen M Horton, Elliot K Fishman

Siva P Raman, Karen M Horton, Elliot K Fishman, Department of Radiology, Johns Hopkins University School of Medicine, Johns Hoplins Outpatient Center, Baltimore, MD 21287, United States

Author contributions: All three authors contributed to the writing and editing of this manuscript; Raman SP was the primary author of the paper; Both Horton KM and Fishman EK played a major role in image selection.

Correspondence to: Siva P Raman, MD, Department of Radiology, Johns Hopkins University School of Medicine, Johns Hoplins Outpatient Center, Room 3251, 601 N Caroline Street, Baltimore, MD 21287, United States. srsraman3@gmail.com
Telephone: +1-410-9555173 Fax: +1-410-6140341

Received: January 7, 2013 Revised: April 18, 2013
Accepted: May 17, 2013
Published online: May 28, 2013

Abstract

Crohn's disease, a transmural inflammatory bowel disease, remains a difficult entity to diagnose clinically. Over the last decade, multidetector computed tomography (CT) has become the method of choice for non-invasive evaluation of the small bowel, and has proved to be of significant value in the diagnosis of Crohn's disease. Advancements in CT enterography protocol design, three dimensional (3-D) post-processing software, and CT scanner technology have allowed increasing accuracy in diagnosis, and the acquisition of studies at a much lower radiation dose. The cases in this review will illustrate that the use of 3-D technique, proper enterography protocol design, and a detailed understanding of the different manifestations of Crohn's disease are all critical in properly diagnosing the full range of possible complications in Crohn's patients. In particular, CT enterography has proven to be effective in identifying involvement of the small and large bowel (including active inflammation, stigmata of chronic inflammation, and Crohn's-related bowel neoplasia) by Crohn's disease, as well as the extra-enteric manifestations of the disease, including fistulae, sinus tracts, abscesses, and urologic/hepatobiliary/osseous complications. Moreover, the proper use of 3-D technique (including volume rendering and maximum intensity projection) as a routine component of enterography interpretation can play a vital role in improving diagnostic accuracy.

Key words: Crohn's disease; Computed tomography angiography; Multidetector computed tomography; Three dimensional technique; Volume rendering; Maximum intensity projection; Fistula; Dose reduction

Core tip: Advancements in computed tomography (CT) enterography protocol design, three dimensional (3-D) post-processing software, and CT scanner technology have allowed increasing accuracy in diagnosis, and the acquisition of studies at a much lower radiation dose. The cases in this review will illustrate that the use of 3-D technique, proper enterography protocol design, and a detailed understanding of the different manifestations of Crohn's disease are all critical in properly diagnosing the full range of possible complications in Crohn's patients.

Raman SP, Horton KM, Fishman EK. Computed tomography of Crohn's disease: The role of three dimensional technique. *World J Radiol* 2013; 5(5): 193-201 Available from: URL: http://www.wjgnet.com/1949-8470/full/v5/i5/193.htm DOI: http://dx.doi.org/10.4329/wjr.v5.i5.193

INTRODUCTION

Crohn's disease, a form of transmural inflammatory bowel disease affecting over 1.5 million Americans and Europeans, remains a difficult entity to diagnose clinically: While involvement of any segment of the gastrointestinal tract is possible, the disease most often affects the mesenteric small bowel, making direct endoscopic evaluation and biopsy difficult. Moreover, symptoms tend to be nonspecific, and there are no clinical symptoms or labora-

tory markers which allow a specific diagnosis[1]. With the development of the newest generation of drugs aimed at the treatment of Crohn's disease (including tumor necrosis factor-α inhibitors, steroids, and salicylic acid), some of which have proven efficacious even in moderate to severe cases, the accurate, timely diagnosis of Crohn's has become increasingly important[1,2].

Over the last decade, multidetector computed tomography (MDCT) has become the method of choice for non-invasive evaluation of the small bowel, and has proved to be of significant value in the diagnosis of Crohn's disease[3]. Computed tomography (CT) enterography has proven to be quite effective not only in identifying involvement of the small and large bowel by Crohn's, but also in the diagnosis of the extra-enteric manifestations of the disease, including fistulae, sinus tracts, and abscesses[4,5]. Improvements in enterography protocols, MDCT scanner technology, and image post-processing software have further improved the utility of MDCT in Crohn's, allowing increasingly subtle diagnoses, while at the same time, allowing acquisition of studies with markedly reduced radiation doses. This review will focus on the enteric and extra-enteric manifestations of Crohn's disease on MDCT, the importance of proper MDCT enterography protocols, the use of low-radiation techniques on modern MDCT scanners, and the utility of three dimensional (3-D) technique in improving diagnostic accuracy.

CT ENTEROGRAPHY TECHNIQUE

At our institution, all patients undergoing CT enterography are told to avoid any oral intake for at least 4-6 h prior to the study. Positive oral contrast is never used, as beam-hardening artifact from such contrast agents can obscure subtle bowel wall thickening, and make it difficult to appreciate changes in bowel wall and mucosal enhancement. Moreover, positive oral contrast agents can interfere with 3-D post-processing of MDCT data sets, an increasingly important component of enterography interpretation.

Instead, neutral contrast agents are preferred, typically 0.1% wt/vol barium sulfate suspension (VoLumen; Braco Diagnostics, Princeton, NJ, United States), although a few other products are also commercially available[6,7]. Notably, the literature suggests that VoLumen (compared to other neutral and positive contrast media) provides the best distension of the small bowel. Neutral contrast agents, which are near water density (but are not absorbed as rapidly as ingested water), are effective in distending the small bowel, but at the same time, allow detailed evaluation of small bowel wall thickness, density, and enhancement, without any negative impact upon 3-D post-processing[1,8].

Several different protocols have been described in the literature regarding the administration of oral contrast media for CT enterography, including protocols solely comprised of VoLumen, protocols with a combination of water and VoLumen, and protocols composed almost entirely of water[9]. Our institution's enterography protocol involves the administration of a total of 1350 cc of VoLumen (450 cc at 60 min prior to scanning, 450 cc at 40 min prior to scanning, and 450 cc at 20 min prior to scanning), followed by 500 cc of water 10 min before scanning. While this administration schedule represents the ideal, it is important to note that many patients may be unable to tolerate the ingestion of this large a volume of contrast media[1]. Even when patients are unable to drink the entire volume of oral contrast, adequate distension is still often possible.

Subsequently, a rapid injection of 100 cc of intravenous (IV) contrast is performed (3-5 cc/s), with the acquisition of both arterial and venous phase images at 30 s and 60 s respectively. The arterial phase images are critical for appreciating subtle bowel wall or mucosal hyperenhacement, as well as engorgement of the adjacent vasa recta, all of which are important signs of bowel inflammation. The venous phase images are important not only for evaluating the bowel, but also the other parenchymal organs of the abdomen (*i.e.*, liver, spleen, *etc.*), the extra-enteric manifestations of Crohn's disease, the venous mesenteric vasculature, and hypovascular bowel tumors.

Images are acquired with thin collimation, with acquisition of 0.625-0.75 mm slices, which are then reconstructed into 3-5 mm axial slices for routine interpretation. Coronal and sagittal multiplanar reconstructions are directly created at the CT scanner following the acquisition of the axial source images. At the same time, isotropic 0.5-0.75 mm images are used for 3-D post-processing.

3-D TECHNIQUE

At our institution, two separate sets of 3-D reconstructions are interactively created by the interpreting radiologist at an independent workstation: (1) Maximum intensity projection (MIP) imaging is based upon a computer algorithm which extracts the highest attenuation voxels in a data set, and projects these voxels into a 3-D display which can be manipulated and rotated by the radiologist into the desired plane. These images have proven the most effective for evaluation of the mesenteric vasculature, and are useful not only for visualizing the main aortic branch vessels, but also tiny mesenteric branches which are typically not readily visualized on the axial source images. Areas of bowel hyperemia and mesenteric vascular engorgement (*i.e.*, "comb sign", opacification of the vasa recta) are also easily identified using this technique; and (2) Volume rendering (VR) is based upon a more complex computer algorithm which assigns a specific color and transparency to each voxel in a data set based on its underlying attenuation (and relationship to other adjacent voxels), before projecting this data into an interactive 3-D display. We have found this technique to be most useful in displaying the entirety of the small bowel, and illustrating the relationship of adjacent small bowel loops, subtle areas of bowel wall thickening, abnormal mucosal enhancement, and extra-enteric manifestations of Crohn's disease[10-12].

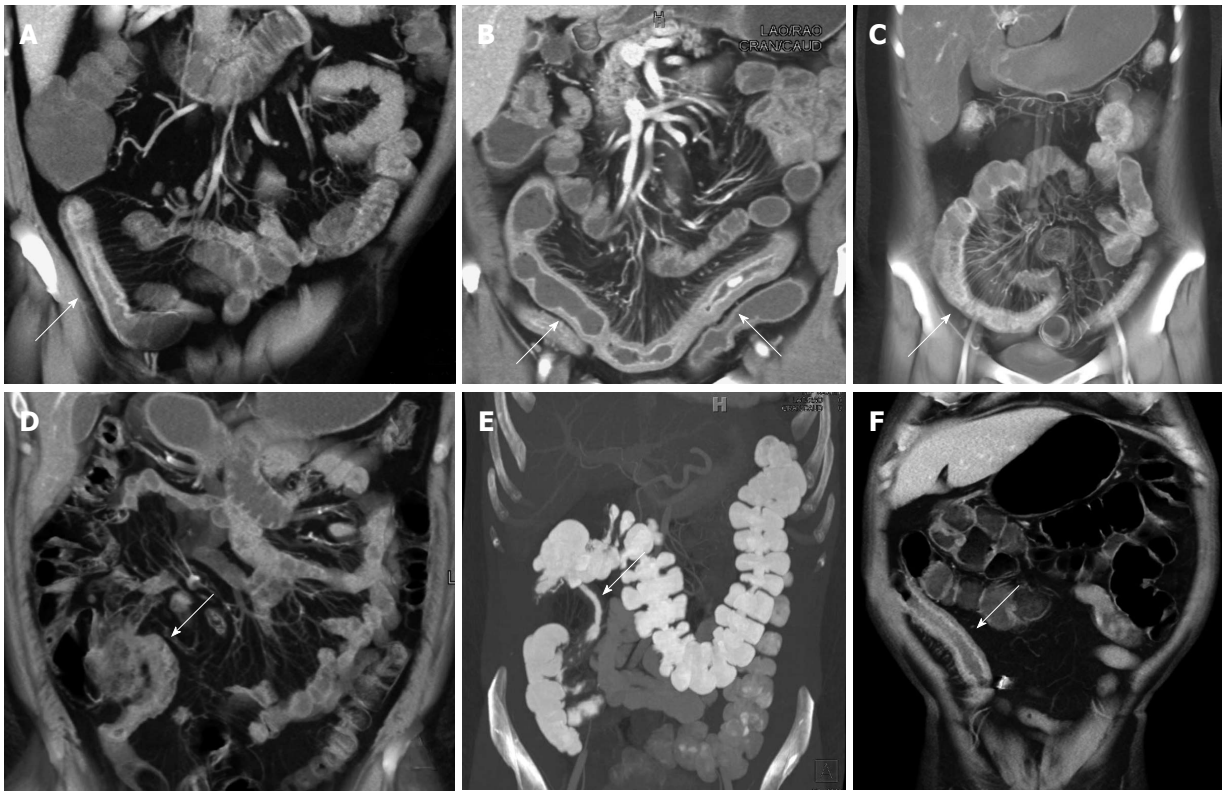

Figure 1 Active Crohn's disease. A: Fifty-four-year-old male with Crohn's disease. Coronal volume rendered image demonstrates prominent wall thickening and mucosal hyperemia encompassing a 10 cm segment of ileum (arrow). The volume rendered three dimensional (3-D) image nicely accentuates the marked mesenteric hyperemia and vasa recta engorgement adjacent to the inflamed loop of bowel; B: Sixty-two-year-old male with Crohn's disease. Coronal volume rendered images demonstrate a long segment of markedly thickened, inflamed bowel in the pelvis (arrows). Notably, the 3-D images accentuate the marked engorgement of the vasa recta ("comb sign") adjacent to the inflamed loop of bowel; C: Twenty-two-year-old with Crohn's disease. Coronal volume rendered image demonstrates an acutely inflamed loop of colon (arrow) with mucosal hyperemia and wall thickening, as well as adjacent engorgement of the vasa recta; D: Thirty-eight-year-old male with Crohn's disease. Coronal volume rendered image demonstrates thickening and mucosal hyperemia of the terminal ileum, a classic appearance and location for acute Crohn's related inflammation; E: Thirty-four-year-old male with Crohn's disease. Coronal volume rendered image demonstrates thickening of an intermediate length segment of terminal ileum (arrow); F: Sixty-year-old male with Crohn's disease and history of prior ileal resection and reanastomosis. Coronal volume rendered image demonstrates marked thickening, mucosal hyperemia, and adjacent vasa recta engorgement of the neo-terminal ileum (arrow).

LOW-DOSE CT TECHNIQUE

It is important to be cognizant that (1) the peak incidence of Crohn's disease is in patients between the ages of 20-40 years; (2) a sizeable percentage of cases are diagnosed in children (15%); and (3) the disease has a mild female predominance[13,14]. In other words, Crohn's disease is most often diagnosed in a particularly radiation-sensitive population, and the waxing and waning course of the disease (with multiple relapses over the patient's lifetime) places the patient at risk for a significant cumulative lifetime radiation dose[13-16]. However, several dose-reduction techniques are now available on the latest generation of CT scanners, all of which should be used for Crohn's patients (when available). These include (1) automated tube current modulation, which alters the tube current (mAs) based on the patient's size and density; (2) automated tube potential modulation, which alters the scanner's tube potential (kVp) based on the patient's size and density; and (3) iterative reconstruction, an alternative to traditional filtered back projection reconstruction techniques, which allows the acquisition and reconstruction of diagnostic quality images at far lower radiation doses[17]. Notably, while the details of each of these dose-reduction techniques is beyond the scope of this article, several studies have illustrated that enterography studies in patients with Crohn's disease can be performed at substantially lower radiation doses using these techniques, and can still be interpreted with a high degree of diagnostic confidence by the radiologist[13-17].

ENTERIC MANIFESTATIONS OF CROHN'S DISEASE

Active small bowel inflammation

Crohn's disease can involve any portion of the gastrointestinal tract from the mouth to the anus, although the small bowel is the most commonly affected portion of the bowel, particularly the distal and terminal ileum (Figure 1)[18]. The earliest phases of small bowel inflammation may be characterized only by subtle mucosal hyperenhancement on the arterial phase images, with little or no wall thickening or venous phase enhancement abnormalities[19,20]. However, as the degree of inflammation progresses, thickening of the bowel wall is typi-

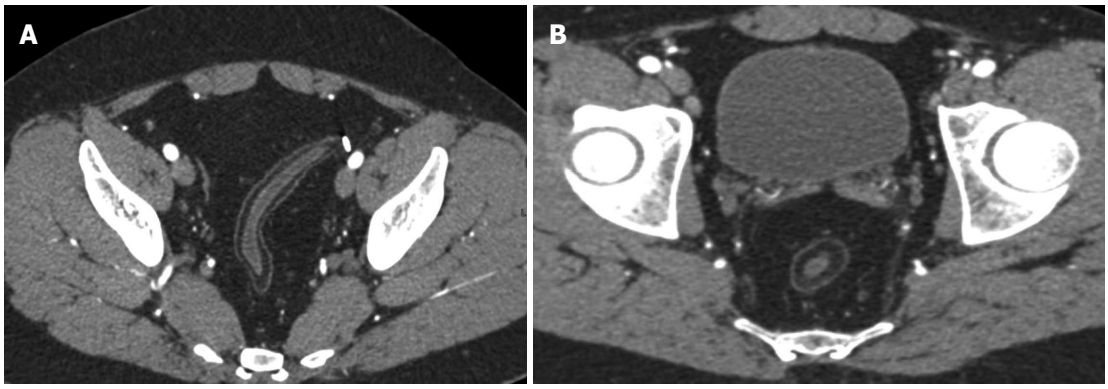

Figure 2 Sequela of chronic Crohn's related bowel inflammation. Twenty-seven year-old male with Crohn's disease. Axial images demonstrate diffuse fat deposition in the wall of the rectosigmoid colon (A, B), as well as marked fibrofatty proliferation ("creeping fat") (B) surrounding the rectum.

cally visualized (in addition to frank mucosal hyperemia on the venous phase images), with evidence of mural stratification ("target" or "double-halo appearance")[19]. This mural stratification most often represents the juxtaposition of avidly enhancing mucosa with hypodense submucosal edema in the bowel wall itself, and in some cases, hyperemia of the serosal surface of the bowel[21].

Clearly, interpretation of wall thickening must take into account the degree of luminal distention, but a wall thickness of > 3 mm in well distended small bowel loops has traditionally been considered as abnormal[22]. Although sometimes difficult to appreciate even on the highest quality studies, this wall thickening usually begins on the mesenteric side of the bowel, before progressing towards the antimesenteric side[19]. Notably, more than the wall thickening itself, the degree of mucosal enhancement most highly correlates with disease activity, although one must be careful not to confuse pathologic hyperenhancement with the normal greater enhancement of the jejunum relative to the ileum on arterial phase images. Similarly, collapsed bowel loops often appear to have higher attenuation walls, a finding which should not be confused with pathologic hyperenhancement[18,23].

Coronal multiplanar reformats, volume rendered images, and MIP images can be very helpful in properly evaluating abnormal small bowel loops. The coronal reformats are often most useful to visualize the small bowel as a whole, and better gauge which small bowel loops are truly abnormal, rather than simply collapsed. In a study by Liu *et al*[19], several instances of abnormal small bowel loops were not perceptible on the standard axial images, but were clearly present on coronal multiplanar reformats. The coronal reformations can also be helpful in cases of small bowel obstruction as a result of active inflammation, particularly in identifying the site of transition. Moreover, subtle mucosal hyperemia and thickening is often best appreciated on the volume rendered and MIP images, which accentuate these abnormalities. The use of clip planes is helpful to ensure visualization of the entire mesenteric small bowel, by removing overlapping loops, and following the entire bowel from duodenum to the terminal ileum.

Active colonic inflammation

While involvement of the small bowel is more common, Crohn's disease can also involve the large bowel, and in some cases, affect only the large bowel without small bowel involvement. While findings similar to those previously described in the small bowel should be sought, it should be noted that CT enterography studies are not designed to optimally distend the colon. As a result, the determination of bowel wall thickening and mucosal hyperenhancement should be made carefully, particularly when the colon is largely decompressed.

Chronic bowel disease

In the chronic phases of the disease, intramural deposition of fat is a common finding, and hypodense/soft tissue attenuation wall thickening and mucosal hyperemia should not be present in the absence of active inflammation (Figure 2). Notably, however, intramural fat deposition is a nonspecific finding that can be seen not only in other causes of chronic bowel inflammation, but also in the setting of obesity, steroid use, and diabetes[8]. As a result of the disease's preferential involvement of the mesenteric side of the bowel, asymmetric fibrosis and pseudosacculations along the mesenteric border are also common in the chronic setting[6].

CT enterography can also be helpful in identifying sites of strictures and narrowing, representing sites of fibrosis as a result of prior bouts of active inflammation. However, while sites of narrowing and thickening can be identified on CT, it is not always easy to distinguish a true stricture from peristalsis. Signs of true bowel obstruction should be sought, including proximal bowel dilatation with a discrete caliber transition at the stricture, distal decompression of small bowel loops, and fecal material in the proximal small bowel as a result of delayed bowel transit and stasis (Figure 3A-C). In some cases, it can be difficult to determine if a site of luminal narrowing is secondary to active inflammation or chronic fibrosis, particularly in the absence of adjacent inflammatory change and mesenteric hyperemia[24]. Regardless of whether luminal narrowing is acute or chronic, the presence of a stricture is a critical finding to communi-

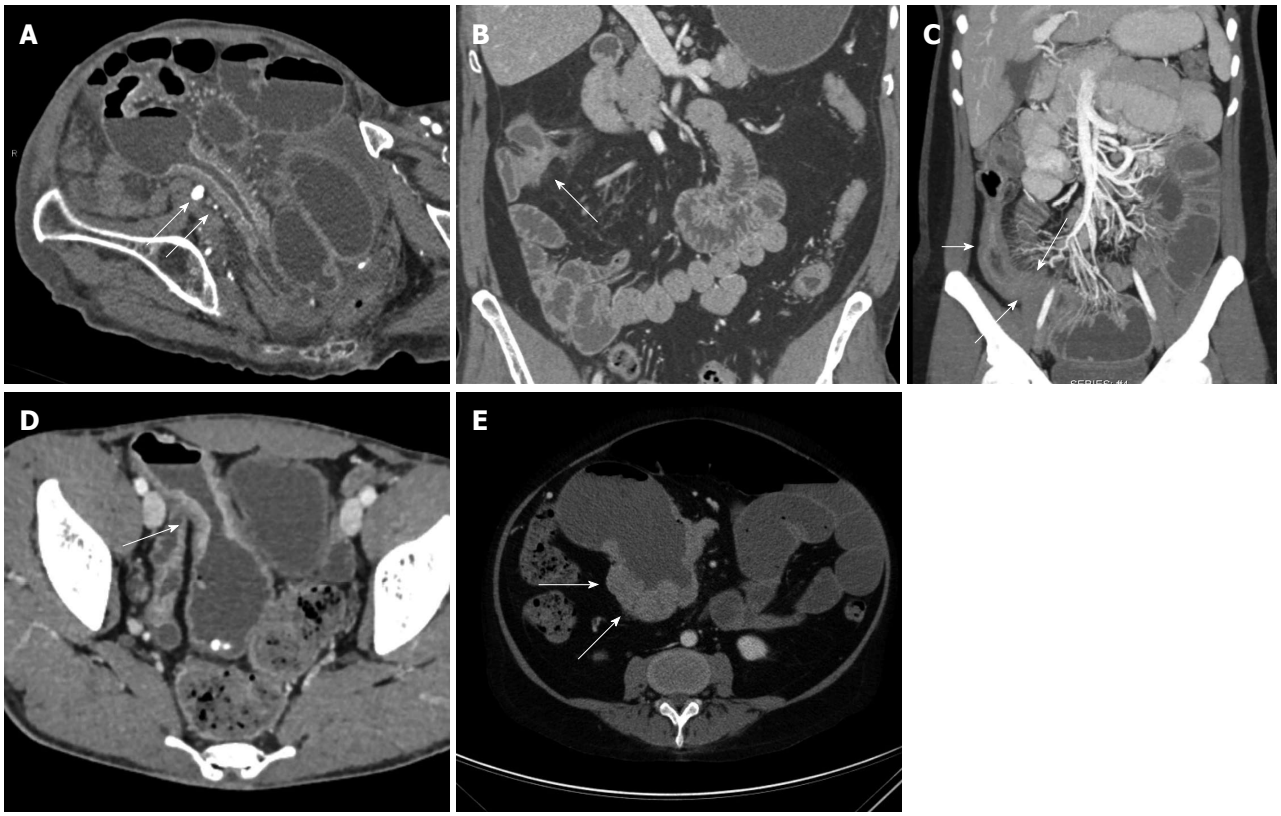

Figure 3 Bowel-related complications of Crohn's disease. A: Eighty-four-year-old who presented with abdominal pain. Axial contrast-enhanced image demonstrates multiple dilated loops of small bowel, in keeping with a small bowel obstruction. This image also demonstrates a long segment of bowel wall thickening and mucosal hyperemia with luminal narrowing (arrows). Given the patient's age, this was originally thought to represent a neoplastic or ischemic stricture, but was found to represent late-onset Crohn's disease after surgery; B: Forty-nine-year-old male with Crohn's disease. Coronal volume rendered computed tomography image demonstrates a short segment stricture and focal thickening of the hepatic flexure of the colon, with minimal adjacent induration, but no significant mesenteric hyperemia. This was thought to be a chronic-appearing stricture. Colonoscopy was performed to exclude an underlying neoplasm, and the patient was found to have a chronic stricture in this location without acute inflammation or evidence of tumor; C: Twenty-four-year-old female with Crohn's disease. Coronal volume rendered image demonstrates several dilated loops of small bowel in the left abdomen, with a discrete transition point (long arrows) in the distal ileum, at the site of a long segment of narrowed, hyperemic, thickened, inflamed small bowel (short arrow); D: Twenty-five-year-old male with Crohn's disease. Axial contrast enhanced image demonstrates thickening of a loop of small bowel in the pelvis, with dilatation proximal to the site of stricturing. Given the irregular thickening (arrow) at this site, the possibility of a malignancy could not be excluded. As a result, the patient underwent surgical resection and was found to have a small bowel adenocarcinoma; E: Fifty-one-year-old female with a history of Crohn's disease. Axial image demonstrates nodular soft tissue thickening (arrows) surrounding an aneurysmally dilated loop of bowel in the right abdomen. This was found to represent B-cell lymphoma following surgical resection.

cate to gastroenterologists, as small bowel endoscopy in this setting can result in capsule retention and small bowel obstruction[6].

Bowel neoplasia

Patients with Crohn's disease are at increased risk for both small bowel and colonic adenocarcinoma and lymphoma (Figure 3D and E). Corresponding to the most common sites of inflammation in Crohn's disease patients, the most common sites of small bowel adenocarcinoma are in the distal and terminal ileum, as opposed to the general population, where small bowel adenocarcinomas are most common in the duodenum. The overall risk of small bowel adenocarcinoma may be 15-50 times greater than in the general population, and are most commonly seen at the sites of greatest inflammation in each specific patient[25].

As a result, given the absence of any other clear means by which to screen the small bowel for tumors, the possibility of a tumor must be considered when evaluating any CT enterography study. In addition to the classic appearances of a tumor (*i.e.*, focal soft tissue mass, ulcerated nodule, annular constricting mass or "apple-core" lesion), any abnormal bowel loop must be evaluated critically: Any fixed site of narrowing (whether inflammatory or fibrotic) should be treated as a site of suspicion until proven otherwise, even if a discrete soft tissue mass is not identified. Moreover, asymmetric wall thickening and irregularity should not automatically be assumed to simply represent a site of active inflammation, particular if mural stratification of the thickened wall is not seen.

In a series by Soyer *et al*[25], four different patterns were seen with Crohn's related small bowel adenocarcinomas: (1) focal soft tissue mass; (2) short severe stenosis; (3) long stenosis with wall irregularity; and (4) irregular circumferential wall thickening of a bowel loop. The use of VR techniques in the coronal plane can be particularly useful in some of these cases, nicely illustrating the irreg-

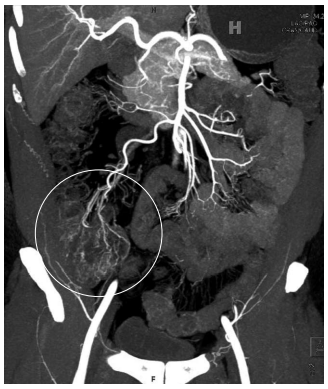

Figure 4 Identification of early Crohn's disease using maximum intensity projection images. Forty-seven-year-old male with abdominal pain. While no significant abnormality was appreciated on the axial source images or multiplanar reformats, coronal maximum intensity projection images raised the possibility of mild mesenteric hyperemia and vasa recta engorgement (circle) adjacent to the cecum. The patient underwent colonoscopy, and was found to have Crohn's colitis.

ularity and mass-like nature of some areas of wall thickening, and suggesting the presence of a neoplasm. It is also critical to assess local adenopathy. Although reactive nodes are commonly noted in patients with active Crohn's disease, large nodes (> 2 cm) should raise the possibility of an underlying malignancy.

EXTRA-ENTERIC MANIFESTATIONS OF CROHN'S DISEASE

Acute mesenteric findings

In the acute inflammatory setting, engorgement of the vasa recta, mesenteric hyperemia, fat stranding, and increased attenuation of the mesenteric fat are all common imaging findings, and are typically localized adjacent to the sites of greatest bowel inflammation (Figures 1A-C and 4). These signs are particularly important in those cases where bowel wall thickening and mucosal hyperemia are equivocal, as well as those cases where collapsed loops of bowel limit subtle evaluation of the bowel wall and mucosa (Figure 4). All of these mesenteric findings have been associated with active bowel inflammation, elevated C-reactive protein levels, and severity of disease, and are important findings to note in every examination[22]. In particular, engorgement of the vasa recta (sometimes termed the "comb" sign) is often best appreciated on coronal MIP images, which accentuate those areas of greatest vascular engorgement.

Chronic mesenteric findings

Over time, as a result of multiple bouts of active inflammation, fibrofatty proliferation (often termed as "creeping fat") can develop along the mesenteric border of the involved bowel segments (Figure 2). This fatty proliferation is associated with chronic disease, although it is unclear whether this fat is merely reactive to the patient's chronic inflammation, or alternatively, is hormonally active and may potentially drive the patient's inflammation[8,22].

Abscesses and fistulas

Up to 1/3 of Crohn's patients develop a fistula within the first ten years after exhibiting symptoms of Crohn's disease (Figures 5 and 6A). While the perianal region is the most common site of fistula formation, fistulas can develop anywhere in the abdomen, including enteroenteric, coloenteric, colocolic, rectovaginal, enterocutaneous, and enterovesicular fistulas. The sensitivity of CT for fistulas may be as high as 94%, although the appearance can be subtle in some cases. In the most obvious cases, an enhancing tract can be traced, clearly identifying the presence of a fistula[8].

However, in many cases a discrete tract will not be identified, and the presence of a fistula must be surmised by secondary signs. In particular, the presence of ectopic gas in the midst of bowel loops, tethering and spiculation of adjacent bowel loops, and soft tissue stranding and density in the midst of tethered bowel loops can be seen in the presence "complex fistulizing" Crohn's disease. In such cases, these imaging features are suggestive of the presence of fistulous tracts connecting these abnormally oriented loops of bowel (Figure 5A, C and E). Ectopic gas in other locations, including the bladder and subcutaneous soft tissues, should also raise concern for a fistula, and should not automatically be assumed to be secondary to a foley catheter or soft tissue injections[22]. Notably, CT is much less sensitive to the presence of a perianal fistula compared to magnetic resonance imaging, and a discrete tract or hyperenhancement is very rarely visualized on CT[26]. Nevertheless, the presence of any soft tissue stranding, induration, or fluid in this location should raise concern, and at the very least, should precipitate clinical examination of this area (Figure 6A)[8].

From a protocol perspective, while the use of a neutral oral contrast agent is the norm in CT enterography studies, better delineation of a fistula is one of the few indications where a positive oral contrast agent may be helpful. The use of volume rendered images can also be very useful in delineating the full extent of a patient's fistulous disease, particularly in cases of complex fistulizing Crohn's disease with multiple involved bowel loops. Coronal VR images can improve visualization of sites of involvement, delineate the size and extent of fistulous tracts, and in some cases, can facilitate visualization of fistulous tracts which are difficult to appreciate on routine axial images. Finally, patients with Crohn's disease are at high risk of developing abscesses in the leaves of the mesentery, some of which can fistulize with the adjacent bowel (Figure 6B). These abscesses can be difficult to visualize, and can blend in with adjacent bowel loops given the routine use of VoLumen in CT enterography studies.

Urological complications

In the setting of acute Crohn's-related inflammatory disease in the abdomen, the two most common severe urological complications are the development of (1) obstructive uropathy; and (2) enterovesicular fistulas: The development of obstructive uropathy is relatively

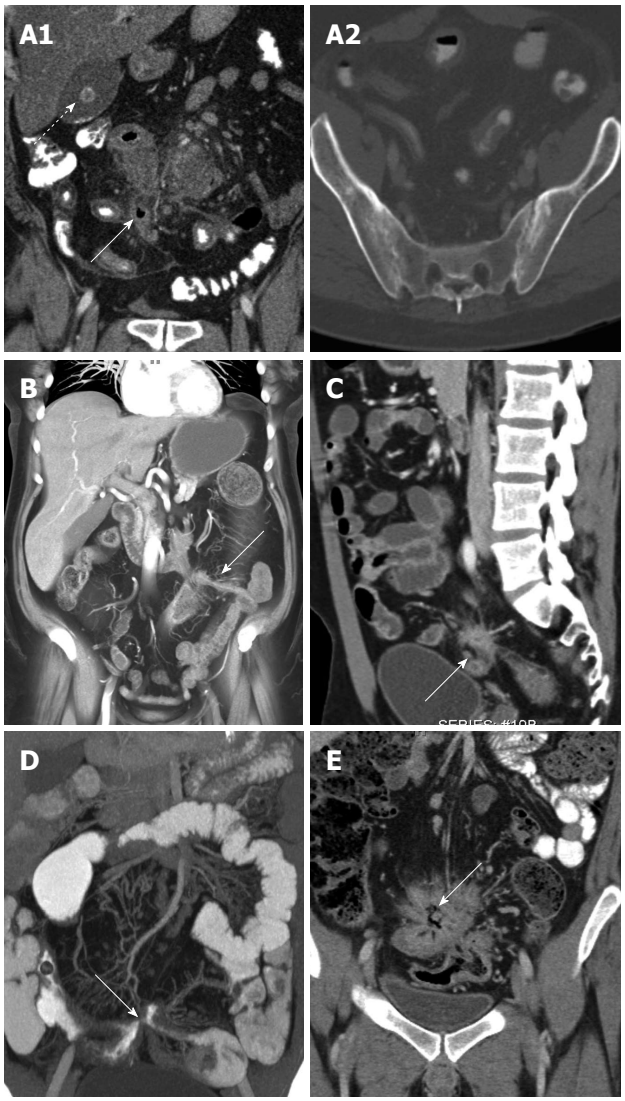

Figure 5 Fistulas and sinus tracts related to Crohn's disease. A: Thirty-nine-year-old male with Crohn's disease. Coronal image demonstrates several thick-walled, inflamed loops of small bowel tethered and matted together in the right lower abdomen, with ectopic gas (solid arrow), fluid, and phlegmonous change at the center of this collection of bowel loops. While discrete fistulous tracts could not be visualized, this constellation of findings is highly suggestive of complex fistulizing Crohn's disease. A gallstone (dashed arrow) is incidentally visualized in the gallbladder, a commonly associated finding in Crohn's disease (A1). Image of the bony pelvis demonstrates bilateral narrowing, sclerosis, and partial ankylosis of the sacroiliac joints (A2); B: Sixty-nine-year-old male with Crohn's disease. Coronal volume rendered (VR) image demonstrates several thickened, inflamed bowel loops in the mid and left abdomen with mucosal hyperemia and adjacent vasa recta engorgement. A clear enhancing fistulous tract (arrow) is identified connecting adjacent tethered bowel loops; C: Twenty-four-year-old male with Crohn's disease. Sagittal contrast-enhanced image demonstrates clumping (arrow) and matting of two immediately adjacent, inflamed loops of ileum and sigmoid colon. This appearance persisted on follow-up examination, and was highly concerning for an enterocolonic fistula; D: Twenty-eight-year-old female with Crohn's disease. Coronal volume rendered image demonstrates an enteroenteric fistulae (arrow) connecting adjacent loops of small bowel; E: Twenty-six-year-old female with Crohn's disease. Coronal multiplanar reformatted image demonstrates multiple loops of bowel tethered together and matted in the central abdomen. Especially given the linear gas (arrow) at the center of these bowel loops, this appearance is strongly suggestive of multiple enteroenteric and enterocolic fistulae.

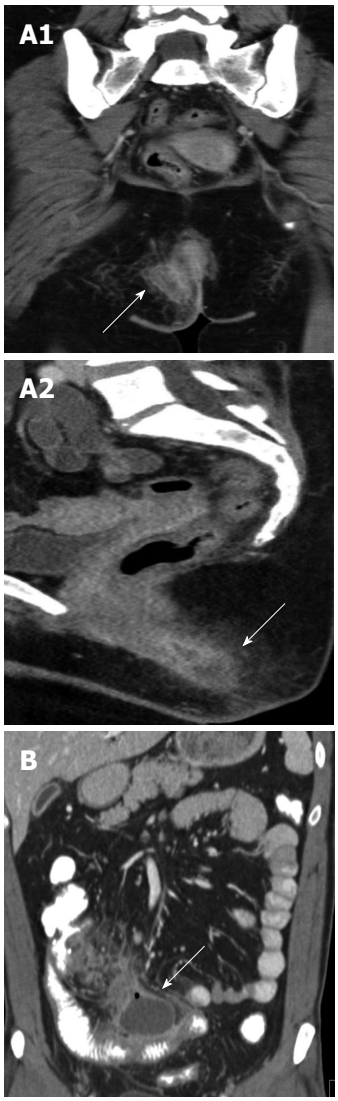

Figure 6 Abscesses related to Crohn's disease. A: Forty-three-year-old female with Crohn's disease. Coronal and sagittal computed tomography images with contrast demonstrate a right-sided perianal rim-enhancing fluid collection/abscess (A1 and A2, arrows) with a direct tract extending from the abscess to the rectum; B: Thirty-six-year-old male with Crohn's disease. Coronal contrast-enhanced image demonstrates a thickened loop of ileum in the right lower quadrant with marked adjacent phlegmonous change and inflammation, as well as an abscess (arrow) along the mesenteric border of the inflamed loop of bowel.

common in Crohn's, and may be present in up to 6% of patients with acute inflammatory disease. Most common on the right side, hydronephrosis and hydroureter are typically the result of either acute inflammatory change enveloping a portion of the ureter, or alternatively, fibrotic narrowing of the ureter as a result of a prior inflammatory episode[27].

Enterovesicular fistulas are a rare, but serious, complication, present in up to 3.5% of patients. Typically the result of an adjacent inflamed loop of bowel, women are less likely to develop this complication because of the protective presence of the uterus and adnexa. In the most obvious cases, a direct enhancing tract can be identified extending from an adjacent bowel loop (usually ileum) to the bladder. However, in the absence of directly visualizing a tract, the presence of ectopic gas in the bladder, focal bladder wall thickening adjacent to

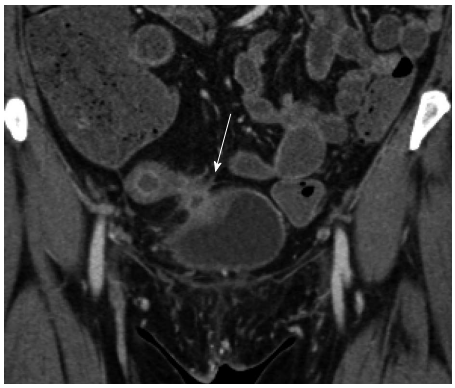

Figure 7 Enterovesicular fistula. Fifty-two-year-old female with Crohn's disease. Coronal contrast-enhanced computed tomography image demonstrates a markedly thickened, hyperemic loop of bowel in the pelvis, in keeping with acute Crohn's related inflammation. The bowel loop directly abuts the bladder, which is focally thickened (arrow) at the site of contact, although no gas was identified in the bladder. The patient was ultimately proven to have an enterovesicular fistula.

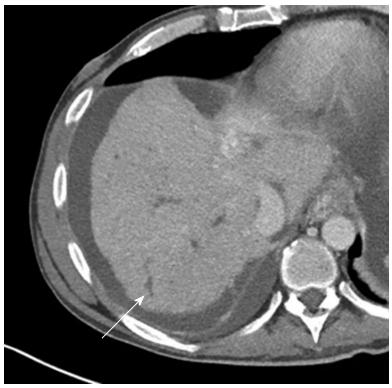

Figure 8 Primary sclerosing cholangitis and Crohn's disease. Twenty-four-year-old female with inflammatory bowel disease and primary sclerosing cholangitis. Axial contrast enhanced image demonstrates beading and irregular dilatation of the peripheral intrahepatic biliary tree (arrow). Massive enlargement of the caudate lobe with nodularity of the liver capsule was also noted (not shown).

an inflamed loop of bowel, or the tethering of a bowel loop towards the bladder should all raise concern for the presence of a fistula. Evaluation of the bladder in the coronal plane using multiplanar reformations and VR is a necessity, especially when abnormal bowel loops are identified in close proximity to the bladder (Figure 7)[27]. Notably, patients with Crohn's disease are also at increased risk of developing both renal stones and urinary infections, even in the absence of an active inflammatory episode[27].

Hepatic and biliary complications

In addition to the previously mentioned predilection for renal stones, patients with Crohn's disease also demonstrate an increased incidence of gallstones (perhaps up to 9.3% in one series)[28] (Figure 5A). Moreover, although rare, there is a known association between Crohn's disease and primary sclerosing cholangitis (PSC). Although this entity may sometimes be difficult to appreciate on CT, the presence of ductal beading and irregularity, cirrhosis, and significant enlargement of the caudate lobe are all signs which should be suggestive of PSC in the setting of known Crohn's disease (Figure 8).

Osseous complications

The association between sacroiliitis and Crohn's disease has been well described in the literature, with between 11%-35% of patients with Crohn's disease demonstrating evidence of bilateral, symmetric sacroiliitis on either CT or nuclear medicine studies[29]. Careful attention should be paid to the sacroiliac joints on every study in a Crohn's patient, searching for evidence of joint space narrowing, erosions, sclerosis, and fusion[5] (Figure 5A). Moreover, given the relatively common use of steroids and other immunomodulators in the treatment of Crohn's, the radiologist must carefully note any evidence of new sclerosis, deformity, or irregularity of either the femoral or humeral heads, as the use of these medications places this patient population at increased risk of avascular necrosis[5].

Lymphoma

There is a roughly four-fold increased risk of non-Hodgkins lymphoma in patients with Crohn's disease, although it is unclear whether this increased risk is secondary to these patients' underlying Crohn's disease (and disease severity), or the use of immunomodulating drugs (such as azathioprine and 6-mercaptopurine)[30] (Figure 3E).

CONCLUSION

The utility of MDCT in the diagnosis of Crohn's disease and its complications is undeniable, with a proven efficacy in identifying the enteric and extra-enteric manifestations of the disease. However, advancements in CT enterography protocol design, 3-D post-processing software, and CT scanner technology have allowed increasing accuracy in diagnosis, and the acquisition of studies at a much lower radiation dose. As the cases in this review illustrate, the use of 3-D technique, proper protocol design, and a detailed understanding of the different manifestations of Crohn's disease are all critical in properly diagnosing the full range of possible complications in Crohn's patients.

REFERENCES

1 **Huprich JE**, Fletcher JG. CT enterography: principles, technique and utility in Crohn's disease. *Eur J Radiol* 2009; **69**: 393-397 [PMID: 19118968 DOI: 10.1016/j.ejrad.2008.11.014]

2 **Wu YW**, Tang YH, Hao NX, Tang CY, Miao F. Crohn's disease: CT enterography manifestations before and after treatment. *Eur J Radiol* 2012; **81**: 52-59 [PMID: 21185142 DOI: 10.1016/j.ejrad.2010.11.010]

3 **Raptopoulos V**, Schwartz RK, McNicholas MM, Movson J, Pearlman J, Joffe N. Multiplanar helical CT enterography in patients with Crohn's disease. *AJR Am J Roentgenol* 1997; **169**: 1545-1550 [PMID: 9393162 DOI: 10.2214/ajr.169.6.9393162]

4 **Hara AK**, Leighton JA, Heigh RI, Sharma VK, Silva AC, De Petris G, Hentz JG, Fleischer DE. Crohn disease of the small bowel: preliminary comparison among CT enterography, capsule endoscopy, small-bowel follow-through, and ileoscopy. *Radiology* 2006; **238**: 128-134 [PMID: 16373764 DOI: 10.1148/radiol.2381050296]

5 **Kerner C**, Carey K, Mills AM, Yang W, Synnestvedt MB, Hilton S, Weiner MG, Lewis JD. Use of abdominopelvic computed tomography in emergency departments and rates of urgent diagnoses in Crohn's disease. *Clin Gastroenterol Hepatol* 2012; **10**: 52-57 [PMID: 21946122 DOI: 10.1016/j.cgh.2011.09.005]

6 **Elsayes KM**, Al-Hawary MM, Jagdish J, Ganesh HS, Platt JF. CT enterography: principles, trends, and interpretation of findings. *Radiographics* 2010; **30**: 1955-1970 [PMID: 21057129 DOI: 10.1148/rg.307105052]

7 **Al-Hawary M**, Zimmermann EM. A new look at Crohn's disease: novel imaging techniques. *Curr Opin Gastroenterol* 2012; **28**: 334-340 [PMID: 22678451 DOI: 10.1097/MOG.0b013e3283540705]

8 **Paulsen SR**, Huprich JE, Fletcher JG, Booya F, Young BM, Fidler JL, Johnson CD, Barlow JM, Earnest F. CT enterography as a diagnostic tool in evaluating small bowel disorders: review of clinical experience with over 700 cases. *Radiographics* 2006; **26**: 641-657; discussion 657-662 [PMID: 16702444 DOI: 10.1148/rg.263055162]

9 **Furukawa A**, Saotome T, Yamasaki M, Maeda K, Nitta N, Takahashi M, Tsujikawa T, Fujiyama Y, Murata K, Sakamoto T. Cross-sectional imaging in Crohn disease. *Radiographics* 2004; **24**: 689-702 [PMID: 15143222 DOI: 10.1148/rg.243035120]

10 **Johnson PT**, Horton KM, Fishman EK. Nonvascular mesenteric disease: utility of multidetector CT with 3D volume rendering. *Radiographics* 2009; **29**: 721-740 [PMID: 19448112 DOI: 10.1148/rg.293085113]

11 **Raman SP**, Horton KM, Fishman EK. Transitional cell carcinoma of the upper urinary tract: optimizing image interpretation with 3D reconstructions. *Abdom Imaging* 2012; **37**: 1129-1140 [PMID: 22207253 DOI: 10.1007/s00261-011-9838-2]

12 **Raman SP**, Horton KM, Fishman EK. Multimodality imaging of pancreatic cancer-computed tomography, magnetic resonance imaging, and positron emission tomography. *Cancer J* 2012; **18**: 511-522 [PMID: 23187837 DOI: 10.1097/PPO.0b013e318274a461]

13 **Kambadakone AR**, Chaudhary NA, Desai GS, Nguyen DD, Kulkarni NM, Sahani DV. Low-dose MDCT and CT enterography of patients with Crohn disease: feasibility of adaptive statistical iterative reconstruction. *AJR Am J Roentgenol* 2011; **196**: W743-W752 [PMID: 21606263 DOI: 10.2214/AJR.10.5303]

14 **Kambadakone AR**, Prakash P, Hahn PF, Sahani DV. Low-dose CT examinations in Crohn's disease: Impact on image quality, diagnostic performance, and radiation dose. *AJR Am J Roentgenol* 2010; **195**: 78-88 [PMID: 20566800 DOI: 10.2214/AJR.09.3420]

15 **Kielar AZ**, Tao H, McKeever C, El-Maraghi RH. Low-Radiation-Dose Modified Small Bowel CT for Evaluation of Recurrent Crohn's Disease. *Gastroenterol Res Pract* 2012; **2012**: 598418 [PMID: 21785584 DOI: 10.1155/2012/598418]

16 **Lee SJ**, Park SH, Kim AY, Yang SK, Yun SC, Lee SS, Jung GS, Ha HK. A prospective comparison of standard-dose CT enterography and 50% reduced-dose CT enterography with and without noise reduction for evaluating Crohn disease. *AJR Am J Roentgenol* 2011; **197**: 50-57 [PMID: 21701010 DOI: 10.2214/AJR.11.6582]

17 **Raman SP**, Johnson PT, Deshmukh S, Mahesh M, Grant KL, Fishman EK. CT dose reduction applications: available tools on the latest generation of CT scanners. *J Am Coll Radiol* 2013; **10**: 37-41 [PMID: 23290672 DOI: 10.1016/j.jacr.2012.06.025]

18 **Zalis M**, Singh AK. Imaging of inflammatory bowel disease: CT and MR. *Dig Dis* 2004; **22**: 56-62 [PMID: 15292695 DOI: 10.1159/000078735]

19 **Liu YB**, Liang CH, Zhang ZL, Huang B, Lin HB, Yu YX, Xie SF, Wang QS, Zheng JH. Crohn disease of small bowel: multidetector row CT with CT enteroclysis, dynamic contrast enhancement, CT angiography, and 3D imaging. *Abdom Imaging* 2006; **31**: 668-674 [PMID: 16967238 DOI: 10.1007/s00261-006-9092-1]

20 **Gatta G**, Di Grezia G, Di Mizio V, Landolfi C, Mansi L, De Sio I, Rotondo A, Grassi R. Crohn's disease imaging: a review. *Gastroenterol Res Pract* 2012; **2012**: 816920 [PMID: 22315589 DOI: 10.1155/2012/816920]

21 **Lalitha P**, Reddy MCh, Reddy KJ, Kumari MV. Computed tomography enteroclysis: a review. *Jpn J Radiol* 2011; **29**: 673-681 [PMID: 22009417 DOI: 10.1007/s11604-011-0621-7]

22 **Hara AK**, Swartz PG. CT enterography of Crohn's disease. *Abdom Imaging* 2009; **34**: 289-295 [PMID: 18649092 DOI: 10.1007/s00261-008-9443-1]

23 **Booya F**, Fletcher JG, Huprich JE, Barlow JM, Johnson CD, Fidler JL, Solem CA, Sandborn WJ, Loftus EV, Harmsen WS. Active Crohn disease: CT findings and interobserver agreement for enteric phase CT enterography. *Radiology* 2006; **241**: 787-795 [PMID: 17032911 DOI: 10.1148/radiol.2413051444]

24 **Dillman JR**, Adler J, Zimmermann EM, Strouse PJ. CT enterography of pediatric Crohn disease. *Pediatr Radiol* 2010; **40**: 97-105 [PMID: 19936733 DOI: 10.1007/s00247-009-1465-5]

25 **Soyer P**, Hristova L, Boudghène F, Hoeffel C, Dray X, Laurent V, Fishman EK, Boudiaf M. Small bowel adenocarcinoma in Crohn disease: CT-enterography features with pathological correlation. *Abdom Imaging* 2012; **37**: 338-349 [PMID: 21671043 DOI: 10.1007/s00261-011-9772-3]

26 **Pariente B**, Peyrin-Biroulet L, Cohen L, Zagdanski AM, Colombel JF. Gastroenterology review and perspective: the role of cross-sectional imaging in evaluating bowel damage in Crohn disease. *AJR Am J Roentgenol* 2011; **197**: 42-49 [PMID: 21701009 DOI: 10.2214/AJR.11.6632]

27 **Tonolini M**, Villa C, Campari A, Ravelli A, Bianco R, Cornalba G. Common and unusual urogenital Crohn's disease complications: spectrum of cross-sectional imaging findings. *Abdom Imaging* 2013; **38**: 32-41 [PMID: 22456714 DOI: 10.1007/s00261-011-9764-3]

28 **Bruining DH**, Siddiki HA, Fletcher JG, Tremaine WJ, Sandborn WJ, Loftus EV. Prevalence of penetrating disease and extraintestinal manifestations of Crohn's disease detected with CT enterography. *Inflamm Bowel Dis* 2008; **14**: 1701-1706 [PMID: 18623171 DOI: 10.1002/ibd.20529]

29 **Steer S**, Jones H, Hibbert J, Kondeatis E, Vaughan R, Sanderson J, Gibson T. Low back pain, sacroiliitis, and the relationship with HLA-B27 in Crohn's disease. *J Rheumatol* 2003; **30**: 518-522 [PMID: 12610811]

30 **Koronakis N**, Lagoudianakis E, Keramidaris D, Pappas A, Gemenetzis G, Seretis C, Chrysikos J, Manouras A. Mesentery lymphoma in a patient with Crohn's disease: An extremely rare entity. *Int J Surg Case Rep* 2012; **3**: 343-345 [PMID: 22580080 DOI: 10.1016/j.ijscr.2012.04.005]

P- Reviewer Plataniotis G **S- Editor** Huang XZ
L- Editor A **E- Editor** Ma S

World Journal of Radiology

Online Submissions: http://www.wjgnet.com/esps/
wjr@wjgnet.com
doi:10.4329/wjr.v5.i5.202

World J Radiol 2013 May 28; 5(5): 202-207
ISSN 1949-8470 (online)

BRIEF ARTICLE

Correlation analysis of dual-energy CT iodine maps with quantitative pulmonary perfusion MRI

Jan Hansmann, Paul Apfaltrer, Frank G Zoellner, Thomas Henzler, Mathias Meyer, Gerald Weisser, Stefan O Schoenberg, Ulrike I Attenberger

Jan Hansmann, Paul Apfaltrer, Thomas Henzler, Mathias Meyer, Gerald Weisser, Stefan O Schoenberg, Ulrike I Attenberger, Institute of Clinical Radiology and Nuclear Medicine, University Medical Center Mannheim, Medical Faculty Mannheim, Heidelberg University, D-68167 Mannheim, Germany
Frank G Zoellner, Computer Assisted Clinical Medicine, Medical Faculty Mannheim, Heidelberg University, D-68167 Mannheim, Germany
Author contributions: All authors made substantial contributions to the conception and design of the study, drafting or revising the article critically for important intellectual content; Hansmann J, Apfaltrer P, Zoellner FG and Attenberger UI contributed to the data analysis and interpretation.
Correspondence to: Jan Hansmann, MD, Institute of Clinical Radiology and Nuclear Medicine, University Medical Center Mannheim, Medical Faculty Mannheim, University of Heidelberg, Theodor-Kutzer-Ufer 1-3, D-68167 Mannheim, Germany. jan.hansmann@medma.uni-heidelberg.de
Telephone: +49-621-3832067 Fax: +49-621-3833817
Received: January 14, 2013 Revised: May 3, 2013
Accepted: May 16, 2013
Published online: May 28, 2013

Abstract

AIM: To correlate dual-energy computed tomography (DECT) pulmonary angiography derived iodine maps with parameter maps of quantitative pulmonary perfusion magnetic resonance imaging (MRI).

METHODS: Eighteen patients with pulmonary perfusion defects detected on DECT derived iodine maps were included in this prospective study and additionally underwent time-resolved contrast-enhanced pulmonary MRI [dynamic contrast enhanced (DCE)-MRI]. DCE-MRI data were quantitatively analyzed using a pixel-by-pixel deconvolution analysis calculating regional pulmonary blood flow (PBF), pulmonary blood volume (PBV) and mean transit time (MTT) in visually normal lung parenchyma and perfusion defects. Perfusion parameters were correlated to mean attenuation values of normal lung and perfusion defects on DECT iodine maps. Two readers rated the concordance of perfusion defects in a visual analysis using a 5-point Likert-scale (1 = no correlation, 5 = excellent correlation).

RESULTS: In visually normal pulmonary tissue mean DECT and MRI values were: 22.6 ± 8.3 Hounsfield units (HU); PBF: 58.8 ± 36.0 mL/100 mL per minute; PBV: 16.6 ± 8.5 mL; MTT: 17.1 ± 10.3 s. In areas with restricted perfusion mean DECT and MRI values were: 4.0 ± 3.9 HU; PBF: 10.3 ± 5.5 mL/100 mL per minute, PBV: 5 ± 4 mL, MTT: 21.6 ± 14.0 s. The differences between visually normal parenchyma and areas of restricted perfusion were statistically significant for PBF, PBV and DECT ($P < 0.0001$). No linear correlation was found between MRI perfusion parameters and attenuation values of DECT iodine maps (PBF: $r = 0.35$, $P = 0.15$; PBV: $r = 0.34$, $P = 0.16$; MTT: $r = 0.41$, $P = 0.08$). Visual analysis revealed a moderate correlation between perfusion defects on DECT iodine maps and the parameter maps of DCE-MRI (mean score 3.6, κ 0.45).

CONCLUSION: There is a moderate visual but not statistically significant correlation between DECT iodine maps and perfusion parameter maps of DCE-MRI.

Key words: Dual-energy computed tomography; Time-resolved magnetic resonance imaging; Pulmonary perfusion; Iodine maps

Core tip: Dual-energy derived iodine maps and dynamic contrast enhanced magnetic resonance imaging (DCE-MRI) may allow evaluation of pulmonary perfusion. Hypothetical the decrease in pulmonary perfusion detected on DCE-derived iodine maps would correlate highly with perfusion parameters derived from DCE-MRI in patients with restricted pulmonary perfusion.

However, against our hypothesis, we did not find a significant correlation between pulmonary perfusion defects detected on dual-energy computed tomography-derived iodine maps and perfusion parameters derived from time-resolved MRI. In addition, there was only a moderate level of visual correlation. This is in contrast with prior studies that investigated the role of pulmonary iodine maps to serve as an additional tool providing a functional evaluation of pulmonary perfusion.

Hansmann J, Apfaltrer P, Zoellner FG, Henzler T, Meyer M, Weisser G, Schoenberg SO, Attenberger UI. Correlation analysis of dual-energy CT iodine maps with quantitative pulmonary perfusion MRI. *World J Radiol* 2013; 5(5): 202-207 Available from: URL: http://www.wjgnet.com/1949-8470/full/v5/i5/202.htm DOI: http://dx.doi.org/10.4329/wjr.v5.i5.202

INTRODUCTION

Dual-energy computed tomography (DECT) was first introduced in the late 1970s and allows for the differentiation of materials based on their X-ray attenuation at different tube voltages[1]. Different vendors have reintroduced DECT and in recent years the technique has become clinically feasible[2,3]. DECT has been investigated for a variety of organ systems[4-8], however, pulmonary imaging and in particular dual-energy derived iodine maps have been the focus of multiple previous studies[9-12]. Dual-energy derived iodine maps allow the visualization of parenchymal iodine distribution in relation to a previously defined scan delay, which might be considered as a surrogate of pulmonary perfusion and has shown good correlation compared to nuclear medicine based imaging modalities[9,10,13]. Another modality that allows an evaluation of pulmonary perfusion disorders is dynamic contrast enhanced magnetic resonance imaging (DCE-MRI)[14-17]. Multiple pulmonary perfusion parameters can be derived from DCE-MRI by means of post-processing, including pulmonary blood flow (PBF), pulmonary blood volume (PBV) and mean transit time (MTT). To our knowledge, no prior study correlated the perfusion changes shown in time resolved perfusion imaging modalities such as DCE-MRI to the perfusion changes displayed in DECT-derived iodine maps. We hypothesized that a decrease in pulmonary perfusion detected on DECT-derived iodine maps would correlate highly with perfusion parameters derived from DCE-MRI in patients with restricted pulmonary perfusion regardless of the underlying cause of pulmonary perfusion restriction.

MATERIALS AND METHODS

Patients

This monocentric, prospective, non-randomized study was approved by our institutional review board. The nature of our study was explained entirely to all patients prior to enrollment and written informed consent was obtained from all participants. Eighteen consecutive patients (11 men and 7 women, mean age 61 years, range 20-81 years) were prospectively enrolled in our study. The inclusion criterion was a perfusion defect detected on iodine maps derived from DECT pulmonary angiography (DE-CTPA). Exclusion criteria were renal insufficiency defined as a serum creatinine level > 1.5 mg/d, hemodynamic instability or general contraindications to MRI. Pulmonary perfusion deficits were due to a number of underlying pathology, including pulmonary embolism (n = 8), severe emphysema (n = 5) and postobstructive perfusion defects due to lung cancer (n = 5).

Dual energy computed tomography

All examinations were performed on a 64-channel first generation dual-source computed tomography (CT) scanner (Somatom Definition, Siemens Health Care, Forchheim, Germany). The system is equipped with two X-ray tubes and two corresponding detectors mounted in a 90 degree angle to each other in the gantry. One detector array (corresponding to tube A) provides a field of view of 50 cm, while the other detector array (corresponding to tube B) is limited to field of view of 26 cm. Tube voltages for tube A were set to 140 kV and to 80 kV for tube B. To compensate for the lower photon output of tube B, the quality reference tube current was set to 235 mAs for tube B and 50 mAs for tube A. Tube rotation time was 0.33 s. Automatic tube current modulation (CARE Dose 4D, Siemens Health Care Sector, Forchheim, Germany) was used in all patients. According to the manufacturer's recommendations, the detector collimation was set to 14 mm × 1.2 mm to minimize beam-hardening artefacts and improve signal-to-noise ratio. A separate dataset for each tube kV as well as a linearly weighted average dataset ("virtual 120 kV", using 70% tube A and 30% tube B) was calculated with a slice thickness of 2 mm and a reconstruction increment of 1.5 mm using a soft tissue kernel (D30f). All scans were performed in caudocranial direction during a midinspiratory breath-hold.

Contrast material was injected using 18 or 20 G intravenous catheters placed in the left or right antecubital vein using an automated power injector (Stellant D CT Injection System MEDRAD Inc, Warrendale, PA) and utilizing a bolus tracking technique, in which the scan was started with a 10 s delay after a threshold of 100 Hounsfield units (HU) was reached in the pulmonary trunk. Injection rate was 3.5 mL/s. All contrast injections were followed by an additional saline (NaCl) flush of 50 mL, injected at the same rate used for the previous contrast agent injection.

MRI

All pulmonary time resolved magnetic resonance angiography (MRA) exams were performed on a 3.0 Tesla 128 channel MR system (Magnetom Skyra, Siemens AG, Healthcare Sector, Erlangen, Germany). For signal reception, a body matrix coil with 18 elements as well as 18 elements of the inbuilt spine matrix were used. First, 2D gradient echo localizers and a coronal T_2-weighted

half acquisition turbo spin echo sequence were applied to ensure correct preparation of the MRA exam. Time resolved MRA was applied using a 3D time resolved angiography with interleaved stochastic trajectories pulse sequence, which combines parallel imaging with view-sharing to decrease the acquisition time. In detail, the following imaging parameters were used: echo time = 0.8 ms, repetition time = 2.2 ms, bandwidth = 815 Mhz/px, generalized autocalibrating partially parallel acquisition = 2, field of view = 375 × 500, voxel size = 2.0 × 2.0 × 5.0 mm^3, acquisition time was 58 s. Patients were asked to hold their breath in mid inspiratory breathhold as long as possible and to continue shallow breathing until completion of the sequence. Eighteen or 20 G access was obtained in the left or right antecubital fossa. An automated power injector (Medrad Spectris Solaris EP, Medrad Indianola, PA) was used for the injection of the contrast agent. A dose of 0.07 mmol/kg per body weight of gadoterate meglumine (Dotarem, Guerbet, France) was used. The injection rate of the contrast material was 3.0 mL/s followed by a 20 mL chaser of saline (NaCl), injected at the same rate.

Data analysis

Iodine maps were generated on a commercially available workstation (Leonardo, Siemens Healthcare) using the commercially available Syngo Pulmonary Blood Volume software (Syngo VA 21, Siemens Health Care Sector, Forchheim, Germany). After loading both 80-kV and 140-kV images into the software, the iodine content of each voxel is derived through a three-material-decomposition algorithm for air, soft tissue, and iodine. Multiplanar reformations for iodine maps were generated using a slice thickness of 2 mm, with a 1.5 mm increment.

MRA data were quantitatively analyzed using a pixel-by-pixel deconvolution analysis using an in-house developed software plugin, integrated into a standard digital imaging and communications in medicine viewer (the OsiriX Foundation, Geneva, Switzerland). The underlying algorithm is a modification of the highly successful truncated singular value decomposition algorithm with a fixed regularization parameter, as first proposed for DCE-MRI by Ostergaard *et al*[18]. To allow for perfusion analysis of T1-weighted DCE-MRI, the conversion of signal to concentration is modified and the convolution product is discretised using the Volterra formula as proposed by Sourbron *et al*[19,20]. Using an in-house test suite of artificial data demonstrated that the plug-in can produce similar values as a published and widely used reference implementation in PMI 0.4[19,20]. Here, on average the difference on pixel basis for the parameters plasma flow (in units of mL/100 mL per minute), volume of distribution (in units of mL/100 mL), and MTT (in units of second) was less than 0.05.

Image evaluation

Parenchymal attenuation was measured in perfusion defects and visually normal parenchyma on DECT-derived iodine maps using the previously described Pulmonary Blood Volume software (Syngo VA 21, Siemens Health Care Sector, Forchheim, Germany). Three region of interests (ROIs) were placed on consecutive slices in areas of restricted perfusion. Three ROIs were placed on consecutive slices in visually normal parenchyma of the same lung (*i.e.*, right or left). Care was taken to exclude pulmonary vessels in order to avoid artifacts. The mean "overlay value" of the ROIs was noted which represents the pure dual-energy calculated iodine distribution within the parenchyma. The mean value as well as the standard deviation of the three measurements were calculated. ROI size was not standardized between patients due to the different size of perfusion defects encountered but was identical between areas of restricted perfusion and normal parenchyma.

ROIs corresponding to the location of the ROIs placed for DECT iodine maps were placed in the areas of restricted perfusion as well as normal parenchyma on MRI parameter maps. Again, three consecutive slices were chosen and the mean regional PBF, PBV and MTT were averaged from the ROI measurements. Perfusion parameters were correlated to mean attenuation values measured in perfusion defects and normal parenchyma in DECT-derived iodine maps using Pearsons's correlation analysis.

In addition, two readers both with more than 10 years of experience in thoracic imaging rated the correlation of perfusion defects between the two modalities in a visual analysis using a 5-point Likert scale (1 = no correlation, 2 = poor correlation, 3 = fair correlation, 4 = good correlation, 5 = excellent correlation). The correlation between modalities was first assessed by each reader individually before a consensus was established for each patient. Readers were blinded to the patients' history and diagnosis. Figure 1 provides an example of the perfusion deficits observed in this study. Inter-reader correlation was assessed using kappa statistics.

Statistical analysis

Statistical analysis was performed using JMP 9.0 (SAS Institute, Cary, NC, United States). Continuous variables are expressed as mean ± SD. The Shapiro-Wilk test was applied to determine probability distribution; a two-tailed Student's *t*-test was subsequently used to compare groups with normal distribution, while the Mann-Whitney-*U*-test was used if the data were not normally distributed. The χ^2 test was applied for dichotomous variables. Pearson's correlation was used to correlate perfusion defects detected on DECT-derived iodine maps with to the corresponding PBF, PBV and MTT. A 2-tailed *P*-value of < 0.05 was considered statistically significant.

RESULTS

Mean time delay between DECT and DCE-MRI was 2.6 d (range 0-12 d). In acute pulmonary perfusion disorders (*e.g.*, pulmonary embolism) the mean time between examinations was 22 h (range 4-48 h). In 14 of 18 patients undergoing DECT up to 3.4 cm of the peripheral lung

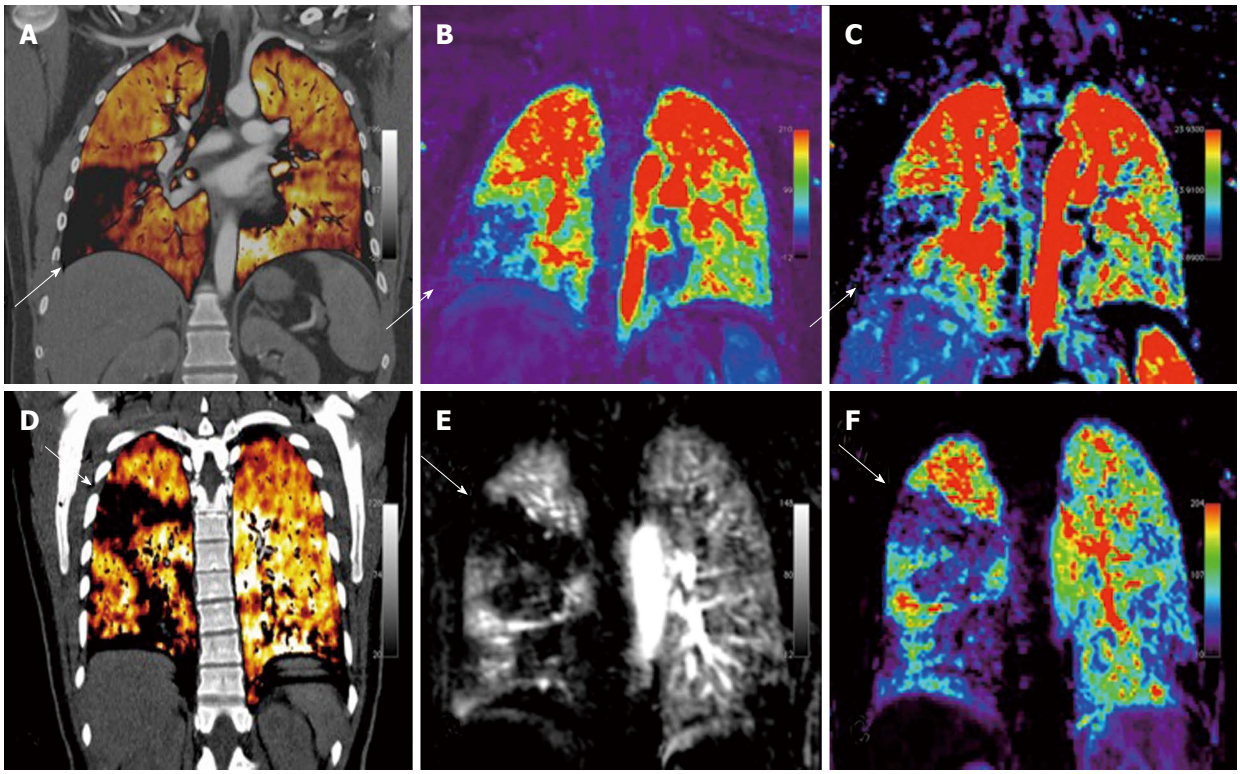

Figure 1 Correlation of perfusion deficits in a 20-year-old male and 42-year-old female male with pulmonary embolism (arrows pointing to perfusion defects). A, D: Dual-energy computed tomography derived iodine map; B, E: Pulmonary blood flow; C, F: Pulmonary blood volume.

Table 1 Mean dynamic contrast enhanced-magnetic resonance imaging and dual-energy computed tomography values and SD in visually normal pulmonary parenchyma and areas with restricted perfusion

	Visually normal parenchyma	Perfusion defect	*P* value
PBF (mL/100 mL per minute)	58.8 ± 36	10.3 ± 5.5	< 0.0001
PBV (mL)	16.6 ± 8.5	5.0 ± 4.0	< 0.0001
MTT (s)	17.1 ± 10.3	21.6 ± 14	0.28
Lodine map (HU)	22.6 ± 8.3	4.0 ± 3.9	< 0.0001

The attenuation given for the Iodine Map represents the pure dual-energy calculated iodine distribution within the pulmonary parenchyma. PBF: Pulmonary blood flow; PBV: Pulmonary blood volume; MTT: Mean transit time; HU: Hounsfield units.

parenchyma was not covered due to the reduced field of view of the second detector of the first generation dual-source CT, thus not allowing for perfusion analysis in these areas.

Mean attenuation values in DE derived iodine maps were significantly lower in perfusion defects compared to normal parenchyma [4 HU (SD ± 3.9) *vs* 22.6 HU (SD ± 8.3), $P < 0.0001$]. The mean values of the quantitative perfusion parameters in the correlating perfusion defects detected on DCE-MRA were 10.3 mL/100 mL per minute (SD ± 5.5) for PBF, 5 mL (SD ± 4) for PBV and 21.6 s (SD ± 14) for MTT. In visually normal pulmonary tissue mean PBF values were 58.8 mL/ 100 mL per minute (SD ± 36), mean PBV was 16.6 mL (SD ± 8.5) and mean MTT was 17.1 s (SD ± 10.3). Statistically significant differences were observed between PBF and PBV measurements in perfusion defects compared to healthy pulmonary parenchyma with a *P* value of < 0.0001. No statistically significant difference was found for MTT measured in perfusion defects compared to healthy pulmonary parenchyma ($P = 0.28$). Table 1 summarizes the findings.

Pearson correlation showed no correlation between perfusion defects measured on DECT-derived iodine maps and PBF, PBV or MTT measured in the corresponding perfusion defects on DCE-MRI (PBF: $r = 0.35$, $P = 0.15$; PBV: $r = 0.34$, $P = 0.16$; MTT: $r = 0.41$, $P = 0.08$).

The visual analysis showed a moderate correlation between the two modalities, with a median score of 3.8 (SD ± 0.8) for reader 1 and 3.6 (SD ± 0.9) for reader 2. The consensus read revealed a median score of 3.6 (SD ± 0.9) for both readers. Interreader agreement was moderate with a kappa of 0.45 ($P = 0.02$).

DISCUSSION

Our results did not show a significant correlation between pulmonary perfusion defects detected on DECT-derived iodine maps and perfusion parameters derived from time-resolved MRI. In addition, there was only a moderate level of visual correlation. This is in contrast with prior studies that investigated the role of pulmonary iodine maps to serve as an additional tool providing a functional evaluation of pulmonary perfusion. Thieme *et al*[9,10] found a sensitivity/specificity of 100% and 100% of DE-CTPA for the diagnosis of acute pulmonary per-

fusion deficits compared to SPECT/CT and a per segment sensitivity/specificity of 83%/99% with a negative predictive value of 93% for DECT when correlated with pulmonary scintigraphy. In acute pulmonary perfusion disorders such as pulmonary embolism, perfusion defects detected on iodine maps have shown good correlation with morphologic CTPA data[13,21-26]. In pulmonary embolism iodine maps add a further diagnostic criterion whether or not a perfusion defect is present, since small subsegmental pulmonary emboli are sometimes challenging to detect on standard CTPA-images. Perfusion defects caused by these small emboli can be detected on iodine maps, thus possibly raising the detection rate of small, subsegmental pulmonary emboli and at the same time allowing for an assessment of the perfusion deficit associated with the detected embolus. The fact that we did not observe a strong correlation between the two modalities investigated in our study might be related to the broad inclusion criteria for our study since we included patients with a variety of underlying pulmonary pathology including lung cancer, emphysema and acute perfusion disorders such as pulmonary embolism. In addition, only a small number of patients were included in this study, and therefore our results should be viewed as preliminary. Certainly further studies including a larger number of patients and focusing on one disease entity (*e.g.*, pulmonary embolism) seem warranted. Despite the potential advantage of DECT-derived iodine maps, applying them to pulmonary imaging is not without pitfalls. Iodine maps are prone to artifacts due to hyperdense contrast material especially in the inflow tract of the upper thoracic vasculature[12]. Therefore, iodine perfusion maps should not be used as a standalone tool but should only be used in conjunction with standard morphological CTPA data. Generation of iodine maps on a standard workstation is not a time consuming task and can be easily integrated alongside standard reconstructions already used in a routine setting. Radiation dose for DECT has been reported to be within the range of 2-6 mSv and is thus comparable to standard MDCT.

Limitations

Several limitations exist for our study: As this was an initial study only a small sample size of 18 patients was included. A well known limitation of first-generation DE scanners is the 26 cm detector width of the second detector, thus not allowing for the lung periphery in larger patients to be included in the calculations of iodine maps. This problem has been addressed with second-generation scanners. Dual-energy derived iodine maps are prone to artifacts due to beam-hardening from hyperdense contrast material especially in the superior vena cava and the right heart. Nance *et al*[12] found these artifacts to be present in 97% of iodine maps in of a sample of 100 patients. These artifacts have the potential to obscure true perfusion defects or to cause false-positive results. This prevents iodine maps from being used as the sole means to detect pulmonary perfusion disorders and make it mandatory to correlate findings to standard CTPA images. There was a time delay between image acquisition in both modalities, however, in acute pulmonary perfusion disorders such as pulmonary embolism the mean time between DECT and MRI was 24 h with a maximum delay of 48 h in one patient.

Our findings show that perfusion deficits detected on static dual-energy derived iodine maps show a moderate visual correlation with time-resolved DCE-MRI, thus allowing for an assessment of pulmonary perfusion changes as related to a variety of pathology. However, there was no statistically significant correlation between the two modalities, and therefore a prospective study focusing on one entity of pulmonary perfusion disorders (*e.g.*, pulmonary embolism) seems warranted.

COMMENTS

Background

Both, dual-energy computed tomography (DECT) and dynamic contrast enhanced magnetic resonance imaging (DCE-MRI) have been applied for evaluation of pulmonary perfusion. Dual-energy derived iodine maps allow the visualization of parenchymal iodine distribution in relation to a previously defined scan delay, which might be considered as a surrogate of pulmonary perfusion and has shown good correlation compared to nuclear medicine based imaging modalities. However, no prior study correlated the perfusion changes shown in time resolved perfusion imaging modalities such as DCE-MRI to the perfusion changes displayed in DECT-derived iodine maps.

Research frontiers

Time resolved perfusion-imaging modalities such as DCE-MRI and dual-source DECT.

Innovations and breakthroughs

Authors' study shows that perfusion deficits detected on static dual-energy derived iodine maps show a moderate visual correlation with time-resolved DCE-MRI, thus allowing for an assessment of pulmonary perfusion changes as related to a variety of pathology. This is in contrast with prior studies that investigated the role of pulmonary iodine maps to serve as an additional tool providing a functional evaluation of pulmonary perfusion.

Applications

Both, DECT and DCE-MRI should be applied pulmonary embolism imaging. However, the authors think that the results of this study should be viewed as preliminary as only a small number of patients were included and broad inclusion criteria including patients with a variety of underlying pulmonary pathology were applied

Peer review

The authors investigated whether there is correlation between DECT derived iodine maps and parameter maps of quantitative pulmonary perfusion MRI. This is a well-written manuscript, which should be suitable for publication.

REFERENCES

1 **Chiro GD**, Brooks RA, Kessler RM, Johnston GS, Jones AE, Herdt JR, Sheridan WT. Tissue signatures with dual-energy computed tomography. *Radiology* 1979; **131**: 521-523 [PMID: 441344]

2 **Flohr TG**, McCollough CH, Bruder H, Petersilka M, Gruber K, Süss C, Grasruck M, Stierstorfer K, Krauss B, Raupach R, Primak AN, Küttner A, Achenbach S, Becker C, Kopp A, Ohnesorge BM. First performance evaluation of a dual-source CT (DSCT) system. *Eur Radiol* 2006; **16**: 256-268 [PMID: 16341833 DOI: 10.1007/s00330-005-2919-2]

3 **Johnson TR**, Krauss B, Sedlmair M, Grasruck M, Bruder H, Morhard D, Fink C, Weckbach S, Lenhard M, Schmidt B, Flohr T, Reiser MF, Becker CR. Material differentiation by dual energy CT: initial experience. *Eur Radiol* 2007; **17**: 1510-1517 [PMID: 17151859 DOI: 10.1007/s00330-006-0517-6]

4 **Apfaltrer P**, Meyer M, Meier C, Henzler T, Barraza JM, Dint-

er DJ, Hohenberger P, Schoepf UJ, Schoenberg SO, Fink C. Contrast-enhanced dual-energy CT of gastrointestinal stromal tumors: is iodine-related attenuation a potential indicator of tumor response? *Invest Radiol* 2012; **47**: 65-70 [PMID: 21934517 DOI: 10.1097/RLI.0b013e31823003d2]

5 **Ascenti G**, Mazziotti S, Lamberto S, Bottari A, Caloggero S, Racchiusa S, Mileto A, Scribano E. Dual-energy CT for detection of endoleaks after endovascular abdominal aneurysm repair: usefulness of colored iodine overlay. *AJR Am J Roentgenol* 2011; **196**: 1408-1414 [PMID: 21606306 DOI: 10.2214/AJR.10.4505]

6 **Gnannt R**, Fischer M, Goetti R, Karlo C, Leschka S, Alkadhi H. Dual-energy CT for characterization of the incidental adrenal mass: preliminary observations. *AJR Am J Roentgenol* 2012; **198**: 138-144 [PMID: 22194489 DOI: 10.2214/AJR.11.6957]

7 **Guggenberger R**, Gnannt R, Hodler J, Krauss B, Wanner GA, Csuka E, Payne B, Frauenfelder T, Andreisek G, Alkadhi H. Diagnostic performance of dual-energy CT for the detection of traumatic bone marrow lesions in the ankle: comparison with MR imaging. *Radiology* 2012; **264**: 164-173 [PMID: 22570505]

8 **Kim JE**, Lee JM, Baek JH, Han JK, Choi BI. Initial assessment of dual-energy CT in patients with gallstones or bile duct stones: can virtual nonenhanced images replace true nonenhanced images? *AJR Am J Roentgenol* 2012; **198**: 817-824 [PMID: 22451546 DOI: 10.2214/AJR.11.6972]

9 **Thieme SF**, Becker CR, Hacker M, Nikolaou K, Reiser MF, Johnson TR. Dual energy CT for the assessment of lung perfusion--correlation to scintigraphy. *Eur J Radiol* 2008; **68**: 369-374 [PMID: 18775618 DOI: 10.1016/j.ejrad.2008.07.031]

10 **Thieme SF**, Graute V, Nikolaou K, Maxien D, Reiser MF, Hacker M, Johnson TR. Dual Energy CT lung perfusion imaging--correlation with SPECT/CT. *Eur J Radiol* 2012; **81**: 360-365 [PMID: 21185141]

11 **Thieme SF**, Johnson TR, Lee C, McWilliams J, Becker CR, Reiser MF, Nikolaou K. Dual-energy CT for the assessment of contrast material distribution in the pulmonary parenchyma. *AJR Am J Roentgenol* 2009; **193**: 144-149 [PMID: 19542406 DOI: 10.2214/AJR.08.1653]

12 **Nance JW**, Henzler T, Meyer M, Apfaltrer P, Braunagel M, Krissak R, Schoepf UJ, Schoenberg SO, Fink C. Optimization of contrast material delivery for dual-energy computed tomography pulmonary angiography in patients with suspected pulmonary embolism. *Invest Radiol* 2012; **47**: 78-84 [PMID: 21577132]

13 **Hoey ET**, Gopalan D, Screaton NJ. Dual-energy CT pulmonary angiography: A new horizon in the imaging of acute pulmonary thromboembolism. *AJR Am J Roentgenol* 2009; **192**: W341-W32; author reply W343 [PMID: 19457800]

14 **Fink C**, Ley S, Puderbach M, Plathow C, Bock M, Kauczor HU. 3D pulmonary perfusion MRI and MR angiography of pulmonary embolism in pigs after a single injection of a blood pool MR contrast agent. *Eur Radiol* 2004; **14**: 1291-1296 [PMID: 14997336 DOI: 10.1007/s00330-004-2282-8]

15 **Fink C**, Puderbach M, Ley S, Plathow C, Bock M, Zuna I, Kauczor HU. Contrast-enhanced three-dimensional pulmonary perfusion magnetic resonance imaging: intraindividual comparison of 1.0 M gadobutrol and 0.5 M Gd-DTPA at three dose levels. *Invest Radiol* 2004; **39**: 143-148 [PMID: 15076006 DOI: 10.1097/01.rli.0000101482.79137.f4]

16 **Kuder TA**, Risse F, Eichinger M, Ley S, Puderbach M, Kauczor HU, Fink C. New method for 3D parametric visualization of contrast-enhanced pulmonary perfusion MRI data. *Eur Radiol* 2008; **18**: 291-297 [PMID: 17705043 DOI: 10.1007/s00330-007-0742-7]

17 **Nael K**, Fenchel M, Krishnam M, Finn JP, Laub G, Ruehm SG. 3.0 Tesla high spatial resolution contrast-enhanced magnetic resonance angiography (CE-MRA) of the pulmonary circulation: initial experience with a 32-channel phased array coil using a high relaxivity contrast agent. *Invest Radiol* 2007; **42**: 392-398 [PMID: 17507810 DOI: 10.1097/01.rli.0000261937.77365.6a]

18 **Ostergaard L**, Weisskoff RM, Chesler DA, Gyldensted C, Rosen BR. High resolution measurement of cerebral blood flow using intravascular tracer bolus passages. Part I: Mathematical approach and statistical analysis. *Magn Reson Med* 1996; **36:** 715-725 [PMID: 8916022]

19 **Sourbron S,** Dujardin M, Makkat S, Luypaert R. Pixel-by-pixel deconvolution of bolus-tracking data: optimization and implementation. *Phys Med Biol* 2007; **52:** 429-447 [PMID: 17202625]

20 **Sourbron S,** Luypaert R, Morhard D, Seelos K, Reiser M, Peller M. Deconvolution of bolus-tracking data: a comparison of discretization methods. *Phys Med Biol* 2007; **52:** 6761-6778 [PMID: 17975296]

21 **Geyer LL**, Scherr M, Körner M, Wirth S, Deak P, Reiser MF, Linsenmaier U. Imaging of acute pulmonary embolism using a dual energy CT system with rapid kVp switching: initial results. *Eur J Radiol* 2012; **81**: 3711-3718 [PMID: 21420812]

22 **Fink C**, Johnson TR, Michaely HJ, Morhard D, Becker C, Reiser M, Nikolaou K. Dual-energy CT angiography of the lung in patients with suspected pulmonary embolism: initial results. *Rofo* 2008; **180**: 879-883 [PMID: 19238637]

23 **Pontana F**, Faivre JB, Remy-Jardin M, Flohr T, Schmidt B, Tacelli N, Pansini V, Remy J. Lung perfusion with dual-energy multidetector-row CT (MDCT): feasibility for the evaluation of acute pulmonary embolism in 117 consecutive patients. *Acad Radiol* 2008; **15**: 1494-1504 [PMID: 19000866 DOI: 10.1016/j.acra.2008.05.018]

24 **Hoey ET**, Mirsadraee S, Pepke-Zaba J, Jenkins DP, Gopalan D, Screaton NJ. Dual-energy CT angiography for assessment of regional pulmonary perfusion in patients with chronic thromboembolic pulmonary hypertension: initial experience. *AJR Am J Roentgenol* 2011; **196**: 524-532 [PMID: 21343493 DOI: 10.2214/AJR.10.4842]

25 **Fink C**, Risse F, Buhmann R, Ley S, Meyer FJ, Plathow C, Puderbach M, Kauczor HU. Quantitative analysis of pulmonary perfusion using time-resolved parallel 3D MRI - initial results. *Rofo* 2004; **176**: 170-174 [PMID: 14872369 DOI: 10.1055/s-2004-817624]

26 **Ingrisch M**, Dietrich O, Attenberger UI, Nikolaou K, Sourbron S, Reiser MF, Fink C. Quantitative pulmonary perfusion magnetic resonance imaging: influence of temporal resolution and signal-to-noise ratio. *Invest Radiol* 2010; **45**: 7-14 [PMID: 19996761 DOI: 10.1097/RLI.0b013e3181bc2d0c]

P- Reviewer Ma LS **S- Editor** Wen LL
L- Editor A **E- Editor** Xiong L

World Journal of Radiology

Online Submissions: http://www.wjgnet.com/esps/
wjr@wjgnet.com
doi:10.4329/wjr.v5.i5.208

World J Radiol 2013 May 28; 5(5): 208-214
ISSN 1949-8470 (online)

BRIEF ARTICLE

Chronic hepatitis B: Enlarged perihepatic lymph nodes correlated with hepatic histopathology

Jian Shu, Jian-Nong Zhao, Fu-Gang Han, Guang-Cai Tang, Yin-Deng Luo, Li Luo, Xin Chen

Jian Shu, Fu-Gang Han, Guang-Cai Tang, Li Luo, Xin Chen, Department of Radiology, Affiliated Hospital of Luzhou Medical College, Luzhou 646000, Sichuan Province, China
Jian-Nong Zhao, Yin-Deng Luo, Department of Radiology, Second Affiliated Hospital of Chongqing Medical University, Chongqing 400010, China
Author contributions: Shu J performed the majority of procedures and wrote the manuscript; Zhao JN was involved in conception and design for the manuscript; Han FG and Tang GC edited the manuscript; Luo YD, Luo L and Chen X contributed to data analysis and interpretation.
Correspondence to: Jian Shu, MD, Department of Radiology, Affiliated Hospital of Luzhou Medical College, 319 Zhongshan Road, Luzhou 646000, Sichuan Province, China. shujiannc@163.com
Telephone: +86-830-3165738 Fax: +86-830-3165738
Received: January 7, 2013 Revised: April 23, 2013
Accepted: May 9, 2013
Published online: May 28, 2013

Abstract

AIM: To assess the value of enlarged perihepatic lymph nodes in determining hepatic histopathology for chronic hepatitis B (CHB) by magnetic resonance imaging (MRI).

METHODS: Sixty-seven patients who were clinically and histologically diagnosed with CHB and 18 healthy subjects without history of liver disease underwent abdominal MRI. Histological diagnosis and hepatic inflammation (grade 0-4) and fibrosis (stage 0-4) were assessed by a simplified system for scoring in chronic viral hepatitis. The major imaging protocol included an axial breath-hold fat suppressed fast spoiled gradient echo T_2-weighted imaging (T_2WI), axial breath-trigger fat suppressed fast recovery fast spin echo T_2WI, and axial and coronal fast imaging employing steady-state acquisition. Perihepatic lymph nodes larger than 5 mm in shortest diameter were noted.

RESULTS: The numbers and size indexes of lymph nodes greater than 5 mm in shortest diameter in hepatic hilum suggested inflammatory activity for subjects with grade 2 or higher, with a high accuracy of diagnosis (the area under the curves > 0.9, $P < 0.001$). The numbers of lymph nodes were 2 or more with a sensitivity of 87.27%, a specificity of 90.00%, an accuracy of 88.24%, a positive predictive value of 94.12%, and a negative predictive value of 79.41% in patients with grade 2 or higher, and the size indexes were no less than 180 mm^2 with a sensitivity of 83.64%, a specificity of 100%, an accuracy of 89.41%, a positive predictive value of 100%, and a negative predictive value of 76.92%. The numbers and size indexes of lymph nodes were not correlated with hepatic fibrosis. The signal intensity indexes of lymph nodes were no significant correlation with histological grading or staging of liver.

CONCLUSION: The numbers and size indexes of enlarged perihepatic lymph nodes for patients with CHB suggest inflammatory activity for subjects with grade 2 or higher.

Key words: Chronic hepatitis B; Magnetic resonance imaging; Lymph nodes; Histopathology; Inflammatory activity

Core tip: Chronic hepatitis B (CHB) is frequently associated with hyperplasia of lymph nodes in the hepatic hilum, and the enlarged lymph nodes can be a good indicator for inflammatory activity of the liver. Enlarged perihepatic lymph nodes for the patients with CHB can be sensitively demonstrated by magnetic resonance imaging, especially fat suppressed T_2-weighted imaging. The numbers and size indexes of lymph nodes larger than 5 mm in shortest diameter suggest inflammatory activity for subjects with grade 2 or higher, with a high accuracy of diagnosis at a cutoff value of 2 for the numbers or 180 mm^2 for the size indexes of lymph nodes.

Shu J, Zhao JN, Han FG, Tang GC, Luo YD, Luo L, Chen X. Chronic hepatitis B: Enlarged perihepatic lymph nodes correlated with hepatic histopathology. *World J Radiol* 2013; 5(5): 208-214 Available from: URL: http://www.wjgnet.com/1949-8470/full/v5/i5/208.htm DOI: http://dx.doi.org/10.4329/wjr.v5.i5.208

INTRODUCTION

Hepatitis B virus (HBV) is one of the most common causes of chronic hepatitis, and infected individuals are at an increased risk of developing cirrhosis, liver failure, and hepatocellular carcinoma (HCC)[1-3]. Several effective medications are available to inhibit HBV replication with liver fibrosis regression by reducing liver inflammation and cellular damage in most patients with chronic hepatitis B (CHB)[3-5]. These include injectable interferon and the oral nucleoside analogues: adefovir, lamivudine, and tenofovir[2,4,6]. So, the assessment of liver necroinflammatory activity (grading) and fibrosis (staging) for patients with CHB is helpful for determining prognosis and treatment strategy[4,7]. Liver biopsy is the gold standard for the assessment of liver histology for patients with CHB. However, it is more invasive, and often more expensive, than modern imaging methods, such as sonography, computed tomography (CT), or magnetic resonance imaging (MRI).

CHB is frequently associated with hyperplasia of lymph nodes in the hepatic hilum for patients with CHB[8-10], and enlarged lymph nodes can be a good indicator of inflammatory activity by the liver in CHB[9,10]. Sonography is frequently used to evaluate lymph nodes in the hepatic hilum for the patients with CHB and chronic hepatitis C (CHC)[8-12]. MRI can not only show the anatomy of the liver and pancreas clearly but can also depict enlarged perihepatic lymph nodes and their locations relative to adjacent bile ducts or vascular structures[13-15]. MRI can provide better contrast between the lymph nodes and adjacent tissue than does sonography or CT, and is superior to sonography for visualizing enlarged lymph nodes in the porta hepatis[13-16]. In patients with chronic hepatitis, MRI is usually performed to detect the presence of cirrhosis or HCC. In addition to the MRI features that may be present in acute hepatitis, focal inflammatory activity or fibrosis may develop in chronic hepatitis, resulting in diffuse or regional high signal intensity (SI) on T_2-weighted images (T_2WI) and early patchy enhancement or late linear enhancement on gadolinium-enhanced dynamic magnetic resonance images[17,18]. The magnetic resonance appearance of perihepatic lymph nodes in patients with CHC has been reported[14,15]. However, to our knowledge, there are no previous studies using MRI that reveal the significance of lymph nodes in the porta hepatis for patients with CHB.

The purposes of this study were to assess the value of enlarged perihepatic lymph nodes in determining the histopathology of CHB by magnetic resonance fat suppressed T_2WI.

MATERIALS AND METHODS

Patients

This study was conducted in accordance with the guidelines of the review board of our institution. Between January 2005 and July 2010, all consecutive inpatients at our medical center with chronic HBV infection who had undergone an abdominal magnetic resonance examination before antiviral treatment were selected retrospectively. In patients with CHB, MRI was usually performed to detect the presence of cirrhosis or HCC. The selection criteria for patients were a diagnosis of CHB with available pathology reports from the biopsy and clinical evaluation including positive serumal hepatitis B surface antigen for at least 6 mo. Patients with hepatic malignant neoplastic diseases such as HCC, or with other diseases of the liver and gallbladder such as cholecystitis, hepatic abscess and cholangitis, or with other hepatitis such as alcoholic hepatitis, viral hepatitis except hepatitis B and autoimmune hepatitis, or with systemic or abdominal diseases inducing hyperplasia of lymph nodes in the hepatic hilum such as lymphoma, abdominal tuberculosis and malignant neoplasm, were excluded following appropriate clinical, laboratory, and radiological investigations.

Finally, a total of 67 patients met the criteria for inclusion in this study. As controls, 18 subjects were recruited without liver biopsy, selected randomly from 45 healthy volunteers without abdominal disease on magnetic resonance images by a random digits table. In addition to the exclusion criteria mentioned above, the controls were normal for liver function tests and negative for hepatitis B surface antigen. All of the patients and controls were negative for anti-human immunodeficiency virus antibody.

Liver pathology

Experienced hepatologists performed percutaneous liver biopsies in the right lobe of the liver with sonographic guidance using an 18-gauge spring-loaded biopsy device. All core biopsy samples with common 1.5 cm length were obtained within 3 d after the MRI examination and examined by the same pathologist, who was unaware of the clinical, biochemical and imaging data. Histological diagnosis, hepatic inflammation (grade 0-4) and fibrosis (stage 0-4) were assessed by a simplified system for scoring in chronic viral hepatitis according to Scheuer (1991)[19,20].

MRI technique

All magnetic resonance examinations were performed on a 1.5 T MRI scanner (Signa, GE Healthcare, United States) with 38 mT/m gradient subsystems and 120 T/m/s gradient switch rates using a phased-array torso coil. The imaging protocols mainly included an axial breath-hold fat suppressed fast spoiled gradient echo, T_1-weighted imaging, axial breath-trigger fat suppressed fast recovery fast spin echo (FRFSE) T_2WI, and axial and coronal fast imaging employing steady-state acquisition. Forty-one of the 67 patients underwent triple-phase dynamic MRI with liver acquisition in a volume acceleration

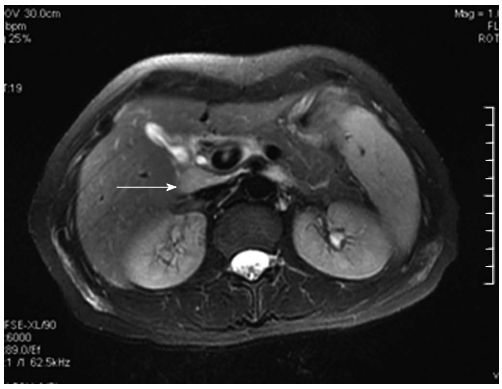

Figure 1 Enlarged lymph node (arrow) in the hepatic hilum in the patients with chronic hepatitis B on magnetic resonance fat suppressed T2-weighted imaging.

sequence. Among the various sequences included in clinical examinations, only the FRFSE T2WI were reviewed for the purpose of this study with the following parameters: repetition time = 6000 ms, echo time = 89 ms, echo train length = 19, bandwidth = 62.5 kHz, matrix = 320 × 224, number of excitations = 2, section thickness = 8 mm, gap = 1 mm.

Imaging analysis

The original data were transferred to the workstation (Advanced Workstation 4.3, GE Healthcare) with 0.1 mm accuracy for distance and 0.01 for SI. All reviews and measurement of images were carried out on the workstation by two experienced radiologists blinded to clinical and pathologic findings with consensus opinions comparing each observation item and standard together.

Perihepatic lymph nodes greater than 5 mm in shortest diameter were counted[14,21], and the long and short axis diameters of each node were measured using electronic calipers on magnified fat suppressed FRFSE T2WI. The size of the lymph nodes were defined as an index, obtained as the product of the long and short axes. A size index of lymph nodes for each patient was recorded as the sum of the diameter products of all nodes (nodal numbers were less than or equal to 3) or the three largest nodes when there were more than three nodes[14,21]. The SI of these lymph nodes was measured for each patient and expressed as ratios relative to spleen on fat suppressed FRFSE T2WI[21]. A SI index of lymph nodes for each patient was recorded as the mean of all the ratios. The SI for each lymph node was measured in a circular region of interest with range in area from 10 to 30 mm^2. The spleen region of interest, ranging in area from 200 to 500 mm^2, was placed in the same or adjacent magnetic resonance section as the corresponding lymph node to avoid artifacts, spleen vessels, and heterogeneous areas. Each diameter or SI was measured three times, and the average of the three measurements was considered true measurements.

Statistical analysis

Quantitative data are presented as mean ± SD. The differences for multi-group quantitative data were analyzed for variance at a P value ≤ 0.05 level of significance, and for two groups by the independent-samples t test when the distribution of data was normal. When the distribution of data was not normal or there was homogeneity of variances, a nonparametric test was used, the differences for multi-group quantitative data were analyzed with the Kruskall-Wallis test, and the comparisons for two groups were assessed using the Mann-Whitney U test. In qualitative data, the comparisons among groups were assessed using χ^2 test or Fischer's exact test.

Because the size or SI indexes of the lymph nodes could simultaneously correlate with the grade and stage of liver histology, partial correlation was used to test the relationship between the nodal size indexes and the grade or stage, or between the nodal SI indexes and the grade or stage of liver histology. The accuracy of diagnostic criteria for the size indexes or numbers of lymph nodes in predicting inflammatory activity was determined by calculating the area under the curve from corresponding receiver operative characteristics (ROC) curves.

Values of P ≤ 0.05 were considered statistically significant. All statistical analyses were performed with SPSS 13.0 for Windows (SPSS Inc., Chicago, IL, United States).

RESULTS

Sample characteristics

Sixty-seven patients with CHB, comprising 52 men and 15 women (age range, 18-63 years; mean age, 40.8 ± 8.3 years), and 18 healthy volunteers, 13 men and 5 women (age range, 24-63 years; mean age, 42.4 ± 11.4 years), met the criteria for inclusion in this study. Between the patients and controls, there were no statistical differences between genders (P = 0.755, Fischer's exact test) and ages (t = 0.550, P = 0.588). Liver histological findings for all subjects are shown in Table 1.

Size and SI index of lymph nodes

Enlarged perihepatic lymph nodes for the patients with CHB on magnetic resonance fat suppressed T2WI are shown in Figure 1. In the subjects without lymph nodes greater than 5 mm in shortest diameter in hepatic hilum, the size and SI index of lymph nodes was considered zero. The size and SI indexes of lymph nodes in hepatic hilum according to grade and stage groups are shown in Table 1. The average nodal size index was greater in individuals with grade 2 or higher than that in individuals with grades 0 and 1 [43.52 ± 58.38 mm^2 for grade 0 (n = 18), 77.70 ± 74.12 mm^2 for grade 1 (n = 12), 273.65 ± 155.04 mm^2 for grade 2 (n = 19), 492.12 ± 324.97 mm^2 for grade 3 (n = 20), and 404.58 ± 198.42 mm^2 for grade 4 (n = 16)]. The average size index of lymph nodes for all subjects was 218.18 ± 262.65 mm^2.

The partial correlation coefficient between the nodal size indexes and histological grading was 0.376 (P = 0.000), and 0.194 (P = 0.077) between the SI indexes and grading when controlling staging variables. There was no statistically significant correlation between the nodal size

Table 1 The size and signal intensity indexes of lymph nodes greater than 5 mm in shortest diameter in hepatic hilum (mean ± SD)

Grading	Staging	Sample size (*n*)	Size indexes (mm^2)	SI indexes
G0 (controls)	S0	18	43.52 ± 58.38	0.572 ± 0.599
G1	S0	6	63.33 ± 74.27	0.474 ± 0.519
	S1	3	92.48 ± 87.29	0.720 ± 0.627
	S2	2	137.50 ± 50.20	1.130 ± 0.500
	S3	1	0	0
G2	S1	6	221.16 ± 68.83	1.218 ± 0.167
	S2	10	268.22 ± 164.69	1.213 ± 0.210
	S3	1	162.06	1.878
	S4	2	514.09 ± 141.30	1.301 ± 0.204
G3	S1	3	404.33 ± 191.74	1.172 ± 0.153
	S2	6	647.02 ± 238.31	1.169 ± 0.171
	S3	9	413.88 ± 417.78	1.094 ± 0.454
	S4	2	511.21 ± 172.53	1.383 ± 0.152
G4	S2	4	398.09 ± 219.81	1.209 ± 0.350
	S3	7	471.95 ± 154.13	1.065 ± 0.247
	S4	5	315.45 ± 240.52	1.114 ± 0.073

SI: Signal intensity.

indexes and histological staging ($r = 0.063$, $P = 0.572$), or between the SI indexes and staging ($r = 0.134$, $P = 0.226$) when controlling grading variables.

The data for the nodal size indexes among partial groups of grading (grades 0 and 1) did not show normal distribution by tests of normality ($P < 0.05$, Shapiro-Wilk test) or by tests of homogeneity of variances for the nodal size indexes among groups of grading indicate heterogeneity of variance ($F = 2.452$, $P = 0.006$). The nonparametric Kruskall-Wallis test showed significant difference for the nodal size indexes among grading groups ($\chi^2 = 49.557$, $P = 0.000$). The nonparametric Mann-Whitney *U* test (exact probability) showed no significant difference for the nodal size indexes between grades 0 and 1 ($P = 0.232$), grade 2 and grade 4 ($P = 0.061$), and grade 3 and grade 4 ($P = 0.498$). However, there was a statistically significant difference between grades 1 and 2 ($P = 0.000$, Mann-Whitney *U* test with exact probability), which could suggest that the nodal size indexes in individuals with grade 2 or higher were larger than that in individuals with grades 0 and 1. All subjects were grouped into two new groups, group A comprising grades 0 and 1 (the average nodal size index, 57.19 ± 66.12 mm^2) and group B comprising grade 2-4 (the average nodal size index, 391.18 ± 254.54 mm^2). There was a statistically significant difference between groups A and B ($U = 94.000$, $W = 559.000$, $Z = -6.741$, $P = 0.000$, Mann-Whitney *U* test).

The ROC curve for the size indexes of lymph nodes predicting individuals with grade 2 or higher is shown in Figure 2A. The area under the curve was 0.943 ($P = 0.000$) with a cutoff value of 180.8 mm^2. A cutoff value of 180 mm^2 for the size indexes of lymph nodes had a sensitivity of 83.64%, a specificity of 100%, an accuracy of 89.41%, a positive predictive value of 100%, and a negative predictive value of 76.92% for a MR diagnosis of hepatic inflammation with grade 2 or higher.

Table 2 The number of lymph nodes greater than 5 mm in shortest diameter in hepatic hilum among grading groups *n* (%)

Grading	Sample size (*n*)	Subjects with various numbers of lymph nodes			
		0	⩾ 1	⩾ 2	⩾ 3
G0	18	9 (50.00)	9 (50.00)	1 (5.56)	0
G1	12	5 (41.67)	7 (58.33)	2 (16.67)	1 (8.33)
G2	19	0	19 (100)	15 (78.95)	10 (56.63)
G3	20	1 (5.00)	19 (95.00)	18 (90.00)	16 (80.00)
G4	16	0	16 (100)	15 (93.75)	10 (62.50)
Total	85	15 (17.65)	70 (82.35)	51 (60.00)	37 (43.53)

Number of lymph nodes

The numbers of lymph nodes greater than 5 mm in shortest diameter in hepatic hilum among grade groups are shown in Table 2. There was statistically significant difference for the subjects with one lymph node or more among the grade groups ($P = 0.000$, Fischer's exact test for R × C Table), for the subjects with two lymph nodes or more ($\chi^2 = 49.556$, $P = 0.000$), and for the subjects with three lymph nodes or more ($\chi^2 = 33.727$, $P = 0.000$), respectively. Presence rates of subjects with differing numbers of lymph nodes were larger in individuals with grade 2 or higher than that in individuals with grades 0 and 1 in Table 2. *P* value was 0.722 for subjects with one lymph node or more, 0.548 for subjects with two lymph nodes or more and 0.400 for subjects with three lymph nodes or more between grades 0 and 1, respectively (Fischer's exact test). *P* value was 0.005 for subjects with one lymph node or more, 0.001 for subjects with two lymph nodes or more and 0.020 for subjects with three lymph nodes or more between grades 1 and 2, respectively (Fischer's exact test). *P* value was 1.000 for subjects with one lymph node or more, 0.474 for subjects with two lymph nodes or more and 0.182 for subjects with three lymph nodes or more among grades 2-4, respectively (Fischer's exact test). All subjects were grouped into two new groups, group A comprising grades 0 and 1 and group B comprising grades 2-4. There was a statistically significant difference between groups A and B ($\chi^2 = 26.866$, $P = 0.000$; $\chi^2 = 48.295$, $P = 0.000$; and $\chi^2 = 30.475$, $P = 0.000$, respectively) for the subjects with various numbers of lymph nodes.

There were 15 subjects without lymph node greater than 5 mm in shortest diameter in hepatic hilum (9 subjects with grade 0, 5 subjects with grades 1 and 1 subjects with grade 3), 19 subjects with a single lymph node (8 subjects with grade 0, 5 subjects with grade 1, 4 subjects with grade 2, 1 subjects with grade 3 and 1 subjects with grade 4), 14 subjects with two lymph nodes (1 subjects with grade 0, 1 subjects with grade 1, 5 subjects with grade 2, 2 subjects with grade 3 and 5 subjects with grade 4), and 37 subjects with three or more lymph nodes (1 subjects with grade 1, 10 subjects with grade 2, 16 subjects with grade 3 and 10 subjects with grade 4). The ROC curve for the numbers of lymph nodes predicting individuals with grade 2 or higher is shown in Figure 2B. There was a high accuracy for numbers of lymph nodes predicting individuals with grade 2 or higher (the area under the curve = 0.926, $P = 0.000$, and cutoff value = 2). The sensitivity,

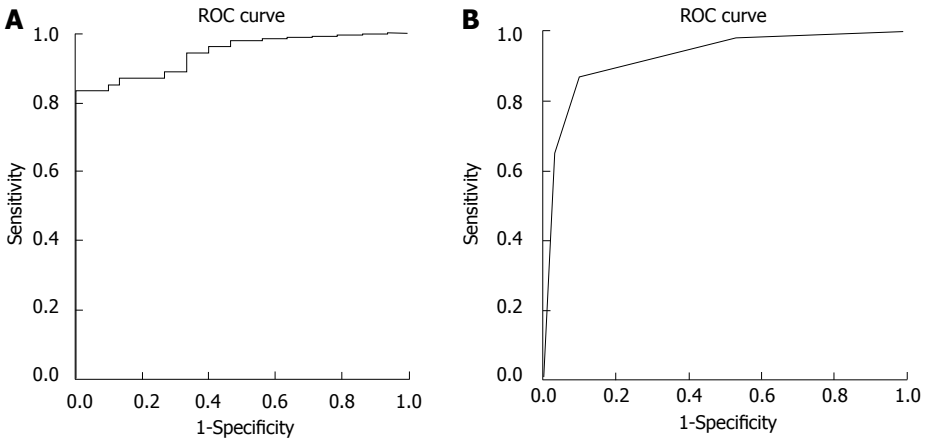

Figure 2 The receiver operative characteristics curve. A: The size indexes of lymph nodes predicting individuals with grade 2 or higher. The area under the curve was 0.943 (P = 0.000) with a cutoff value of 180.8 mm^2; B: The number of lymph nodes predicting individuals with grade 2 or higher. The area under the curve was 0.926 (P = 0.000) with a cutoff value of 2. ROC: Receiver operative characteristics.

specificity, accuracy, positive predictive value and negative predictive value for the diagnosis of hepatic inflammation with grade 2 or higher using 2 or more lymph nodes greater than 5 mm in shortest diameter in hepatic hilum were 87.27%, 90.00%, 88.24%, 94.12% and 79.41%, respectively.

There was a statistically significant difference for all subjects with one lymph node or more among stage groups (12 subjects with stage 0, 11 subjects with stage 1, 22 subjects with stage 2, 16 subjects with stage 3 and 9 subjects with stage 4, respectively), for subjects with two lymph nodes or more (1 subjects with stage 0, 9 subjects with stage 1, 19 subjects with stage 2, 14 subjects with stage 3 and 8 subjects with stage 4, respectively), and for subjects with three lymph nodes or more (5 subjects with stage 1, 14 subjects with stage 2, 11 subjects with stage 3 and 7 subjects with stage 4, respectively) (all three P value = 0.000, Fischer's exact test for R × C table). However, there was no statistically significant difference between fibrosis groups (stages 1-4) (P = 0.305, 0.779 and 0.432, respectively, Fischer's exact test for R × C table), which indicates that the presence of the lymph nodes could be not correlated with hepatic fibrosis and the difference between normal (stage 0) and fibrosis groups could come from differences in inflammatory activity of the liver.

DISCUSSION

In our study, we retrospectively reviewed the appearances of lymph nodes on axial fat suppressed FRFSE T_2WI in patients with CHB, measured the presence, number, size, and SI of perihepatic lymph node, and assessed the relationship of these MR findings with liver histology for patients with CHB. We found that the number and size indexes of lymph nodes greater than 5 mm in shortest diameter in hepatic hilum suggested inflammatory activity for subjects with grade 2 or higher, with a high accuracy of diagnosis (the area under the curves > 0.9, P < 0.001). The number of lymph nodes was 2 or more with a sensitivity of 87.27%, a specificity of 90.00%, an accuracy of 88.24%, a positive predictive value of 94.12%, and a negative predictive value of 79.41% in patients with grade 2 or higher, and the size indexes were no less than 180 mm^2 with a sensitivity of 83.64%, a specificity of 100%, an accuracy of 89.41%, a positive predictive value of 100%, and a negative predictive value of 76.92%. The number and size indexes of lymph nodes were not correlated with hepatic fibrosis. The SI indexes of lymph nodes were not significantly correlated with histological grading or staging of liver.

Lymph nodes are well known to exist in the hepatoduodenal ligament. They can consistently be detected in the dorsal part of the hepatoduodenal ligament adjacent to the cystic duct and common bile duct, and in the ventral hepatoduodenal ligament close to the orifice of the foramen epiploicum[22]. Enlarged lymph nodes in the hepatoduodenal ligament were prevalent in chronic viral hepatitis, especially CHC and CHB[8-12,23]. In ultrasound study, enlarged lymph nodes could be demonstrated in the hilus hepatis of almost all patients with CHB or CHC[8,9]. Lymph nodes in the hepatoduodenal ligament, especially those wider than 5 mm, suggested chronic HBV or HCV infection instead of only chronic hepatitis[8], and there was no significant difference in lymph node volume between patients with hepatitis B and those with hepatitis C[9]. Enlarged lymph nodes within the dorsal portion of the hepatoduodenal ligament can easily be identified on sonography, although it may be more difficult to detect lymph nodes in the ventral portion of the hepatoduodenal ligament because of surrounding fat deposition and connective tissue[22]. There was generally higher SI for enlarged perihepatic lymph nodes on magnetic resonance fat suppressed T_2WI and better contrast between the lymph nodes and adjacent tissue than that on sonography or CT, which was superior to sonography for visualizing enlarged lymph nodes in the porta hepatica[14,21].

In patients with CHC, enlargement of perihepatic lymph nodes was associated with viremia and was predictive for the presence of severe inflammatory activity on sonography[9,22,24]. Total perihepatic lymph node volume

changed according to the antiviral response: patients with CHC without response to antiviral therapy did not normalize the size of perihepatic lymph nodes, but successful antiviral therapy with histological improvement was reflected in a decline in perihepatic lymph node size[12,25].

In patients with CHB, the sonographically determined lymph node volume showed a significant correlation with serum aspartate transaminase, alanine transaminase, gamma-glutamyl-transpeptidase, histologic activity index, and necroinflammatory score, but not with fibrosis score and serum hepatitis B viremia[10].

Zhang *et al*[14] studied the magnetic resonance appearance of lymph nodes in relation to activity of CHC. They found that MRI could depict perihepatic lymph nodes in most patients with CHC, and that the number, size, and hyperintensity of lymph nodes were related to the activity of CHC while the results of liver function tests were not. Mitchell *et al*[21] found that the size index of lymph nodes was correlated with inflammatory activity of CHC but there was no correlation between Lymph node SI and any pathology using unenhanced MRI.

In our study, perihepatic lymph nodes in the patients with CHB were evaluated with MRI, especially fat suppressed FRFSE T_2WI. Our results indicated that the number and size indexes of lymph nodes greater than 5 mm in shortest diameter in hepatic hilum correlated with inflammatory activity of CHB and did not correlate with fibrosis, in accordance with previous research for CHC or CHB[9,10,14,21]. The SI indexes of lymph nodes were not significantly correlated with histological grading or staging of liver, in accordance with research on CHC by Mitchell *et al*[21]. In our study, we also found that the number and size indexes of lymph nodes greater than 5 mm in shortest diameter suggested inflammatory activity for subjects with grade 2 or higher, with a high accuracy of diagnosis at a cutoff value of 2 for the numbers or 180 mm^2 for the size indexes of lymph nodes. The findings suggest that MRI may reduce or displace liver biopsy for assessing liver inflammation in patients with CHB. Moreover, other liver diseases, such as CHC, may lead to perihepatic lymphadenectasis. The etiology diagnosis of this lymphadenectasis was difficult when depending only on MRI. In such cases, other tools such as serological examination, were available[26].

One limitation of our study is the relatively small sample size of groups. However, this should not significantly affect our results because appropriate statistical methods were applied. Additionally, in our study sequence one slice was obtained every 9 mm , with a slice-thickness of 8 mm and a gap of 1 mm. So, effect of partial volume cannot be ignored in the size index of lymph nodes for each subject. In addition, the size of the lymph nodes obtained as the product of the long and short axes could be slightly different from the true size. However, these would be only random errors without directionality in measurements, could not significantly affect our overall results.

In conclusion, enlarged perihepatic lymph nodes for the patients with CHB can be sensitively demonstrated by MRI, especially fat suppressed FRFSE T_2WI. The number and size indexes of lymph nodes greater than 5 mm in shortest diameter suggest inflammatory activity for subjects with grade 2 or higher, with a high accuracy of diagnosis at a cutoff value of 2 for the numbers or 180 mm^2 for the size indexes of lymph nodes.

COMMENTS

Background

Hepatitis B virus (HBV) is one of the most common causes of chronic hepatitis, and the infected individuals are at an increased risk of developing cirrhosis, liver failure, and hepatocellular carcinoma. Several effective medications are available to inhibit HBV replication with liver fibrosis regression by reducing liver inflammation and cellular damage in most patients with chronic hepatitis B (CHB). So, the assessment of liver necroinflammatory activity and fibrosis for patients with CHB is helpful for determining prognosis and treatment strategy.

Research frontiers

CHB is frequently associated with hyperplasia of lymph nodes in the hepatic hilum, and these enlarged lymph nodes can be a good indicator for inflammatory activity of the liver in patients with CHB. Magnetic resonance imaging (MRI) can provide better contrast between the lymph nodes and adjacent tissue, especially T_2-weighted imaging (T_2WI). This has been reported for the magnetic resonance appearance of perihepatic lymph nodes in patients with chronic hepatitis C. However, there are no previous studies using MRI that reveal the significance of lymph nodes in the porta hepatis for patients with CHB.

Innovations and breakthroughs

Enlarged perihepatic lymph nodes in patients with CHB can be sensitively demonstrated by MRI, especially fat suppressed fast recovery fast spin echo T_2WI. The number and size indexes of lymph nodes greater than 5 mm in shortest diameter suggest inflammatory activity for subjects with grade 2 or higher, with a high accuracy of diagnosis at a cutoff value of 2 for the numbers or 180 mm^2 for the size indexes of lymph nodes.

Applications

The results support the suitability of MRI for assessment of liver inflammation in patients with CHB. Liver biopsy for assessment of inflammation can be reduced or displaced in patients with CHB. The study was performed directly on clinical subjects, and the findings can be readily applied to patient care

Peer review

The authors attempt to validate the potential of using magnetic resonance fat suppressed T_2WI in diagnosing inflammatory lymph nodes that lead to CHB. The study is a systematic and well thought out approach which, clearly shows the added advantages of magnetic resonance fat suppressed T_2WI. Being a non-invasive tool for diagnosing the nodal inflammation, and the study was performed directly on clinical subjects; the findings can be readily applied to patient care.

REFERENCES

1 **Robotin MC**. Hepatitis B prevention and control: Lessons from the East and the West. *World J Hepatol* 2011; **3**: 31-37 [PMID: 21423912 DOI: 10.4254/wjh.v3.i2.31]

2 **Pradeep Kumar S**, Medhi S, Asim M, Das BC, Gondal R, Kar P. Evaluation of adefovir & amp; lamivudine in chronic hepatitis B: correlation with HBV viral kinetic, hepatic-necro inflammation & amp; fibrosis. *Indian J Med Res* 2011; **133**: 50-56 [PMID: 21321419]

3 **Lin CL**, Kao JH. Recent advances in the treatment of chronic hepatitis B. *Expert Opin Pharmacother* 2011; **12**: 2025-2040 [PMID: 21682661 DOI: 10.1517/14656566.2011.590474]

4 **Kim SU**, Park JY, Kim do Y, Ahn SH, Choi EH, Seok JY, Lee JM, Park YN, Chon CY, Han KH. Non-invasive assessment of changes in liver fibrosis via liver stiffness measurement in patients with chronic hepatitis B: impact of antiviral treatment on fibrosis regression. *Hepatol Int* 2010; **4**: 673-680 [PMID: 21286337 DOI: 10.1007/s12072-010-9201-7]

5 **Dienstag JL**, Goldin RD, Heathcote EJ, Hann HW, Woessner M, Stephenson SL, Gardner S, Gray DF, Schiff ER. Histological outcome during long-term lamivudine therapy.

Gastroenterology 2003; **124**: 105-117 [PMID: 12512035]
6 **Lok AS**, McMahon BJ. Chronic hepatitis B: update 2009. *Hepatology* 2009; **50**: 661-662 [PMID: 19714720 DOI: 10.1002/hep.23190]
7 **Wright TL**. Introduction to chronic hepatitis B infection. *Am J Gastroenterol* 2006; **101 (**Suppl 1): S1-S6 [PMID: 16448446]
8 **Kuo HT**, Lin CY, Chen JJ, Tsai SL. Enlarged lymph nodes in porta hepatis: sonographic sign of chronic hepatitis B and C infections. *J Clin Ultrasound* 2006; **34**: 211-216 [PMID: 16673362]
9 **Dietrich CF**, Gottschalk R, Herrmann G, Caspary WF, Zeuzem S. Sonographic detection of lymph nodes in the hepatoduodenal ligament. *Dtsch Med Wochenschr* 1997; **122**: 1269-1274 [PMID: 9378062]
10 **Choi MS**, Lee JH, Koh KC, Paik SW, Rhee PL, Kim JJ, Rhee JC, Choi KW, Kim SH. Clinical significance of enlarged perihepatic lymph nodes in chronic hepatitis B. *J Clin Gastroenterol* 2001; **32**: 329-332 [PMID: 11276277]
11 **Nakanishi S**, Shiraki K, Sugimoto K, Tameda M, Yamamoto K, Masuda C, Iwata M, Koyama M. Clinical significance of ultrasonographic imaging of the common hepatic arterial lymph node (No. 8 LN) in chronic liver diseases. *Mol Med Rep* 2010; **3**: 679-683 [PMID: 21472298 DOI: 10.3892/mmr_00000316]
12 **Dietrich CF**, Stryjek-Kaminska D, Teuber G, Lee JH, Caspary WF, Zeuzem S. Perihepatic lymph nodes as a marker of antiviral response in patients with chronic hepatitis C infection. *AJR Am J Roentgenol* 2000; **174**: 699-704 [PMID: 10701612]
13 **Kim SY**, Kim MJ, Chung JJ, Lee JT, Yoo HS. Abdominal tuberculous lymphadenopathy: MR imaging findings. *Abdom Imaging* 2000; **25**: 627-632 [PMID: 11029097]
14 **Zhang XM**, Mitchell DG, Shi H, Holland GA, Parker L, Herrine SK, Pasqualin D, Rubin R. Chronic hepatitis C activity: correlation with lymphadenopathy on MR imaging. *AJR Am J Roentgenol* 2002; **179**: 417-422 [PMID: 12130443]
15 **Papakonstantinou O**, Maris TG, Kostaridou S, Ladis V, Vasiliadou A, Gourtsoyiannis NC. Abdominal lymphadenopathy in beta-thalassemia: MRI features and correlation with liver iron overload and posttransfusion chronic hepatitis C. *AJR Am J Roentgenol* 2005; **185**: 219-224 [PMID: 15972427]
16 **Norton ID**, Clain JE. The role of transabdominal ultrasonography, helical computed tomography, and magnetic resonance cholangiopancreatography in diagnosis and management of pancreatic disease. *Curr Gastroenterol Rep* 2000; **2**: 120-124 [PMID: 10981013]
17 **Mortele KJ**, Ros PR. MR imaging in chronic hepatitis and cirrhosis. *Semin Ultrasound CT MR* 2002; **23**: 79-100 [PMID: 11866224]
18 **Semelka RC**, Chung JJ, Hussain SM, Marcos HB, Woosley JT. Chronic hepatitis: correlation of early patchy and late linear enhancement patterns on gadolinium-enhanced MR images with histopathology initial experience. *J Magn Reson Imaging* 2001; **13**: 385-391 [PMID: 11241811]
19 **Scheuer PJ**. Classification of chronic viral hepatitis: a need for reassessment. *J Hepatol* 1991; **13**: 372-374 [PMID: 1808228]
20 **Hübscher SG**. Histological grading and staging in chronic hepatitis: clinical applications and problems. *J Hepatol* 1998; **29**: 1015-1022 [PMID: 9875653]
21 **Mitchell DG**, Navarro VJ, Herrine SK, Bergin D, Parker L, Frangos A, McCue P, Rubin R. Compensated hepatitis C: unenhanced MR imaging correlated with pathologic grading and staging. *Abdom Imaging* 2008; **33**: 58-64 [PMID: 17387539]
22 **Dietrich CF**, Lee JH, Herrmann G, Teuber G, Roth WK, Caspary WF, Zeuzem S. Enlargement of perihepatic lymph nodes in relation to liver histology and viremia in patients with chronic hepatitis C. *Hepatology* 1997; **26**: 467-472 [PMID: 9252160]
23 **Soresi M**, Bonfissuto G, Magliarisi C, Riili A, Terranova A, Di Giovanni G, Bascone F, Carroccio A, Tripi S, Montalto G. Ultrasound detection of abdominal lymph nodes in chronic liver diseases. A retrospective analysis. *Clin Radiol* 2003; **58**: 372-377 [PMID: 12727165]
24 **Cassani F**, Valentini P, Cataleta M, Manotti P, Francesconi R, Giostra F, Ballardini G, Lenzi M, Zauli D, Bianchi FB. Ultrasound-detected abdominal lymphadenopathy in chronic hepatitis C: high frequency and relationship with viremia. *J Hepatol* 1997; **26**: 479-483 [PMID: 9075652]
25 **Dietrich CF**, Zeuzem S. [Sonographic detection of perihepatic lymph nodes: technique and clinical value]. *Z Gastroenterol* 1999; **37**: 141-151 [PMID: 10190247]
26 **Akcam FZ**, Tigli A, Kaya O, Ciris M, Vural H. Cytokine levels and histopathology in chronic hepatitis B and chronic hepatitis C. *J Interferon Cytokine Res* 2012; **32**: 570-574 [PMID: 23067363 DOI: 10.1089/jir.2012.0048]

P- Reviewers Darge K, Karmy-Jones R, Natarajan M
S- Editor Huang XZ **L- Editor** Hughes D **E- Editor** Ma S

World Journal of Radiology

Online Submissions: http://www.wjgnet.com/esps/
wjr@wjgnet.com
doi:10.4329/wjr.v5.i5.215

World J Radiol 2013 May 28; 5(5): 215-219
ISSN 1949-8470 (online)

CASE REPORT

Incidental meandering right pulmonary vein, literature review and proposed nomenclature revision

Mark Alexander Rodrigues, Gillian Ritchie, John Tallach Murchison

Mark Alexander Rodrigues, Gillian Ritchie, John Tallach Murchison, Department of Radiology, Royal Infirmary of Edinburgh, Edinburgh, Scotland EH16 4SA, United Kingdom

Author contributions: Ritchie G reported the chest X-ray; Murchison JT reported the computed tomography; Rodrigues MA performed the case research; Rodrigues MA, Ritchie G and Murchison JT contributed to the literature research, manuscript preparation and editing; Rodrigues MA and Murchison JT contributed to the image preparation.

Correspondence to: Dr. Mark Alexander Rodrigues, Radiology Registrar, Department of Radiology, Royal Infirmary of Edinburgh, 51 Little France Crescent, Edinburgh EH16 4SA, United Kingdom. mark.a.rodrigues@gmail.com

Telephone: +44-131-5361000 Fax: +44-131-5361000

Received: January 30, 2013 Revised: March 29, 2013
Accepted: May 8, 2013
Published online: May 28, 2013

Abstract

We report a case of an anomalous pulmonary vein on chest X-ray resembling a scimitar sign in an 80-year-old female undergoing investigation of syncope. Multislice computed tomography (CT) with multiplanar reformatting and maximum intensity projections demonstrated an aberrant right inferior pulmonary vein coursing inferomedially towards the diaphragm before turning superiorly and draining normally into the left atrium. The diagnosis of an incidental meandering right pulmonary vein was established. The case is used to review the literature on this rare pulmonary anomaly, including pathogenesis, its relationship with scimitar syndrome and scimitar variant, and diagnosis, with an emphasis on the role modern CT techniques can play in non-invasive diagnosis. A revision to the nomenclature of pulmonary vascular anomalies is proposed to help reduce confusion in the literature.

Key words: Incidental findings; Pulmonary veins/abnormalities; Scimitar syndrome/radiography; Tomography; X-ray computed

Core tip: This case highlights the chest X-ray features of scimitar syndrome are not diagnostic and a meandering right pulmonary vein (MRPV) should be considered in the differential diagnosis. The nomenclature used in the literature to describe these pulmonary vascular anomalies is inconsistent. We therefore propose a revision to the nomenclature to avoid confusion. Differentiation between pulmonary vascular anomalies is required to help decide whether treatment is necessary. Modern multislice computed tomography technology allows clear depiction of the vascular connections and associated anatomy, and has superseded invasive pulmonary angiography and cardiac catheterization as the investigation of choice for MRPV.

Rodrigues MA, Ritchie G, Murchison JT. Incidental meandering right pulmonary vein, literature review and proposed nomenclature revision. *World J Radiol* 2013; 5(5): 215-219 Available from: URL: http://www.wjgnet.com/1949-8470/full/v5/i5/215.htm DOI: http://dx.doi.org/10.4329/wjr.v5.i5.215

INTRODUCTION

Meandering right pulmonary vein (MRPV) is a rare pulmonary vascular anomaly. Cases are often confused with the more common scimitar syndrome as both conditions consist of an anomalous right pulmonary vein, taking a circuitous route through the lung, which usually results in a scimitar sign on chest X-ray. However in contrast to scimitar syndrome, the MRPV terminates normally in the left atrium, rather than the inferior vena cava (IVC). We report a case of an 80-year-old female in which a MRPV coincided with other features of scimitar syndrome. Only a few cases of its type have been reported in the English literature.

CASE REPORT

An 80-year-old female was referred to the geriatric clinic for investigation of recurrent syncope. Her past medical history included mild postural hypotension, temporal arteritis, osteoarthritis and osteoporosis. Clinical examination revealed a small postural drop in blood pressure and an ejection systolic murmur, but was otherwise unremarkable.

A routine chest X-ray demonstrated a curvilinear structure running from the right mid zone towards the right cardiophrenic recess before curving superiorly (Figure 1), resembling a scimitar sign. In addition there was volume loss in the right hemithorax with mediastinal shift to the right suggesting cardiac dextroposition. An anomalous pulmonary vein, such as that seen in scimitar syndrome, was suspected. Contrast-enhanced computed tomography (CT) revealed a dilated right inferior pulmonary vein with an aberrant circuitous route, coursing inferomedially towards the diaphragm before turning upwards and draining normally into the left atrium (Figure 2). There was no connection to the IVC. It also confirmed the X-ray findings of right lung hypoplasia (right lung volume 1.17 L, left lung 1.66 L) and cardiac dextroposition. The right main pulmonary artery was smaller than the left in keeping with mild pulmonary artery hypoplasia. There was no evidence of anomalous systemic arterial supply to the lung. The diagnosis of an incidental MRPV was established and no further investigation or treatment of this was required.

Other investigations did not reveal any significant abnormality; routine blood tests showed an isolated mild hyponatremia (133 mmol/L). Twenty-four-hour electrocardiography monitoring demonstrated sinus rhythm throughout. Echocardiography was limited due to the abnormal positioning of the heart, but revealed mild aortic stenosis and good left ventricular function.

Neurally mediated syncope was deemed the most likely diagnosis and she was managed conservatively with advice on increasing fluid intake and taking care with postural changes.

Interestingly on questioning, the patient explained she had had an abnormal chest X-ray at the age of 5 years that showed "partial collapse" of the right lung. Having worked in the mining industry, she underwent several chest X-rays during her adult life but was told to stop having them because the appearances "always worried the doctors!"

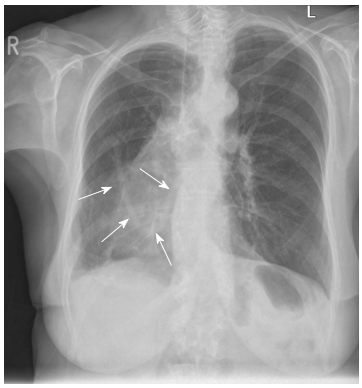

Figure 1 Posteroanterior chest X-ray demonstrating an anomalous curvilinear vessel (white arrows) running from the right mid zone inferomedially before turning superiorly. There is loss of volume within the right hemithorax and mediastinal shift to the right suggesting cardiac dextroposition. L: Left; R: Right.

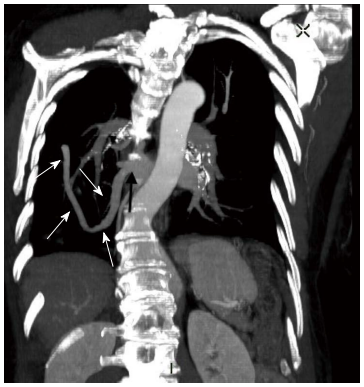

Figure 2 Contrast-enhanced maximum intensity projection multiplanar reformatted coronal image of the computed tomography chest demonstrating the path of the anomalous pulmonary vein (white arrows) and its connection to the left atrium (black arrow). R: Right.

DISCUSSION

The scimitar sign describes a curved vascular shadow on a chest X-ray, which courses along the right cardiac border towards the right cardiophrenic angle. It is so-called because the appearance resembles a Turkish sword or scimitar.

Scimitar syndrome is a rare pulmonary anomaly which consists of anomalous pulmonary venous drainage of the right lung to the IVC (giving rise to the scimitar sign), anomalous systemic arterial supply of the right lower lobe from either the thoracic or abdominal aorta, hypoplasia of the right lung, with resultant cardiac dextroposition and right pulmonary artery hypoplasia[1]. The scimitar sign was originally thought to be diagnostic of scimitar syndrome[2,3], however, a false positive scimitar sign is a rare possibility. Morgan *et al*[4] described the first case in which the scimitar sign and features of scimitar syndrome were present but the aberrant pulmonary vein ultimately drained normally into the left atrium. Other reported causes of the scimitar sign include an anomalous intrapulmonary venous connection to superior vena cava, obstruction of a major pulmonary vein with development of a distended intrapulmonary collateral and an anomalous IVC with normal pulmonary venous drainage[5,6].

The term "meandering right pulmonary vein" was subsequently coined by Goodman *et al*[7] to describe the presence of the scimitar sign and an anomalous right pulmonary vein that drains normally into the left atrium. In contrast to scimitar syndrome, there have only been a handful of cases of MRPV reported in the literature (Table 1). MRPV can occur with or without other fea-

Table 1 Published cases of meandering pulmonary vein

Ref.	Gender	Age (yr)	Symptoms	Scimitar sign	Features of scimitar syndrome	Investigations (in addition to CXR)	Anomalous pulmonary venous drainage	Original diagnosis	Proposed diagnosis
Morgan *et al*[4]	M	22	Incidental	Y	Thoracic aorta supply, right lung hypoplasia, dextroposition	Pulmonary angiography and cardiac catheterization	Single right pulmonary vein to left atrium	Scimitar syndrome with normal pulmonary venous drainage	AUSPV
Goodman *et al*[7]	F	51	Haemoptysis	Y	Dextroposition, right pulmonary artery hypoplasia	Pulmonary angiography and cardiac catheterization	Single right pulmonary vein to left atrium	MRPV	AUSPV
Kanemoto *et al*[15]	F	48	Orthopnea and productive cough	Y	Right lung hypoplasia, dextroposition	Lung perfusion, CT, ECHO, Pulmonary angiography	Single right pulmonary vein to left atrium	Pseudo-scimitar sign	AUSPV
Cukier *et al*[21]	F	27	Haemoptysis	Y	Abdominal aorta supply, right lung hypoplasia	Pulmonary angiography and cardiac catheterization	Inferior right pulmonary vein to left atrium	Scimitar syndrome	MRPV
Holt *et al*[22]	M	2	Murmur and failure to thrive	Y	Systemic supply, right lung hypoplasia, dextroposition	ECHO, cardiac catheterization	Superior and inferior right pulmonary veins to left atrium	Scimitar syndrome variant	MPVs
Tsitouridis *et al*[19]	M	41	Incidental	Y	Right lung hypoplasia, dextroposition	CT	Single right pulmonary vein to left atrium	MPV	AUSPV
Yoo *et al*[20]	F	1	Respiratory distress	Y	Right lung hypoplasia, dextroposition	CT	Single right pulmonary vein to left atrium	MRPV	AUSPV
Siu *et al*[23]	F	43	Incidental	Y	Dextroposition	ECHO, CT	Single right pulmonary vein to left atrium	Scimitar variant	AUSPV
Current case	F	80	Incidental	Y	Right lung hypoplasia, dextroposition, Hypoplasia right pulmonary artery	CT	Inferior right pulmonary vein to left atrium	MRPV	MRPV
Collins *et al*[8]	M	20	Incidental	Y	-	ECHO, cardiac catheterization, pulmonary angiography	All 4 pulmonary veins to left atrium	Idiopathic prominence of pulmonary veins	MPVs
Takeda *et al*[11]	F	28	Incidental	Y	-	Pulmonary angiography	NS	Scimitar variant	-[1]
Kriss *et al*[9]	F	12	Incidental	Y	-	CT, cardiac catheterization, pulmonary angiography	Right superior and inferior and left inferior pulmonary veins to left atrium	MPV	MPVs
Salazar-Mena *et al*[14]	F	15	Incidental	Y	-	Pulmonary angiography and cardiac catheterization	Right inferior pulmonary vein to left atrium	MRPV	MRPV
Al-Naami *et al*[24]	M	2/12	Failure to thrive, ASD, VSD	N[2]	-	ECHO, CT, cardiac catheterization	Right inferior pulmonary vein to left atrium	MPV	MRPV

[1]Unable to name due to lack of details in article. [2]Chest X-ray demonstrated cardiomegaly and congested lung fields which may have masked the scimitar sign. M: Male; F: Female; NS: Not stated in article; ASD: Atrial septal defect; AUSPV: Anomalous unilateral single pulmonary vein; CT: Computed tomography; CXR: Chest X-ray; ECHO: Echocardiogram; MPV: Meandering pulmonary vein; MRPV: Meandering right pulmonary vein; VSD: Ventricular septal defect; N: No; Y: Yes.

tures of the classic scimitar syndrome. Whilst most cases involve the right pulmonary veins, cases of anomalous right and left pulmonary veins have been described[8,9]. The scimitar sign is not always present[10].

A further anomaly, termed scimitar variant, describes the connection of an anomalous right pulmonary vein to both the IVC and left atrium[10-13].

A lack of consistency in the literature regarding nomenclature can lead to confusion. Some authors have treated MRPV and scimitar variant as synonymous[14]. Pseudo-scimitar sign has also been used to describe appearances of MRPV[15]. Anomalous unilateral single pulmonary vein (AUSPV) has been used to describe a single anomalous pulmonary vein draining the entire ipsilateral, lung regardless of whether it terminates normally in the left atrium[16,17] or elsewhere[18].

To avoid confusion we advocate using the term MRPV to describe cases in which the anomalous vein draining part of right lung terminates normally into the left atrium, reserving the scimitar variant for those with a dual connection to IVC and the left atrium. Meandering pulmonary veins (MPV) is suggested for cases that have more than one anomalous pulmonary vein draining into the left atrium. AUSPV should be used to describe cases where there is a single anomalous vein draining the entire ipsilateral lung to the left atrium or IVC.

Table 1 compares reported cases of MRPV, scimitar variant and pseudo-scimitar sign. Employing our proposed nomenclature, 2 of these cases would be classified as MRPV with features of scimitar syndrome, 1 as MPVs with features of scimitar syndrome, 2 as MRPV without features of scimitar syndrome, 2 as MPVs without features of scimitar syndrome, with 6 being reclassified as AUSPV.

Scimitar syndrome, scimitar variant and MRPV can be considered as a spectrum of pulmonary anomalies having a common embryological basis, with scimitar syndrome at one extreme, MRPV at the other, and scimitar variant somewhere in between[12,19,20]. It is likely that the stage of embryogenesis at which the anomaly occurs determines which condition develops. For example, persistence of the primitive communications between the pulmonary and systemic vascular supplies may lead to scimitar syndrome if the connection between the right pulmonary vein and left atrium is obstructed, or scimitar variant if this connection is patent[11,14,19]. Abnormally delayed obliteration of the pulmonary and systemic connections may result in a MRPV with an anomalous route in the lungs but ultimately draining normally into the left atrium.

It is important to distinguish between scimitar syndrome and MRPV. Scimitar syndrome results in a left-to-right shunt, which can lead to cyanosis and may require surgical correction. Consequently the patients are often symptomatic and present at a young age. In contrast, there is no left-to-right shunt in MRPV. As in this case, patients are usually asymptomatic, with the diagnosis made incidentally. Treatment has not been required in any reported case of MRPV.

The diagnosis of MRPV has changed drastically thanks to advances in CT technology. Several of the reported cases of MRPV are from the pre-CT era and were investigated with pulmonary angiography and cardiac catheterization, potentially hazardous invasive investigations, particularly considering MRPV is a benign condition requiring no treatment. Of those cases which underwent CT, the older CT technology at the time often did not allow detailed multiplanar reformatting (MPR), limiting the assessment of the anatomy, and therefore necessitating invasive imaging to confirm the diagnosis. This case highlights that non-invasive diagnosis is possible with modern multislice CT technology through the use of detailed MPR and maximum intensity projections, which clearly demonstrate vessel anatomy (Figure 2). Additionally, accurate assessment of lung volumes is possible with modern CT software, allowing assessment of associated lung hypoplasia.

In conclusion, this case highlights that the chest X-ray features of scimitar syndrome are not diagnostic and a MRPV should be considered in their presence. Differentiation between these conditions is required to help decide whether treatment is necessary. Modern multislice CT technology allows clear depiction of the vascular connections and associated anatomy, and has superseded invasive pulmonary angiography and cardiac catheterization as the investigation of choice for MRPV.

REFERENCES

1 **Sanger PW**, Taylor FH, Robicsek F. The "scimitar syndrome". Diagnosis and treatment. *Arch Surg* 1963; **86**: 580-587 [PMID: 13976294 DOI: 10.1001/archsurg.1963.01310100064010]

2 **Neill CA**, Ferencz C, Sabiston DC, Sheldon H. The familial occurrence of hypoplastic right lung with systemic arterial supply and venous drainage "scimitar syndrome". *Bull Johns Hopkins Hosp* 1960; **107**: 1-21 [PMID: 14426379]

3 **Gwinn JL**, Barnes GR. The scimitar syndrome. Anomalies of great vessels associated with lung hypoplasia. *Am J Dis Child* 1967; **114**: 585-586 [PMID: 6058055]

4 **Morgan JR**, Forker AD. Syndrome of hypoplasia of the right lung and dextroposition of the heart: "scimitar sign" with normal pulmonary venous drainage. *Circulation* 1971; **43**: 27-30 [PMID: 5540849 DOI: 10.1161/01.CIR.43.1.27]

5 **Herer B**, Jaubert F, Delaisements C, Huchon G, Chretien J. Scimitar sign with normal pulmonary venous drainage and anomalous inferior vena cava. *Thorax* 1988; **43**: 651-652 [PMID: 3175980 DOI: 10.1136/thx.43.8.651]

6 **Everhart FJ**, Korns ME, Amplatz K, Edwards JE. Intrapulmonary segment in anomalous pulmonary venous connection. Resemblance to scimitar syndrome. *Circulation* 1967; **35**: 1163-1169 [PMID: 6026204 DOI: 10.1161/01.CIR.35.6.1163]

7 **Goodman LR**, Jamshidi A, Hipona FA. Meandering right pulmonary vein simulating the Scimitar syndrome. *Chest* 1972; **62**: 510-512 [PMID: 5078012 DOI: 10.1378/chest.62.4.510]

8 **Collins DR**, Shea PM, Vieweg WV. Idiopathic prominence of pulmonary veins on chest x-ray. *Angiology* 1982; **33**: 613-616 [PMID: 7125297 DOI: 10.1177/000331978203300907]

9 **Kriss VM**, Woodring JH, Cottrill CM. "Meandering" pulmonary veins: report of a case in an asymptomatic 12-year-old girl. *J Thorac Imaging* 1995; **10**: 142-145 [PMID: 7769631 DOI: 10.1097/00005382-199521000-00013]

10 **Gazzaniga AB**, Matloff JM, Harken DE. Anomalous right pulmonary venous drainage into the inferior vena cava and left atrium. *J Thorac Cardiovasc Surg* 1969; **57**: 251-254 [PMID: 5764132]

11 **Takeda S**, Imachi T, Arimitsu K, Minami M, Hayakawa M. Two cases of scimitar variant. *Chest* 1994; **105**: 292-293 [PMID: 8275753 DOI: 10.1378/chest.105.1.292]

12 **Tortoriello TA**, Vick GW, Chung T, Bezold LI, Vincent JA. Meandering right pulmonary vein to the left atrium and inferior vena cava: the first case with associated anomalies. *Tex Heart Inst J* 2002; **29**: 319-323 [PMID: 12484618]

13 **Pearl W**. Scimitar variant. *Pediatr Cardiol* 1987; **8**: 139-141 [PMID: 3628070 DOI: 10.1007/BF02079472]

14 **Salazar-Mena J**, Salazar-Gonzalez J, Salazar-Gonzalez E. Meandering right pulmonary vein: a case of scimitar variant. *Pediatr Radiol* 1999; **29**: 578-580 [PMID: 10415180 DOI: 10.1007/s002470050651]

15 **Kanemoto N**, Sugiyama T, Hirose S, Goto Y. A case with pseudo-scimitar syndrome: "scimitar sign" with normal pulmonary venous drainage. *Jpn Circ J* 1987; **51**: 642-646 [PMID:

3669271 DOI: 10.1253/jcj.51.642]
16 **Engelke C**, Brown K, Sabharwal T, Reidy JF. Anomalous unilateral single pulmonary vein masquerading as a pulmonary arteriovenous malformation. *AJR Am J Roentgenol* 2001; **176**: 1333 [PMID: 11312210 DOI: 10.2214/ajr.176.5.1761333]
17 **Rey C**, Vaksmann G, Francart C. Anomalous unilateral single pulmonary vein mimicking partial anomalous pulmonary venous return. *Cathet Cardiovasc Diagn* 1986; **12**: 330-333 [PMID: 3791408 DOI: 10.1002/ccd.1810120511]
18 **Gilkeson RC**, Haaga JR, Ciancibello LM. Anomalous unilateral single pulmonary vein: multidetector CT findings. *AJR Am J Roentgenol* 2000; **175**: 1464-1465 [PMID: 11044066 DOI: 10.2214/ajr.175.5.1751464]
19 **Tsitouridis I**, Tsinoglou K, Morichovitou A, Stratilati S, Siouggaris N, Kontaki T. Scimitar syndrome versus meandering pulmonary vein: evaluation with three-dimensional computed tomography. *Acta Radiol* 2006; **47**: 927-932 [PMID: 17077042 DOI: 10.1080/02841850600885401]
20 **Yoo SJ**, Al-Otay A, Babyn P. The relationship between scimitar syndrome, so-called scimitar variant, meandering right pulmonary vein, horseshoe lung and pulmonary arterial sling. *Cardiol Young* 2006; **16**: 300-304 [PMID: 16725070 DOI: 10.1017/S1047951106000461]
21 **Cukier A**, Kavakama J, Teixeira LR, Terra-Filho M, Vargas FS. Scimitar sign with normal pulmonary venous drainage and systemic arterial supply. Scimitar syndrome or bronchopulmonary sequestration? *Chest* 1994; **105**: 294-295 [PMID: 8275754 DOI: 10.1378/chest.105.1.294]
22 **Holt PD**, Berdon WE, Marans Z, Griffiths S, Hsu D. Scimitar vein draining to the left atrium and a historical review of the scimitar syndrome. *Pediatr Radiol* 2004; **34**: 409-413 [PMID: 14872299 DOI: 10.1007/s00247-004-1149-0]
23 **Siu CW**, Cheung SC, Chan CW, Jim MH, Tse HF. Contrast-enhanced computed tomography of adult scimitar syndrome (variant form). *Asian Cardiovasc Thorac Ann* 2009; **17**: 662 [PMID: 20026550 DOI: 10.1177/0218492309348643]
24 **Al-Naami GH**, Abu-Sulaiman RM. A familial variant of the Scimitar syndrome with a meandering pulmonary vein. *Cardiol Young* 2006; **16**: 308-309 [PMID: 16725072 DOI: 10.1017/S1047951106000485]

P- Reviewers Ma CS, Marchiori E **S- Editor** Gou SX
L- Editor A **E- Editor** Xiong L

World Journal of Radiology

Online Submissions: http://www.wjgnet.com/esps/
wjr@wjgnet.com
doi:10.4329/wjr.v5.i5.220

World J Radiol 2013 May 28; 5(5): 220-225
ISSN 1949-8470 (online)

CASE REPORT

Sonographic assessment of a suspected biloma: A case report and review of the literature

Claudio Tana, Patrizio D'Alessandro, Armando Tartaro, Marco Tana, Andrea Mezzetti, Cosima Schiavone

Claudio Tana, Patrizio D'Alessandro, Cosima Schiavone, Unit of Internistic Ultrasound, "G. d'Annunzio" University, 66013 Chieti Scalo (CH), Italy
Claudio Tana, Marco Tana, Andrea Mezzetti, Cosima Schiavone, Department of Medicine and Science of Aging, "G. d' Annunzio" University, 66013 Chieti Scalo (CH), Italy
Armando Tartaro, Department of Neurosciences and Imaging, "G. d'Annunzio" University, 66013 Chieti Scalo (CH), Italy
Author contributions: All authors made substantial contributions to conception and design of the manuscript, they were involved in drafting the article and revising it critically for important intellectual content,and gave final approval of the version to be published.
Correspondence to: Cosima Schiavone, Professor, Department of Medicine and Science of Aging, "G. d'Annunzio" University, Via dei Vestini 29, 66013 Chieti Scalo (CH), Italy. cschiavone@unich.it
Telephone: +39-871-358576 Fax: +39-871-358969
Received: March 12, 2013 Revised: April 11, 2013
Accepted: May 16, 2013
Published online: May 28, 2013

Abstract

A biloma is a rare disease characterized by an abnormal intra- or extrahepatic bile collection due to a traumatic or spontaneous rupture of the biliary system. Laboratory findings are nonspecific. The diagnosis is usually suspected on the basis of a typical history (right upper quadrant abdominal pain, chills, fever and recent abdominal trauma or surgery) and is confirmed by detection of typical radiologic features. We report the case of a patient with a history of previous cholecystectomy for lithiasis who presented with clinical symptoms and laboratory data suggestive of acute pancreatitis. Imaging studies also revealed the presence of a chronic and asymptomatic biloma, which could be mistaken for a pseudocyst. The atypical location and ultrasound findings suggested an alternative diagnosis. We therefore reviewed the known literature for bilomas, focusing on the role of ultrasonography, which can reveal some typical aspects, such as location and imaging features. We conclude that ultrasound plays a key role in the assessment of a suspected biloma in patients with appropriate history and clinical features and provides valuable diagnostic clues even in the absence of these.

Key words: Biloma; Bile leakage; Ultrasound; Focused assessment with sonography for trauma; Contrast-enhanced ultrasound; Magnetic resonance cholangiography

Core tip: We report the case of a patient with a history of previous cholecystectomy for lithiasis who presented with a clinical picture suggestive of acute pancreatitis. Imaging studies revealed the presence of an asymptomatic biloma, which could be mistaken for a pseudocyst. We therefore reviewed the literature, focusing on the role of ultrasonography, which can reveal some typical aspects, such as location and imaging features. We conclude that ultrasound plays a key role in the assessment of a suspected biloma in patients with appropriate history and clinical features and provides valuable diagnostic clues even in the absence of these.

Tana C, D'Alessandro P, Tartaro A, Tana M, Mezzetti A, Schiavone C. Sonographic assessment of a suspected biloma: A case report and review of the literature. *World J Radiol* 2013; 5(5): 220-225 Available from: URL: http://www.wjgnet.com/1949-8470/full/v5/i5/220.htm DOI: http://dx.doi.org/10.4329/wjr.v5.i5.220

INTRODUCTION

A biloma is a rare disease characterized by an abnormal intra- or extrahepatic bile collection secondary to a traumatic or spontaneous rupture of the biliary system. Post-traumatic cases were first reported by Whipple[1], who described the case of a patient kicked by a horse, but the term "biloma" was coined by Gould *et al*[2], who

described a subject with extrahepatic bile leakage in the upper right quadrant of the abdomen after trauma from fighting. In the past, the common bile duct damage after open cholecystectomy was rated about 0.1%. Nowadays, with the laparoscopic technique, rates range from 0.3%-0.6%[3]. In a retrospective study that identified 18 patients with one or more documented intra-abdominal bilomas, the most frequent causes were iatrogenic (n = 16), in particular after cholecystectomy, partial hepatectomy and bile-duct catheter drainage; only two were post-traumatic[4]. After laparoscopic cholecystectomy, most of the lesions occur within 7 d[5]. The majority of minor bilomas resolve spontaneously without further complications[6]. Occasionally, spontaneous rupture of the biliary duct is reported, sometimes associated with choledocholithiasis. Other possible causes are cholangiocarcinomas, acute cholecystitis, tuberculosis, hepatic abscesses or infarctions. Rarely, an association with pancreatic cancer is described[7,8]. Biloma can complicate sickle cell disease[9,10]. The clinical features consist primarily of pain or abdominal distension, malaise, anorexia, nausea, chills and fever. If associated with choledocholithiasis, the bilomas may occur with jaundice, dark urine and acholic stools. Less frequently they are asymptomatic. Usually the lesions are diagnosed in an average time of 1-2 wk[11].

Laboratory exams may document the presence of neutrophilic leucocytosis and increased values of erythrocyte sedimentation rate and C-reactive protein (CRP), and these may suggest a concomitant cholangitis[7]. Occasionally, abnormal values of aspartate aminotransferase and alanine aminotransferase may be detected[12]. In the presence of jaundice, laboratory tests may show signs of cholestasis (elevation of serum alkaline phosphatase, total and direct bilirubin) as the result of biliary obstruction by gallstones or, less frequently, of extrahepatic biliary ductal compression caused by the biloma[13,14].

The diagnosis is suspected on the basis of the clinical history (*e.g.*, recent cholecystectomy or abdominal trauma), location of the lesion, ultrasound and computed tomography (CT) appearance and can be confirmed by magnetic resonance (MR) cholangiopancreatography and by the features of the material obtained by ultrasonography-guided percutaneous aspiration. The bilomas must be differentiated from other similar findings, such as lymphocele, abscesses, hematomas, pseudocysts, liver cysts and seroma[4]. Gallbladder scintigraphy with technetium-99 may help to differentiate the biloma from hematomas or liver abscesses. Endoscopic retrograde cholangiography may provide not only further diagnostic confirmation but also a therapeutic option, allowing decompression of the bile duct and biliary drainage of the collection[15-19]. In the case of recurrence or persistence of the biloma, more invasive treatment strategies may be considered. In one study, surgical treatment was found to be associated with a higher complication rate[17]. If the collection is well confined or if there are small residual gallstones, surgical access by subcostal laparotomy is appropriate[20,21]. In case of bile leakage arising after hepatectomy, percutaneous transhepatic biliary drainage is the treatment of choice[21]. Kyoden *et al*[22] evaluated the use of prophylactic abdominal drainage performed in 1269 consecutive cases of elective liver resection in order to reduce the frequency of the development of subphrenic fluid collections and bile leakage. Placement of drains was effective in a significant number of patients undergoing hepatectomy.

CASE REPORT

A 72-year-old woman was admitted to our Hospital for the persistence, from the day before, of acute and stabbing epigastric pain, not associated with nausea, vomiting, diarrhea or fever. The patient did not report unusual food intake or recent travel. She reported a history of ischemic heart disease, previous multiple pulmonary infarctions treated with oral anticoagulants, type 2 diabetes mellitus in good metabolic control, Hashimoto's thyroiditis and a past history of cholecystectomy for lithiasis (12 years before). The physical examination revealed the presence of evoked pain by deep palpation in the epigastrium and torpid peristalsis. The remaining examination was normal. Laboratory tests documented fasting hyperglycemia (> 200 mg/dL), hyperamylasemia (3420 U/L), increased values of lipase (24667 U/L), CRP (8.3 mg/dL) and leukocytosis (14000/mL) with neutrophilia. Hemoglobin, serum electrolytes, indices of cholestasis, liver enzymes and cardiac markers were normal. An electrocardiogram, performed in the emergency room, showed signs of previous myocardial infarction. Abdominal X-ray showed poor distension of the bowel loops in the absence of other findings. An ultrasound examination of the upper abdomen revealed, in the Ⅳ hepatic segment and in proximity of the site of previous cholecystectomy, the presence of a heterogeneous hypo-anechoic rounded lesion, with a maximum size of 3.89 cm × 3.42 cm and hyperechoic, calcified walls; it was equipped with numerous hyperechoic debris generating acoustic shadow (Figure 1A). The lesion did not demonstrate an increase in color Doppler signal (Figure 1B). The pancreas showed a normal size with heterogeneous echotexture and blurred margins. The clinical, laboratory and pancreatic ultrasound findings were suggestive for acute pancreatitis. These data were confirmed by a contrast-enhanced abdominal CT, which showed inflammation of the pancreatic tissue and peritoneal effusion. The focal lesion localized in the Ⅳ hepatic segment had a hypodense appearance and did not enhance after intravenous administration of contrast agent (Figure 2). It was bounded by a wall thickening of a few mm and showed a thin septum in its lateral portion. The lesion's appearance was not specific and was not supported by the clinical and laboratory findings, which strongly indicated a diagnosis of acute pancreatitis.

With the establishment of fasting and appropriate supportive care, the patient became asymptomatic again with optimal values of pancreatic function. However, the hepatic lesion persisted despite adequate treatment and was not due to simple pseudocyst, because of the atypical location and appearance. At magnetic resonance imaging

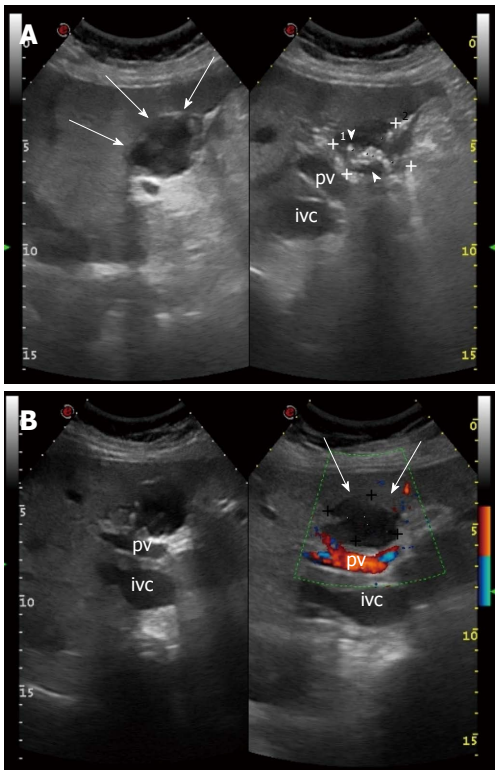

Figure 1 Chronic biloma in a 72-year-old woman: ultrasound findings. A: Oblique view shows a heterogeneous hypo-anechoic rounded lesion with hyperechoic, calcified walls (arrows), numerous hyperechoic debris generating acustic shadow (arrow heads) and maximum size of 3.89 cm (caliper 1) × 3.42 cm (caliper 2); B: Color Doppler sonogram shows absence of vascularity inside the lesion (arrows). pv: Portal vein; ivc: Inferior vena cava.

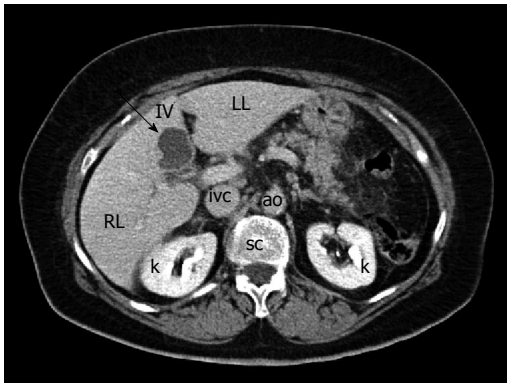

Figure 2 Computed tomography shows the biloma as a hypodense lesion in the Ⅳ hepatic segment, characterized by absence of enhancement after administration of intravenous contrast agent (arrow). RL: Right hepatic lobe; LL: Left hepatic lobe; Ⅳ: Fourth hepatic segment; k: Kidney; ivc: Inferior vena cava; ao: Aorta; sc: Spinal column.

(MRI) the lesion appeared intense on T_1-weighted images and hyperintense on T_2-weighted images (Figure 3A). In addition, because of its location in proximity of the site of the previous cholecystectomy, a contrast-enhanced MR cholangiopancreatography was performed, which revealed a close proximity between the lesion and the stump of the remnant cystic duct. The lesion seemed to arise posteriorly to the confluence of the right and left hepatic ducts into the common hepatic duct (Figure 3B).

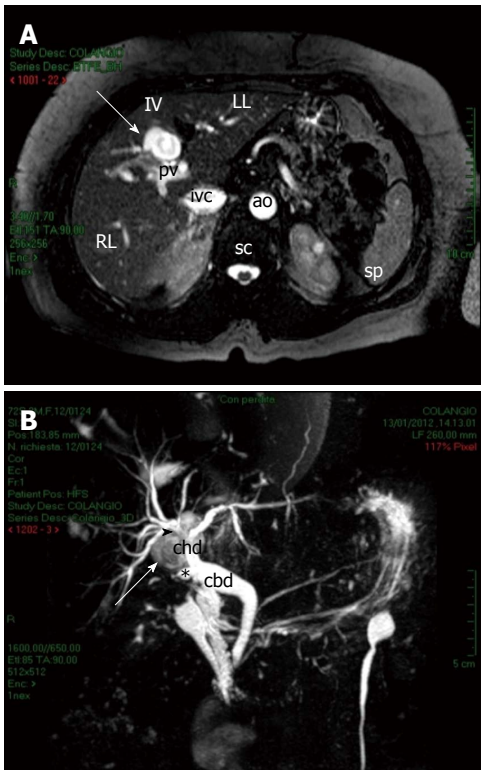

Figure 3 Biloma features on magnetic resonance imaging. A: On T_2-weighted images, the biloma appeared as a hyperintense lesion located in the Ⅳ hepatic segment (arrow); B: Contrast enhanced magnetic resonance cholangiopancreatography shows the biloma as a well-defined, rounded lesion (arrow) arising posteriorly to the confluence of right and left hepatic ducts into the common hepatic duct (arrowhead) in proximity to the stump of the remnant cystic duct (star). RL: Right hepatic lobe; LL: Left hepatic lobe; Ⅳ: Fourth hepatic segment; ivc: Inferior vena cava; ao: Aorta; pv: Portal vein; sc: Spinal column; sp: Spleen; chd: Common hepatic duct; cbd: Common bile duct.

Biloma was diagnosed. Considering the surgical risk of the patient and the fact that the lesion was found many years after cholecystectomy, the surgeon did not advise intervention. The patient is undergoing follow-up with ultrasonography every 6 mo to confirm the stability of the lesion over time.

DISCUSSION

Role of ultrasonography in the assessment of bilomas

Vazquez *et al*[4] identified 21 bilomas in eighteen patients, using ultrasound, CT or both. A solitary bile collection was found in fifteen patients, while two distinct bilomas were detected in three patients each. Width, depth, and axial length ranged from 2 cm × 2 cm × 3 cm to 10 cm × 19 cm × 25 cm, respectively. The maximal transverse diameter was ⩽ 5 cm, between 6 and 10 cm and greater than 10 cm in four, eight and eight bilomas, respectively. Sixteen of these were located in the right upper quadrant of the abdomen, four of which were intrahepatic, six subhepatic, and six subphrenic. The last five were located in the left upper quadrant of the abdomen[4]. Therefore, the right quadrant is more frequently affected[7].

Ultrasound plays a key role in diagnosis of bilomas, representing the first instance investigation[3,15,23,24], with

the advantage of being a non-invasive and rapidly executable exam. This factor is particularly important in post-traumatic cases, where a rapid diagnosis is essential for subsequent therapeutic intervention. Focused assessment with sonography for trauma (FAST) is indicated for screening hemodynamically stable patients with blunt abdominal trauma; in low-grade injuries it may disclose or exclude a potentially unknown pathology, such as bile leaks, free peritoneal fluid and hematomas with a positive cost-to-benefit ratio and high negative predictive value[25-27]. In high-grade injuries, ultrasound may be useful in association with CT for definitive interval assessment[26].

This method is able to show the presence of single or multiple well circumscribed anechoic lesions with prominent distal sonic enhancement[23]. These may contain a small amount of debris or have few septa but are usually devoid of capsules. They are sometimes surrounded by a thin rim which is thicker in the case of longer duration bilomas. The accuracy of ultrasonographic findings in the diagnosis of biloma is enhanced by the clinical pre-test probability, based on a thorough clinical-anamnestic assessment[24]. In the presence of a history of recent trauma or interventions such as cholecystectomy and hepatectomy, usually associated with clinical features (pain or abdominal distension, jaundice, chills, fever) and laboratory abnormalities, the ultrasound finding of well-delimited anechoic lesions in typical locations (sub- or intrahepatic or subphrenic) may suggest the presence of biloma. In this context, ultrasonography-guided percutaneous aspiration can attain a significant diagnostic value; a high aspirated fluid/serum bilirubin ratio is strongly suggestive of bile leakage and can confirm the diagnosis[27]. It may also be useful as a therapeutic option but is associated with discomfort and infection, whereas surgery, which is usually limited to refractory cases, has high morbidity and mortality rates. Therefore, Shami *et al*[28] recently suggested the use of endoscopic ultrasound (EUS) to drain bilomas, obtaining promising results. In this study, a total of five patients underwent EUS-guided transenteric drainage of symptomatic bilomas adjacent to the gastrointestinal lumen. The method included transenteric EUS-guided puncture, placement of a guidewire into the biloma and creation of an enteral-biloma fistula with positioning of a plastic endoprosthesis. This technique was successfully performed, resolving the biloma in all five patients, in the absence of significant morbidity. Recently, contrast-enhanced ultrasound (CEUS) has been applied to detect bile leakage by showing the passage of contrast agent into the perihepatic space[29]. The usefulness of this technique has recently been confirmed by Mao *et al*[30] in the diagnosis of biliary leakage following T-tube removal, but further studies with a larger number of patients are necessary to evaluate this new application of CEUS.

Finally, ultrasonography can be useful in the follow-up of patients undergoing drainage or surgery, to evaluate biloma resolution, and in those conservatively treated in order to document lesion stability without further complications[4].

Other imaging studies

CT can confirm the presence of bilomas, which appear as well-confined collections with low intraparenchymal or perihepatic attenuation values[31]. Bilomas are usually clearly delineated by liver margins, diaphragm, mesenteries and other adjacent structures; however, they have no identifiable capsule. Occasionally, they may have a thin rim of 1-2 mm which can be larger in the case of older biloma; it may be enhanced after administration of intravenous contrast agent[4]. CT cannot show bile duct injuries[17]. Sometimes the lesions are associated with the presence of ascitic fluid in the peritoneal cavity[4].

In doubtful cases and/or in the presence of CT contraindications (severe renal insufficiency or iodinated contrast sensitivity), MRI can be a valuable tool to diagnose and differentiate the biloma from other focal liver lesions, such as subacute hematoma: the biloma can appear heterogeneously intense on T_1-weighted images and homogeneously hyperintense on T_2-weighted images, while the hematoma usually appears hyperintense on both T_1- and T_2-weighted MR sequences[32]. Unlike CT, MR cholangiography enhanced with hepatocyte-specific contrast agents can accurately delineate the anatomy of the biliary system and its relationship with a suspected biloma. This method has proved of high diagnostic accuracy in differentiating biliary from nobiliary lesions[33]. Pecchi *et al*[34] have recently found that MR cholangiography can attain sensitivity, specificity, positive and negative predictive values and diagnostic accuracy of 93.5%, 94.4%, 96.7%, 89.5% and 93.9%, respectively, in the diagnosis of biliary complications (*e.g.*, bilomas) after orthotopic liver transplantation. After the administration of gadolinium-ethoxybenzyl-diethylenetriamine pentaacetic acid (Gd-EOB-DTPA), MR cholangiography can reveal an intrahepatic biloma as a liver fluid accumulation with delayed filling of the contrast agent. Furthermore, by demonstrating the passage of contrast material, such as mangafodipir trisodium or Gd-EOB-DTPA, MR cholangiography can clearly outline an extrahepatic biloma[33,35]. In our case, MR cholangiography confirmed the presence of bile leakage, suspected on the basis of ultrasound findings, in the absence of typical history and clinical features.

In an early stage, the gallbladder scintigraphy with technetium-99 can highlight one or more areas of reduced uptake of the radioactive substance, while in the late phase, 2 h after administration, it can document an uptake area. This examination helps to differentiate the biloma from hematomas or liver abscesses but is currently little used[36].

Endoscopic retrograde cholangiography accurately diagnoses the cause of postcholecystectomy bile leakage and biloma formation, at the same time allowing a definitive treatment determining decompression of the bile duct (through a sphincterotomy or nasobiliary endoprosthesis placement) and biliary drainage of the collection[15,17-19].

In conclusion, ultrasonography plays a key role in the assessment of suspected biloma: in patients with a history of recent trauma or hepatobiliary surgery, who present with right upper quadrant abdominal pain, chills, fever or

other symptoms, the finding of single or multiple well circumscribed anechoic lesions with prominent distal sonic enhancement, debris or few septations, located in typical sites (more often subphrenic, subhepatic or intrahepatic) can orient toward the diagnosis, which can be confirmed by second level imaging and/or ultrasonography-guided percutaneous aspiration or endoscopic drainage. The latter can reveal a high aspirated fluid/serum bilirubin ratio, strongly suggestive of bile leakage, also allowing a rapid resolution of the lesion. In doubtful cases, like our patient, sonography may raise the suspicion of biloma, providing precious diagnostic clues, but confirmation with second level imaging, such as MR cholangiography, is needed. Finally, ultrasonography can be a valuable tool to follow-up untreated lesions in order to document their stability or any increase over time.

REFERENCES

1 **Whipple C**. A case of traumatic rupture of the liver: formation of cystic swelling containing bile stained fluid. *Lancet* 1898; **1**: 719 [DOI: 10.1016/S0140-6736(01)87273-1]

2 **Gould L**, Patel A. Ultrasound detection of extrahepatic encapsulated bile: "biloma". *AJR Am J Roentgenol* 1979; **132**: 1014-1015 [PMID: 108953 DOI: 10.2214/ajr.132.6.1014]

3 **Kannan U**, Parshad R, Regmi SK. An unusual presentation of biloma five years following cholecystectomy: a case report. *Cases J* 2009; **2**: 8048 [PMID: 20181203 DOI: 10.1186/1757-1626-0002-0000008048]

4 **Vazquez JL**, Thorsen MK, Dodds WJ, Quiroz FA, Martinez ML, Lawson TL, Stewart ET, Foley WD. Evaluation and treatment of intraabdominal bilomas. *AJR Am J Roentgenol* 1985; **144**: 933-938 [PMID: 3885693 DOI: 10.2214/ajr.144.5.933]

5 **Kozarek R**, Gannan R, Baerg R, Wagonfeld J, Ball T. Bile leak after laparoscopic cholecystectomy. Diagnostic and therapeutic application of endoscopic retrograde cholangiopancreatography. *Arch Intern Med* 1992; **152**: 1040-1043 [PMID: 1533759 DOI: 10.1001/archinte.1992.00400170118022]

6 **Dev V**, Shah D, Gaw F, Lefor AT. Gastric outlet obstruction secondary to post cholecystectomy biloma: case report and review of the literature. *JSLS* 1998; **2**: 185-188 [PMID: 9876736]

7 **Bas G**, Okan I, Sahin M, Eryılmaz R, Isık A. Spontaneous biloma managed with endoscopic retrograde cholangiopancreatography and percutaneous drainage: a case report. *J Med Case Rep* 2011; **5**: 3 [PMID: 21210994 DOI: 10.1186/1752-1947-5-3]

8 **Trivedi PJ**, Gupta P, Phillips-Hughes J, Ellis A. Biloma: an unusual complication in a patient with pancreatic cancer. *World J Gastroenterol* 2009; **15**: 5218-5220 [PMID: 19891023 DOI: 10.3748/wjg.15.5218]

9 **Middleton JP**, Wolper JC. Hepatic biloma complicating sickle cell disease. A case report and a review of the literature. *Gastroenterology* 1984; **86**: 743-744 [PMID: 6698374]

10 **Lebensburger J**, Esbenshade A, Blakely M, Hankins J, Wang W. Biloma and pneumobilia in sickle cell disease. *Pediatr Blood Cancer* 2008; **51**: 288-290 [PMID: 18421713 DOI: 10.1002/pbc.21575]

11 **Carroll BJ**, Birth M, Phillips EH. Common bile duct injuries during laparoscopic cholecystectomy that result in litigation. *Surg Endosc* 1998; **12**: 310-313; discussion 314 [PMID: 9543519 DOI: 10.1007/s004649900660]

12 **Lee JH**, Suh JI. A case of infected biloma due to spontaneous intrahepatic biliary rupture. *Korean J Intern Med* 2007; **22**: 220-224 [PMID: 17939343 DOI: 10.3904/kjim.2007.22.3.220]

13 **Mansour AY**, Stabile BE. Extrahepatic biliary obstruction due to post-laparoscopic cholecystectomy biloma. *JSLS* 2000; **4**: 167-171 [PMID: 10917126]

14 **Cólović R**, Perisić-Savić M. Retroperitoneal biloma secondary to operative common bile duct injury. *HPB Surg* 1991; **3**: 193-197 [PMID: 2043516 DOI: 10.1155/1991/39181]

15 **Mergener K**, Strobel JC, Suhocki P, Jowell PS, Enns RA, Branch MS, Baillie J. The role of ERCP in diagnosis and management of accessory bile duct leaks after cholecystectomy. *Gastrointest Endosc* 1999; **50**: 527-531 [PMID: 10502175 DOI: 10.1016/S0016-5107(99)70077-5]

16 **Bala M**, Gazalla SA, Faroja M, Bloom AI, Zamir G, Rivkind AI, Almogy G. Complications of high grade liver injuries: management and outcomewith focus on bile leaks. *Scand J Trauma Resusc Emerg Med* 2012; **20**: 20 [PMID: 22444252 DOI: 10.1186/1757-7241-20-20]

17 **Mizuno O**, Kawamoto H, Fukatsu H, Harada R, Tsutsumi K, Fujii M, Kurihara N, Nakanishi T, Ogawa T, Ishida E, Okada H, Sakaguchi K. An iatrogenic hepatic subcapsular biloma successfully treated by percutaneous drainage and endoscopic biliary stenting. *Endoscopy* 2008; **40** (Suppl 2): E42-E43 [PMID: 18300200 DOI: 10.1055/s-2007-966852]

18 **Christoforidis E**, Vasiliadis K, Goulimaris I, Tsalis K, Kanellos I, Papachilea T, Tsorlini E, Betsis D. A single center experience in minimally invasive treatment of postcholecystectomy bile leak, complicated with biloma formation. *J Surg Res* 2007; **141**: 171-175 [PMID: 17499275 DOI: 10.1016/j.jss.2006.07.012]

19 **Miro AG**, De Seta C, Arenga G, Russo M, Lombardi D. Treatment of major iatrogenic lesions of the bile ducts. *Ann Ital Chir* 2002; **73**: 35-39 [PMID: 12148420]

20 **Nordin A**, Halme L, Mäkisalo H, Isoniemi H, Höckerstedt K. Management and outcome of major bile duct injuries after laparoscopic cholecystectomy: from therapeutic endoscopy to liver transplantation. *Liver Transpl* 2002; **8**: 1036-1043 [PMID: 12424717 DOI: 10.1053/jlts.2002.35557]

21 **Hoekstra LT**, van Gulik TM, Gouma DJ, Busch OR. Posthepatectomy bile leakage: how to manage. *Dig Surg* 2012; **29**: 48-53 [PMID: 22441620 DOI: 10.1159/000335734]

22 **Kyoden Y**, Imamura H, Sano K, Beck Y, Sugawara Y, Kokudo N, Makuuchi M. Value of prophylactic abdominal drainage in 1269 consecutive cases of elective liver resection. *J Hepatobiliary Pancreat Sci* 2010; **17**: 186-192 [PMID: 19727544 DOI: 10.1007/s00534-009-0161-z]

23 **Esensten M**, Ralls PW, Colletti P, Halls J. Posttraumatic intrahepatic biloma: sonographic diagnosis. *AJR Am J Roentgenol* 1983; **140**: 303-305 [PMID: 6600348 DOI: 10.2214/ajr.140.2.303]

24 **Sgourakis G**, Lanitis S, Korontzi M, Kontovounisios C, Zacharioudakis C, Armoutidis V, Karaliotas C, Dedemadi G, Lepida N, Karaliotas C. Incidental findings in focused assessment with sonography for trauma in hemodynamically stable blunt trauma patients: speaking about cost to benefit. *J Trauma* 2011; **71**: E123-E127 [PMID: 22182913 DOI: 10.1097/TA.0b013e3182249eaa]

25 **Kornezos I**, Chatziioannou A, Kokkonouzis I, Nebotakis P, Moschouris H, Yiarmenitis S, Mourikis D, Matsaidonis D. Findings and limitations of focused ultrasound as a possible screening test in stable adult patients with blunt abdominal trauma: a Greek study. *Eur Radiol* 2010; **20**: 234-238 [PMID: 19662419 DOI: 10.1007/s00330-009-1516-1]

26 **Chiu WC**, Wong-You-Cheong JJ, Rodriguez A, Shanmuganathan K, Mirvis SE, Scalea TM. Ultrasonography for interval assessment in the nonoperative management of hepatic trauma. *Am Surg* 2005; **71**: 841-846 [PMID: 16468532]

27 **Ahn YJ**, Kim TH, Moon SW, Choi SN, Kim HJ, Jung WT, Lee OJ, Ko GH. [A case of perforated xanthogranulomatous cholecystitis presenting as biloma]. *Korean J Gastroenterol* 2011; **58**: 153-156 [PMID: 21960104 DOI: 10.4166/kjg.2011.58.3.153]

28 **Shami VM**, Talreja JP, Mahajan A, Phillips MS, Yeaton P, Kahaleh M. EUS-guided drainage of bilomas: a new alternative? *Gastrointest Endosc* 2008; **67**: 136-140 [PMID: 18155436 DOI: 10.1016/j.gie.2007.07.040]

29 **Ignee A**, Baum U, Schuessler G, Dietrich CF. Contrast-enhanced ultrasound-guided percutaneous cholangiography and cholangiodrainage (CEUS-PTCD). *Endoscopy* 2009; **41**: 725-726 [PMID: 19670143 DOI: 10.1055/s-0029-1214956]

30 **Mao R**, Xu EJ, Li K, Zheng RQ. Usefulness of contrast-enhanced ultrasound in the diagnosis of biliary leakage following T-tube removal. *J Clin Ultrasound* 2010; **38**: 38-40 [PMID: 19670237 DOI: 10.1002/jcu.20622]

31 **Yoon W**, Jeong YY, Kim JK, Seo JJ, Lim HS, Shin SS, Kim JC, Jeong SW, Park JG, Kang HK. CT in blunt liver trauma. *Radiographics* 2005; **25**: 87-104 [PMID: 15653589 DOI: 10.1148/rg.251045079]

32 **Shigemura T**, Yamamoto F, Shilpakar SK, Kojima T, Yamamoto S, Pu Y. MRI differential diagnosis of intrahepatic biloma from subacute hematoma. *Abdom Imaging* 1995; **20**: 211-213 [PMID: 7620407 DOI: 10.1007/BF00200396]

33 **Lee NK**, Kim S, Lee JW, Lee SH, Kang DH, Kim GH, Seo HI. Biliary MR imaging with Gd-EOB-DTPA and its clinical applications. *Radiographics* 2009; **29**: 1707-1724 [PMID: 19959517 DOI: 10.1148/rg.296095501]

34 **Pecchi A**, De Santis M, Di Benedetto F, Gibertini M, Gerunda G, Torricelli P. Role of magnetic resonance cholangiography in biliary complications of orthotopic liver transplantation. *Radiol Med* 2010; **115**: 1065-1079 [PMID: 20680501 DOI: 10.1007/s11547-010-0563-7]

35 **Park MS**, Kim KW, Yu JS, Kim MJ, Kim KW, Lim JS, Cho ES, Yoon DS, Kim TK, Lee SI, Lee JD, Lee WJ, Ha HK, Lee JT, Yoo HS. Early biliary complications of laparoscopic cholecystectomy: evaluation on T2-weighted MR cholangiography in conjunction with mangafodipir trisodium-enhanced 3D T1-weighted MR cholangiography. *AJR Am J Roentgenol* 2004; **183**: 1559-1566 [PMID: 15547191 DOI: 10.2214/ajr.183.6.01831559]

36 **Barbuscia M**, Ilaqua A, Lemma G, Righettoni A, Nucera D, Sanò M, Pergolizzi FP. [A complication in biliary surgery: the biloma]. *G Chir* 2010; **31**: 523-526 [PMID: 21232197]

P- Reviewers Deter R, Liu YY **S- Editor** Gou SX
L- Editor A **E- Editor** Ma S

World Journal of Radiology

Online Submissions: http://www.wjgnet.com/esps/
wjr@wjgnet.com
doi:10.4329/wjr.v5.i5.226

World J Radiol 2013 May 28; 5(5): 226-228
ISSN 1949-8470 (online)

CASE REPORT

Occlusion of the anterior cerebral artery after head trauma

Wellingson Silva Paiva, Almir Ferreira de Andrade, Matheus Schmidt Soares, Robson Luis Amorim, Eberval Gadelha Figueiredo, Manoel Jacobsen Teixeira

Wellingson Silva Paiva, Almir Ferreira de Andrade, Matheus Schmidt Soares, Robson Luis Amorim, Eberval Gadelha Figueiredo, Manoel Jacobsen Teixeira, Division of Neurological Surgery, Hospital Das Clinicas University of Sao Paulo Medical School, Sao Paulo 05406000, Brazil
Author contributions: Paiva WS, de Andrade AF, Soares MS and Amorim RL had a substantial contributions to conception and design, acquisition and interpretation of data; Figueiredo EG and Teixeira MJ worked in drafting the article and revising it critically for important intellectual content.
Correspondence to: Wellingson Silva Paiva, MD, FRSM, Division of Neurological Surgery, Hospital Das Clinicas University of Sao Paulo Medical School, Eneas Aguiar Street N 255, Sao Paulo 05406000, Brazil. wellingsonpaiva@yahoo.com.br
Telephone: +55-11-25486900 Fax: +55-11-25486906
Received: February 2, 2011 Revised: April 1, 2011
Accepted: April 8, 2011
Published online: May 28, 2013

Abstract

Intracranial arterial occlusion is rarely encountered in association with head injury. Only six cases of traumatic occlusion of the anterior cerebral artery (ACA) have previously been reported. In this paper, the authors describe a case of a posttraumatic occlusion of ACA. A 35-year-old male presented to the emergency room with severe head injury. Computed tomography (CT) scan displayed diffuse brain swelling with multiple skull fractures. Follow up CT scan showed extensive cerebral infarction in the territory of ACA. The patient underwent CT angiography that demonstrated occlusion of the ACA by a fracture of the anterior fossa. He died after 3 d. ACA traumatic occlusion is a rare condition, with poor prognosis. In this case, fracture was responsible for dissection and direct obstruction of the artery.

Key words: Anterior cerebral artery; Brain vascular trauma; Arterial occlusion; Computed tomography; Neurological diagnostic techniques; Brain injury

Paiva WS, de Andrade AF, Soares MS, Amorim RL, Figueiredo EG, Teixeira MJ. Occlusion of the anterior cerebral artery after head trauma. *World J Radiol* 2013; 5(5): 226-228 Available from: URL: http://www.wjgnet.com/1949-8470/full/v5/i5/226.htm DOI: http://dx.doi.org/10.4329/wjr.v5.i5.226

INTRODUCTION

Intracranial arterial occlusion is rare associated with head injury[1,2]. The incidence of this condition with cerebral ischemia in the literature range from 0.2% to 1.6%[3,4]. Most injuries occur in the internal carotid artery, followed by the middle cerebral artery and the vertebrobasilar vessels[1,5]. Occlusion of the anterior cerebral artery (ACA) from head trauma is extremely uncommon. Six cases of traumatic occlusion of the ACA have been reported in literature[1-4,6,7]. In this paper the authors describe a case of severe head injury associated with traumatic occlusion of the ACA.

CASE REPORT

A 35-year-old male was admitted to the emergency room following a motorcycle accident. On admission his Glasgow Coma Score was 4, and he presented isochoric pupils, without systemic lesion. Immediate head multislice computed tomography (CT) scan was performed and showed diffuse brain swelling with multiple skull fractures, included one in the skull base (Figure 1).

The patient developed mydriatic pupils after 24 h and an extensive cerebral infarction in the territory of ACA was found in the CT scan (Figure 2). Patient underwent CT angiography that demonstrated occlusion of the ACA caused by a fracture of the anterior fossa, with partial obstruction of the right and left branches, indicating a traumatic occlusion (Figure 3). Patient deceased after 3 d despite of medical management and intracranial pressure monitoring.

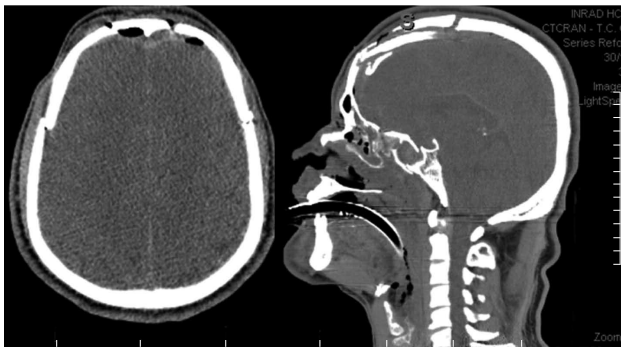

Figure 1 Computed tomography scan showed diffuse brain swelling with multiple skull fractures, including one in the anterior fossa.

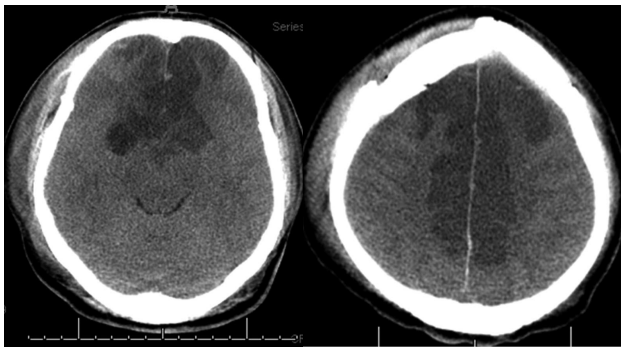

Figure 2 Follow up computed tomography scan showed extensive cerebral infarction in the territory of anterior cerebral artery.

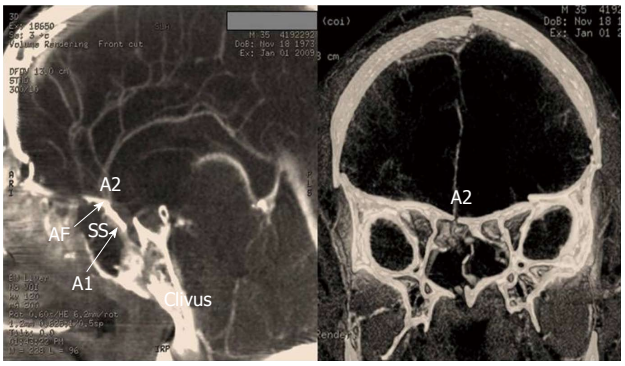

Figure 3 Multislice computed tomography angiography showed occlusion of the anterior cerebral artery adjacent to a fracture in the anterior fossa. AF: Anterior Fossa; A1: First segment of anterior cerebral artery; A2: Second segment of anterior cerebral artery; SS: Sphenoid sinus.

DISCUSSION

Fatal ACA infarct was encountered in half of the reported cases. Only one patient survived without neurological deficits. All patients except one sustained their injury in a road accident. In our patients a severe trauma following motorcycle accident indicates a high energy trauma mechanism.

The initial diagnosis is often delayed because of the low incidence of traumatic ACA occlusion[1]. Lucid intervals are common in patients with traumatic arterial obstruction[3,6]. However in this case, the authors believe that axonal diffuse injury associated with arterial lesion were responsible for the coma, with no lucid interval.

Outcome is generally poor. Three patients died, and one remained in persistent vegetative state. Mechanisms such as direct injury, dissecting aneurysm, thrombosis, and embolism have been reported as cause for intracranial vessel occlusion in association with head injury[1,3]. In this case, occlusion probably was caused by dissection and direct obstruction of artery by fracture. We believe that the extensive line of fracture at the base of the anterior fossa and sella resulted in partial traumatic occlusion by clamping of both anterior cerebral arteries in A1 and A2 segment. The ACA and the terminal branch of internal carotid artery, its first segment, designated A1 presents length ranging from 10 to 20 mm, an average of 15 mm[8]. This segment goes on the optic chiasm in 17% and on the nerve in 83%, while the A2 segment goes hand in hand in 26%[8], as we believe occurred in our patient, which allowed bilateral compression with elevation of bone the fracture and thus clamping these vessels.

Vasospasm is another factor in the pathogenesis of intracranial artery occlusion[9]. Spasm following traumatic subarachnoid hemorrhage is most common in the distal portion of the internal carotid artery and the proximal portion of the middle cerebral artery and ACA[10,11]. The reported incidence of intracranial arterial spasm following moderate to severe head injury range from 5% to 10%[10]. In this patient, presence of early hypodensity on CT skull do not favor spasm as the primary mechanism, nonetheless one may not totally exclude it, mainly in the terminal branches of the anterior cerebral arteries.

REFERENCES

1 **Amagasa M**, Sato S, Shimizu Y, Otabe K, Onuma T. [Post-traumatic occlusion of the anterior cerebral artery]. *No Shinkei Geka* 1988; **16**: 103-107 [PMID: 3362294]
2 **Dratz HM**, Woodhall B. Traumatic dissecting aneurysm of left internal carotid, anterior cerebral and middle cerebral arteries. *J Neuropathol Exp Neurol* 1947; **6**: 286-291 [PMID: 20254509 DOI: 10.1097/00005072-194707000-00009]
3 **Ishibashi A,** Kubota Y, Yokokura Y, Soejima Y, Hiratsuka T. Traumatic occlusion of the anterior cerebral artery: case report. *Neurol Med Chir* (Tokyo) 1995; **35:** 882-885 [DOI: 10.2176/nmc.35.882]
4 **Iwamoto Y,** Fujimoto M, Nakagawa Y, Yamamoto K. Study of the traumatic cerebral infarcti on. *Kyoto Furitsu Ikadaigaku Zasshi* 1993; **102:** 965-971
5 **De Araujo JC**, De Moraes GP. [Traumatic occlusion of the middle cerebral artery: report of a case]. *Arq Neuropsiquiatr* 1984; **42**: 50-54 [PMID: 6732535]
6 **Levin W.** Vascular lesions in head injuries. *Brit J Surg* 1968; **55:** 321-331 [DOI: 10.1002/bjs.1800550502]
7 **Nelson JW**. Dissecting subintimal hematomas of the intracranial arteries: report of a case. *J Am Osteopath Assoc* 1968; **67**: 512-527 [PMID: 5183587]
8 **Perlmutter D**, Rhoton AL. Microsurgical anatomy of the anterior cerebral-anterior communicating-recurrent artery complex. *J Neurosurg* 1976; **45**: 259-272 [PMID: 948013 DOI: 10.3171/jns.1976.45.3.0259]
9 **Mobbs RJ**, Chandran KN. Traumatic middle cerebral artery occlusion: case report and review of pathogenesis. *Neurol India* 2001; **49**: 158-161 [PMID: 11447436]

10 **Yamada K**, Harada M, Hasegawa S, Ushio Y. Delayed post-traumatic middle cerebral artery vasospasm demonstrated by magnetic resonance angiography: case report. *Neurosurgery* 1998; **43**: 153-156 [PMID: 9657203 DOI: 10.1097/0000612-199807000-00101]
11 **Suwanwela C**, Suwanwela N. Intracranial arterial narrowing and spasm in acute head injury. *J Neurosurg* 1972; **36**: 314-323 [PMID: 5059970 DOI: 10.3171/jns.1972.36.3.0314]

P- Reviewer Luo CB **S- Editor** Cheng JX
L- Editor A **E- Editor** Xiong L

World Journal of Radiology

Online Submissions: http://www.wjgnet.com/esps/
wjr@wjgnet.com
www.wjgnet.com

World J Radiol 2013 May 28; 5(5): I-V
ISSN 1949-8470 (online)

INSTRUCTIONS TO AUTHORS

GENERAL INFORMATION

World Journal of Radiology (*World J Radiol*, *WJR*, online ISSN 1949-8470, DOI: 10.4329) is a peer-reviewed open access (OA) academic journal that aims to guide clinical practice and improve diagnostic and therapeutic skills of clinicians.

Aim and scope

WJR covers topics concerning diagnostic radiology, radiation oncology, radiologic physics, neuroradiology, nuclear radiology, pediatric radiology, vascular/interventional radiology, medical imaging achieved by various modalities and related methods analysis. The current columns of *WJR* include editorial, frontier, diagnostic advances, therapeutics advances, field of vision, mini-reviews, review, topic highlight, medical ethics, original articles, case report, clinical case conference (clinicopathological conference), and autobiography.

We encourage authors to submit their manuscripts to *WJR*. We will give priority to manuscripts that are supported by major national and international foundations and those that are of great basic and clinical significance.

WJR is edited and published by Baishideng Publishing Group (BPG). BPG has a strong professional editorial team composed of science editors, language editors and electronic editors. BPG currently publishes 41 OA clinical medical journals, and is one of the leading medical publishers, with the first-class editing and publishing capacity and production.

Columns

The columns in the issues of *WJR* will include: (1) Editorial: The editorial board members are invited to make comments on an important topic in their field in terms of its current research status and future directions to lead the development of this discipline; (2) Frontier: The editorial board members are invited to select a highly cited cutting-edge original paper of his/her own to summarize major findings, the problems that have been resolved and remain to be resolved, and future research directions to help readers understand his/her important academic point of view and future research directions in the field; (3) Diagnostic Advances: The editorial board members are invited to write high-quality diagnostic advances in their field to improve the diagnostic skills of readers. The topic covers general clinical diagnosis, differential diagnosis, pathological diagnosis, laboratory diagnosis, imaging diagnosis, endoscopic diagnosis, biotechnological diagnosis, functional diagnosis, and physical diagnosis; (4) Therapeutics Advances: The editorial board members are invited to write high-quality therapeutic advances in their field to help improve the therapeutic skills of readers. The topic covers medication therapy, psychotherapy, physical therapy, replacement therapy, interventional therapy, minimally invasive therapy, endoscopic therapy, transplantation therapy, and surgical therapy; (5) Field of Vision: The editorial board members are invited to write commentaries on classic articles, hot topic articles, or latest articles to keep readers at the forefront of research and increase their levels of clinical research. Classic articles refer to papers that are included in Web of Knowledge and have received a large number of citations (ranking in the top 1%) after being published for more than years, reflecting the quality and impact of papers. Hot topic articles refer to papers that are included in Web of Knowledge and have received a large number of citations after being published for no more than 2 years, reflecting cutting-edge trends in scientific research. Latest articles refer to the latest published high-quality papers that are included in PubMed, reflecting the latest research trends. These commentary articles should focus on the status quo of research, the most important research topics, the problems that have now been resolved and remain to be resolved, and future research directions. Basic information about the article to be commented (including authors, article title, journal name, year, volume, and inclusive page numbers); (6) Minireviews: The editorial board members are invited to write short reviews on recent advances and trends in research of molecular biology, genomics, and related cutting-edge technologies to provide readers with the latest knowledge and help improve their diagnostic and therapeutic skills; (7) Review: To make a systematic review to focus on the status quo of research, the most important research topics, the problems that have now been resolved and remain to be resolved, and future research directions; (8) Topic Highlight: The editorial board members are invited to write a series of articles (7-10 articles) to comment and discuss a hot topic to help improve the diagnostic and therapeutic skills of readers; (9) Medical Ethics: The editorial board members are invited to write articles about medical ethics to increase readers' knowledge of medical ethics. The topic covers international ethics guidelines, animal studies, clinical trials, organ transplantation, *etc.*; (10) Clinical Case Conference or Clinicopathological Conference: The editorial board members are invited to contribute high-quality clinical case conference; (11) Original Articles: To report innovative and original findings in radiology; (12) Brief Articles: To briefly report the novel and innovative findings in radiology; (13) Meta-Analysis: Covers the systematic review, mixedtreatment comparison, meta-regression, and overview of reviews, in order to summarize a given quantitative effect, *e.g.*, the clinical effectiveness and safety of clinical treatments by combining data from two or more randomized controlled trials, thereby providing more precise and externally valid estimates than those which would stem from each individual dataset if analyzed separately from the others; (15) Letters to the Editor: To discuss and make reply to the contributions published in *WJR*, or to introduce and comment on a controversial issue of general interest; (16) Book Reviews: To introduce and comment on quality monographs of radiology; and (17) Autobiography: The editorial board members are invited to write their autobiography to provide readers with stories of success or failure in their scientific research career. The topic covers their basic personal information and information about when they started doing research work, where and how they did research work, what they have achieved, and their lessons from success or failure.

Name of journal

World Journal of Radiology

ISSN

ISSN 1949-8470 (online)

Launch date

December 31, 2009

Frequency

Monthly

Editor-in-Chief

Filippo Cademartiri, MD, PhD, FESC, FSCCT, Professor, Cardio-Vascular Imaging Unit - Giovanni XXIII Hospital, Via Giovanni XXIII, 7 - 31050 - Monastier di Treviso (TV), Italy. filippocademartiri@gmail.com

Editorial Office
Jian-Xia Cheng, Director
Jin-Lei Wang, Vice Director
World Journal of Radiology
Room 903, Building D, Ocean International Center,
No. 62 Dongsihuan Zhonglu, Chaoyang District,
Beijing 100025, China
Telephone: +86-10-85381891
Fax: +86-10-85381893
E-mail: wjr@wjgnet.com
http://www.wjgnet.com

Publisher
Baishideng Publishing Group Co., Limited
Flat C, 23/F., Lucky Plaza, 315-321 Lockhart Road,
Wanchai, Hong Kong, China
Telephone: +852-58042046
Fax: +852-31158812
E-mail: bpgoffice@wjgnet.com
http://www.wjgnet.com

Production center
Beijing Baishideng BioMed Scientific Co., Limited
Room 903, Building D, Ocean International Center,
No. 62 Dongsihuan Zhonglu, Chaoyang District,
Beijing 100025, China
Telephone: +86-10-85381892
Fax: +86-10-85381893

Representative office
USA Office
8226 Regency Drive,
Pleasanton, CA 94588-3144, United States
Telephone: +1-925-2238242
Fax: +1-925-2238243

Instructions to authors
Full instructions are available online at http://www.wjgnet.com/1948-5204/g_info_20100312180518.htm.

Indexed and Abstracted in
PubMed Central, PubMed, Digital Object Identifier, and Directory of Open Access Journals.

SPECIAL STATEMENT

All articles published in this journal represent the viewpoints of the authors except where indicated otherwise.

Biostatistical editing
Statisital review is performed after peer review. We invite an expert in Biomedical Statistics to evaluate the statistical method used in the paper, including *t*-test (group or paired comparisons), chi-squared test, Ridit, probit, logit, regression (linear, curvilinear, or stepwise), correlation, analysis of variance, analysis of covariance, *etc*. The reviewing points include: (1) Statistical methods should be described when they are used to verify the results; (2) Whether the statistical techniques are suitable or correct; (3) Only homogeneous data can be averaged. Standard deviations are preferred to standard errors. Give the number of observations and subjects (*n*). Losses in observations, such as drop-outs from the study should be reported; (4) Values such as ED50, LD50, IC50 should have their 95% confidence limits calculated and compared by weighted probit analysis (Bliss and Finney); and (5) The word 'significantly' should be replaced by its synonyms (if it indicates extent) or the *P* value (if it indicates statistical significance).

Conflict-of-interest statement
In the interests of transparency and to help reviewers assess any potential bias, *WJR* requires authors of all papers to declare any competing commercial, personal, political, intellectual, or religious interests in relation to the submitted work. Referees are also asked to indicate any potential conflict they might have reviewing a particular paper. Before submitting, authors are suggested to read "Uniform Requirements for Manuscripts Submitted to Biomedical Journals: Ethical Considerations in the Conduct and Reporting of Research: Conflicts of Interest" from International Committee of Medical Journal Editors (ICMJE), which is available at: http://www.icmje.org/ethical_4conflicts.html.

Sample wording: [Name of individual] has received fees for serving as a speaker, a consultant and an advisory board member for [names of organizations], and has received research funding from [names of organization]. [Name of individual] is an employee of [name of organization]. [Name of individual] owns stocks and shares in [name of organization]. [Name of individual] owns patent [patent identification and brief description].

Statement of informed consent
Manuscripts should contain a statement to the effect that all human studies have been reviewed by the appropriate ethics committee or it should be stated clearly in the text that all persons gave their informed consent prior to their inclusion in the study. Details that might disclose the identity of the subjects under study should be omitted. Authors should also draw attention to the Code of Ethics of the World Medical Association (Declaration of Helsinki, 1964, as revised in 2004).

Statement of human and animal rights
When reporting the results from experiments, authors should follow the highest standards and the trial should conform to Good Clinical Practice (for example, US Food and Drug Administration Good Clinical Practice in FDA-Regulated Clinical Trials; UK Medicines Research Council Guidelines for Good Clinical Practice in Clinical Trials) and/or the World Medical Association Declaration of Helsinki. Generally, we suggest authors follow the lead investigator's national standard. If doubt exists whether the research was conducted in accordance with the above standards, the authors must explain the rationale for their approach and demonstrate that the institutional review body explicitly approved the doubtful aspects of the study.

Before submitting, authors should make their study approved by the relevant research ethics committee or institutional review board. If human participants were involved, manuscripts must be accompanied by a statement that the experiments were undertaken with the understanding and appropriate informed consent of each. Any personal item or information will not be published without explicit consents from the involved patients. If experimental animals were used, the materials and methods (experimental procedures) section must clearly indicate that appropriate measures were taken to minimize pain or discomfort, and details of animal care should be provided.

SUBMISSION OF MANUSCRIPTS

Manuscripts should be typed in 1.5 line spacing and 12 pt. Book Antiqua with ample margins. Number all pages consecutively, and start each of the following sections on a new page: Title Page, Abstract, Introduction, Materials and Methods, Results, Discussion, Acknowledgements, References, Tables, Figures, and Figure Legends. Neither the editors nor the publisher are responsible for the opinions expressed by contributors. Manuscripts formally accepted for publication become the permanent property of Baishideng Publishing Group Co., Limited, and may not be reproduced by any means, in whole or in part, without the written permission of both the authors and the publisher. We reserve the right to copy-edit and put onto our website accepted manuscripts. Authors should follow the relevant guidelines for the care and use of laboratory animals of their institution or national animal welfare committee. For the sake of transparency in regard to the performance and reporting of clinical trials, we endorse the policy of the ICMJE to refuse to publish papers on clinical trial results if the trial was not recorded in a publicly-accessible registry at its outset. The only register now available, to our knowledge, is http://www.clinicaltrials.gov sponsored by the United States National Library of Medicine and we encour-

age all potential contributors to register with it. However, in the case that other registers become available you will be duly notified. A letter of recommendation from each author's organization should be provided with the contributed article to ensure the privacy and secrecy of research is protected.

Authors should retain one copy of the text, tables, photographs and illustrations because rejected manuscripts will not be returned to the author(s) and the editors will not be responsible for loss or damage to photographs and illustrations sustained during mailing.

Online submissions

Manuscripts should be submitted through the Online Submission System at: http://www.wjgnet.com/esps/. Authors are highly recommended to consult the ONLINE INSTRUCTIONS TO AUTHORS (http://www.wjgnet.com/1948-5204/g_info_20100312180518.htm) before attempting to submit online. For assistance, authors encountering problems with the Online Submission System may send an email describing the problem to wjr@wjgnet.com, or by telephone: +86-10-85381891. If you submit your manuscript online, do not make a postal contribution. Repeated online submission for the same manuscript is strictly prohibited.

MANUSCRIPT PREPARATION

All contributions should be written in English. All articles must be submitted using word-processing software. All submissions must be typed in 1.5 line spacing and 12 pt. Book Antiqua with ample margins. Style should conform to our house format. Required information for each of the manuscript sections is as follows:

Title page

Title: Title should be less than 12 words.

Running title: A short running title of less than 6 words should be provided.

Authorship: Authorship credit should be in accordance with the standard proposed by International Committee of Medical Journal Editors, based on (1) substantial contributions to conception and design, acquisition of data, or analysis and interpretation of data; (2) drafting the article or revising it critically for important intellectual content; and (3) final approval of the version to be published. Authors should meet conditions 1, 2, and 3.

Institution: Author names should be given first, then the complete name of institution, city, province and postcode. For example, Xu-Chen Zhang, Li-Xin Mei, Department of Pathology, Chengde Medical College, Chengde 067000, Hebei Province, China. One author may be represented from two institutions, for example, George Sgourakis, Department of General, Visceral, and Transplantation Surgery, Essen 45122, Germany; George Sgourakis, 2nd Surgical Department, Korgialenio-Benakio Red Cross Hospital, Athens 15451, Greece

Author contributions: The format of this section should be: Author contributions: Wang CL and Liang L contributed equally to this work; Wang CL, Liang L, Fu JF, Zou CC, Hong F and Wu XM designed the research; Wang CL, Zou CC, Hong F and Wu XM performed the research; Xue JZ and Lu JR contributed new reagents/analytic tools; Wang CL, Liang L and Fu JF analyzed the data; and Wang CL, Liang L and Fu JF wrote the paper.

Supportive foundations: The complete name and number of supportive foundations should be provided, e.g. Supported by National Natural Science Foundation of China, No. 30224801

Correspondence to: Only one corresponding address should be provided. Author names should be given first, then author title, affiliation, the complete name of institution, city, postcode, province, country, and email. All the letters in the email should be in lower case. A space interval should be inserted between country name and email address. For example, Montgomery Bissell, MD, Professor of Medicine, Chief, Liver Center, Gastroenterology Division, University of California, Box 0538, San Francisco, CA 94143, United States. montgomery.bissell@ucsf.edu

Telephone and fax: Telephone and fax should consist of +, country number, district number and telephone or fax number, e.g. Telephone: +86-10-85381891 Fax: +86-10-85381893

Peer reviewers: All articles received are subject to peer review. Normally, three experts are invited for each article. Decision on acceptance is made only when at least two experts recommend publication of an article. All peer-reviewers are acknowledged on Express Submission and Peer-review System website.

Abstract

There are unstructured abstracts (no less than 200 words) and structured abstracts. The specific requirements for structured abstracts are as follows:

An informative, structured abstract should accompany each manuscript. Abstracts of original contributions should be structured into the following sections: AIM (no more than 20 words; Only the purpose of the study should be included. Please write the Aim in the form of "To investigate/study/…"), METHODS (no less than 140 words for Original Articles; and no less than 80 words for Brief Articles), RESULTS (no less than 150 words for Original Articles and no less than 120 words for Brief Articles; You should present *P* values where appropriate and must provide relevant data to illustrate how they were obtained, e.g. 6.92 ± 3.86 *vs* 3.61 ± 1.67, $P < 0.001$), and CONCLUSION (no more than 26 words).

Key words

Please list 5-10 key words, selected mainly from *Index Medicus*, which reflect the content of the study.

Core tip

Please write a summary of less than 100 words to outline the most innovative and important arguments and core contents in your paper to attract readers.

Text

For articles of these sections, original articles and brief articles, the main text should be structured into the following sections: INTRODUCTION, MATERIALS AND METHODS, RESULTS and DISCUSSION, and should include appropriate Figures and Tables. Data should be presented in the main text or in Figures and Tables, but not in both. The main text format of these sections, editorial, topic highlight, case report, letters to the editors, can be found at: http://www.wjgnet.com/1948-5204/g_info_list.htm.

Illustrations

Figures should be numbered as 1, 2, 3, *etc*., and mentioned clearly in the main text. Provide a brief title for each figure on a separate page. Detailed legends should not be provided under the figures. This part should be added into the text where the figures are applicable. Keeping all elements compiled is necessary in line-art image. Scale bars should be used rather than magnification factors, with the length of the bar defined in the legend rather than on the bar itself. File names should identify the figure and panel. Avoid layering type directly over shaded or textured areas. Please use uniform legends for the same subjects. For example: Figure 1 Pathological changes in atrophic gastritis after treatment. A: ...; B: ...; C: ...; D: ...; E: ...; F: ...; G: …*etc*. It is our principle to publish high resolution-figures for the E-versions.

Tables

Three-line tables should be numbered 1, 2, 3, *etc*., and mentioned clearly in the main text. Provide a brief title for each table. Detailed legends should not be included under tables, but rather added into the text where applicable. The information should complement, but not duplicate the text. Use one horizontal line under the title, a second under column heads, and a third below the Table, above any footnotes. Vertical and italic lines should be omitted.

Notes in tables and illustrations

Data that are not statistically significant should not be noted. [a]$P < 0.05$, [b]$P < 0.01$ should be noted ($P > 0.05$ should not be noted). If there are other series of P values, [c]$P < 0.05$ and [d]$P < 0.01$ are used. A third series of P values can be expressed as [e]$P < 0.05$ and [f]$P < 0.01$. Other notes in tables or under illustrations should be expressed as [1]F, [2]F, [3]F; or sometimes as other symbols with a superscript (Arabic numerals) in the upper left corner. In a multi-curve illustration, each curve should be labeled with ●, ○, ■, □, ▲, △, *etc*., in a certain sequence.

Acknowledgments

Brief acknowledgments of persons who have made genuine contributions to the manuscript and who endorse the data and conclusions should be included. Authors are responsible for obtaining written permission to use any copyrighted text and/or illustrations.

REFERENCES

Coding system

The author should number the references in Arabic numerals according to the citation order in the text. Put reference numbers in square brackets in superscript at the end of citation content or after the cited author's name. For citation content which is part of the narration, the coding number and square brackets should be typeset normally. For example, "Crohn's disease (CD) is associated with increased intestinal permeability[1,2]". If references are cited directly in the text, they should be put together within the text, for example, "From references[19,22-24], we know that..."

When the authors write the references, please ensure that the order in text is the same as in the references section, and also ensure the spelling accuracy of the first author's name. Do not list the same citation twice.

PMID and DOI

Pleased provide PubMed citation numbers to the reference list, e.g. PMID and DOI, which can be found at http://www.ncbi.nlm.nih.gov/sites/entrez?db=pubmed and http://www.crossref.org/SimpleTextQuery/, respectively. The numbers will be used in E-version of this journal.

Style for journal references

Authors: the name of the first author should be typed in bold-faced letters. The family name of all authors should be typed with the initial letter capitalized, followed by their abbreviated first and middle initials. (For example, Lian-Sheng Ma is abbreviated as Ma LS, Bo-Rong Pan as Pan BR). The title of the cited article and italicized journal title (journal title should be in its abbreviated form as shown in PubMed), publication date, volume number (in black), start page, and end page [PMID: 11819634 DOI: 10.3748/wjg.13.5396].

Style for book references

Authors: the name of the first author should be typed in bold-faced letters. The surname of all authors should be typed with the initial letter capitalized, followed by their abbreviated middle and first initials. (For example, Lian-Sheng Ma is abbreviated as Ma LS, Bo-Rong Pan as Pan BR) Book title. Publication number. Publication place: Publication press, Year: start page and end page.

Format

Journals

English journal article (list all authors and include the PMID where applicable)

1 **Jung EM**, Clevert DA, Schreyer AG, Schmitt S, Rennert J, Kubale R, Feuerbach S, Jung F. Evaluation of quantitative contrast harmonic imaging to assess malignancy of liver tumors: A prospective controlled two-center study. *World J Gastroenterol* 2007; **13**: 6356-6364 [PMID: 18081224 DOI: 10.3748/wjg.13.6356]

Chinese journal article (list all authors and include the PMID where applicable)

2 **Lin GZ**, Wang XZ, Wang P, Lin J, Yang FD. Immunologic effect of Jianpi Yishen decoction in treatment of Pixu-diarrhoea. *Shijie Huaren Xiaohua Zazhi* 1999; **7**: 285-287

In press

3 **Tian D**, Araki H, Stahl E, Bergelson J, Kreitman M. Signature of balancing selection in Arabidopsis. *Proc Natl Acad Sci USA* 2006; In press

Organization as author

4 **Diabetes Prevention Program Research Group**. Hypertension, insulin, and proinsulin in participants with impaired glucose tolerance. *Hypertension* 2002; **40**: 679-686 [PMID: 12411462 DOI:10.1161/01.HYP.0000035706.28494.09]

Both personal authors and an organization as author

5 **Vallancien G**, Emberton M, Harving N, van Moorselaar RJ; Alf-One Study Group. Sexual dysfunction in 1, 274 European men suffering from lower urinary tract symptoms. *J Urol* 2003; **169**: 2257-2261 [PMID: 12771764 DOI:10.1097/01.ju.0000067940.76090.73]

No author given

6 21st century heart solution may have a sting in the tail. *BMJ* 2002; **325**: 184 [PMID: 12142303 DOI:10.1136/bmj.325.7357.184]

Volume with supplement

7 **Geraud G**, Spierings EL, Keywood C. Tolerability and safety of frovatriptan with short- and long-term use for treatment of migraine and in comparison with sumatriptan. *Headache* 2002; **42** Suppl 2: S93-99 [PMID: 12028325 DOI:10.1046/j.1526-4610.42.s2.7.x]

Issue with no volume

8 **Banit DM**, Kaufer H, Hartford JM. Intraoperative frozen section analysis in revision total joint arthroplasty. *Clin Orthop Relat Res* 2002; (**401**): 230-238 [PMID: 12151900 DOI:10.1097/00003086-200208000-00026]

No volume or issue

9 Outreach: Bringing HIV-positive individuals into care. *HRSA Careaction* 2002; 1-6 [PMID: 12154804]

Books

Personal author(s)

10 **Sherlock S**, Dooley J. Diseases of the liver and billiary system. 9th ed. Oxford: Blackwell Sci Pub, 1993: 258-296

Chapter in a book (list all authors)

11 **Lam SK**. Academic investigator's perspectives of medical treatment for peptic ulcer. In: Swabb EA, Azabo S. Ulcer disease: investigation and basis for therapy. New York: Marcel Dekker, 1991: 431-450

Author(s) and editor(s)

12 **Breedlove GK**, Schorfheide AM. Adolescent pregnancy. 2nd ed. Wieczorek RR, editor. White Plains (NY): March of Dimes Education Services, 2001: 20-34

Conference proceedings

13 **Harnden P**, Joffe JK, Jones WG, editors. Germ cell tumours V. Proceedings of the 5th Germ cell tumours Conference; 2001 Sep 13-15; Leeds, UK. New York: Springer, 2002: 30-56

Conference paper

14 **Christensen S**, Oppacher F. An analysis of Koza's computational effort statistic for genetic programming. In: Foster JA, Lutton E, Miller J, Ryan C, Tettamanzi AG, editors. Genetic programming. EuroGP 2002: Proceedings of the 5th European Conference on Genetic Programming; 2002 Apr 3-5; Kinsdale, Ireland. Berlin: Springer, 2002: 182-191

Electronic journal (list all authors)

15 Morse SS. Factors in the emergence of infectious diseases. Emerg Infect Dis serial online, 1995-01-03, cited 1996-06-05; 1(1): 24 screens. Available from: URL: http://www.cdc.gov/ncidod/eid/index.htm

Patent (list all authors)

16 **Pagedas AC**, inventor; Ancel Surgical R&D Inc., assignee. Flexible endoscopic grasping and cutting device and positioning tool assembly. United States patent US 20020103498. 2002 Aug 1

Statistical data

Write as mean ± SD or mean ± SE.

Statistical expression

Express *t* test as *t* (in italics), *F* test as *F* (in italics), chi square test as χ^2 (in Greek), related coefficient as *r* (in italics), degree of freedom as υ (in Greek), sample number as *n* (in italics), and probability as *P* (in italics).

Units

Use SI units. For example: body mass, m (B) = 78 kg; blood pressure, p (B) = 16.2/12.3 kPa; incubation time, t (incubation) = 96 h, blood glucose concentration, c (glucose) 6.4 ± 2.1 mmol/L; blood CEA mass concentration, p (CEA) = 8.6 24.5 μg/L; CO_2 volume fraction, 50 mL/L CO_2, not 5% CO_2; likewise for 40 g/L formaldehyde, not 10% formalin; and mass fraction, 8 ng/g, *etc*. Arabic numerals such as 23, 243, 641 should be read 23243641.

The format for how to accurately write common units and quantums can be found at: http://www.wjgnet.com/1948-5204/g_info_20100312183048.htm.

Abbreviations

Standard abbreviations should be defined in the abstract and on first mention in the text. In general, terms should not be abbreviated unless they are used repeatedly and the abbreviation is helpful to the reader. Permissible abbreviations are listed in Units, Symbols and Abbreviations: A Guide for Biological and Medical Editors and Authors (Ed. Baron DN, 1988) published by The Royal Society of Medicine, London. Certain commonly used abbreviations, such as DNA, RNA, HIV, LD50, PCR, HBV, ECG, WBC, RBC, CT, ESR, CSF, IgG, ELISA, PBS, ATP, EDTA, mAb, can be used directly without further explanation.

Italics

Quantities: *t* time or temperature, *c* concentration, *A* area, *l* length, *m* mass, *V* volume.
Genotypes: *gyrA*, *arg* 1, *c myc*, *c fos*, *etc*.
Restriction enzymes: *Eco*RI, *Hin*dI, *Bam*HI, *Kbo* I, *Kpn* I, *etc*.
Biology: *H. pylori*, *E coli*, *etc*.

Examples for paper writing

All types of articles' writing style and requirement will be found in the link: http://www.wjgnet.com/esps/NavigationInfo.aspx?id=15

SUBMISSION OF THE REVISED MANUSCRIPTS AFTER ACCEPTED

Authors must revise their manuscript carefully according to the revision policies of Baishideng Publishing Group Co., Limited. The revised version, along with the signed copyright transfer agreement, responses to the reviewers, and English language Grade B certificate (for non-native speakers of English), should be submitted to the online system via the link contained in the e-mail sent by the editor. If you have any questions about the revision, please send e-mail to esps@wjgnet.com.

Language evaluation

The language of a manuscript will be graded before it is sent for revision. (1) Grade A: priority publishing; (2) Grade B: minor language polishing; (3) Grade C: a great deal of language polishing needed; and (4) Grade D: rejected. Revised articles should reach Grade A or B.

Copyright assignment form

Please download a Copyright assignment form from http://www.wjgnet.com/1948-5204/g_info_20100312182928.htm.

Responses to reviewers

Please revise your article according to the comments/suggestions provided by the reviewers. The format for responses to the reviewers' comments can be found at: http://www.wjgnet.com/1948-5204/g_info_20100312182841.htm.

Proof of financial support

For papers supported by a foundation, authors should provide a copy of the approval document and serial number of the foundation.

Links to documents related to the manuscript

WJR will be initiating a platform to promote dynamic interactions between the editors, peer reviewers, readers and authors. After a manuscript is published online, links to the PDF version of the submitted manuscript, the peer-reviewers' report and the revised manuscript will be put on-line. Readers can make comments on the peer reviewer's report, authors' responses to peer reviewers, and the revised manuscript. We hope that authors will benefit from this feedback and be able to revise the manuscript accordingly in a timely manner.

Publication fee

WJR is an international, peer-reviewed, OA online journal. Articles published by this journal are distributed under the terms of the Creative Commons Attribution Non-commercial License, which permits use, distribution, and reproduction in any medium and format, provided the original work is properly cited. The use is non-commercial and is otherwise in compliance with the license. Authors of accepted articles must pay a publication fee. Publication fee: 600 USD per article. All invited articles are published free of charge.

百世登
Baishideng®

Published by **Baishideng Publishing Group Co., Limited**
Flat C, 23/F., Lucky Plaza,
315-321 Lockhart Road, Wan Chai,
Hong Kong, China
Fax: +852-31158812
Telephone: +852-58042046
E-mail: bpgoffice@wjgnet.com
http://www.wjgnet.com